

Smart optics against smart parasites

Towards point-of-care optical diagnosis of malaria and urogenital schistosomiasis

Agbana, Tope

DOI

[10.4233/uuid:4345c365-efd6-49e1-975d-3e66028a8e53](https://doi.org/10.4233/uuid:4345c365-efd6-49e1-975d-3e66028a8e53)

Publication date

2020

Document Version

Final published version

Citation (APA)

Agbana, T. (2020). *Smart optics against smart parasites: Towards point-of-care optical diagnosis of malaria and urogenital schistosomiasis*. [Dissertation (TU Delft), Delft University of Technology]. <https://doi.org/10.4233/uuid:4345c365-efd6-49e1-975d-3e66028a8e53>

Important note

To cite this publication, please use the final published version (if applicable). Please check the document version above.

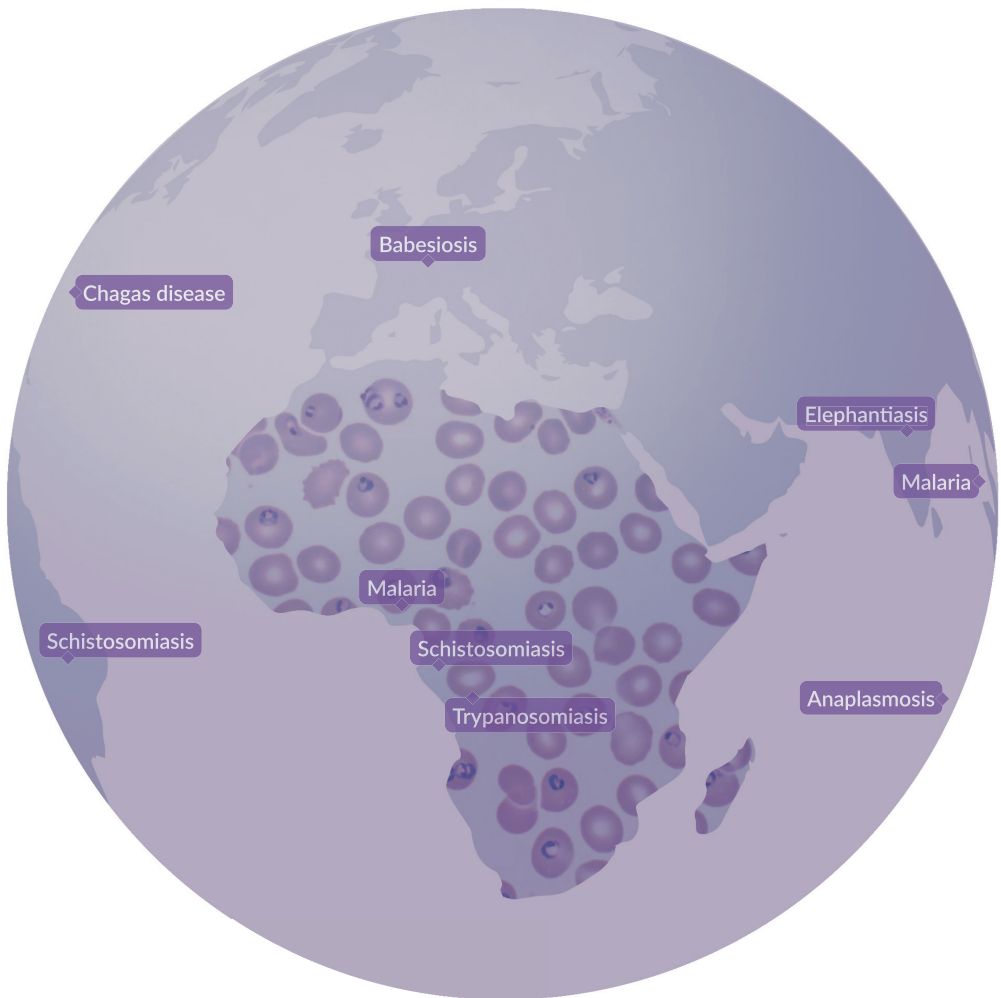
Copyright

Other than for strictly personal use, it is not permitted to download, forward or distribute the text or part of it, without the consent of the author(s) and/or copyright holder(s), unless the work is under an open content license such as Creative Commons.

Takedown policy

Please contact us and provide details if you believe this document breaches copyrights. We will remove access to the work immediately and investigate your claim.

SMART OPTICS AGAINST SMART PARASITES



TEMITOPE EBENEZER AGBANA

Smart Optics against Smart Parasites

Towards point-of-care optical diagnosis of malaria and urogenital schistosomiasis

Smart Optics against Smart Parasites

Towards point-of-care optical diagnosis of malaria and urogenital schistosomiasis

Dissertation

for the purpose of obtaining the degree of doctor
at Delft University of Technology,
by the authority of the Rector Magnificus prof. dr. ir. T.H.J.J. van der Hagen,
chair of the Board for Doctorates,
to be defended publicly on
Wednesday 6 May 2020 at 12:30 o'clock

by

Temitope Ebenezer AGBANA

Master of Science in Electronic Engineering, Delft University of Technology, the Netherlands born in Egbe, Nigeria.

This dissertation has been approved by the promotor.

Composition of the doctoral committee:

Rector Magnificus,	chairperson
Prof. dr. G. V. Vdovine,	Delft University of Technology, promotor
Prof. dr. ir. M. Verhaegen,	Delft University of Technology, promotor

Independent members:

Dr. J. Bergmann	University of Oxford, United Kingdom
Prof. dr. O. Oladimeji	University of Ibadan, Nigeria
Prof. dr. M. Yazdanbakhsh	Leiden University Medical Centrum
Prof. dr ir. R.H.M. Goossens	Delft University of Technology
Prof. Dr. dr. A.G. Yarovoy	Delft University of Technology, reserve member

Other members:

Dr. ir. J.C. Diehl	Delft University of Technology
--------------------	--------------------------------



Keywords: Malaria, diagnostics, smart optics, cell-phone microscopy, holography

Printed by: Gilde Drukkerijen, NL

Front: Distribution of some common parasitic diseases and red blood cells infected with *Plasmodium falciparum*.

Copyright © 2020 by T.E.Agbana

ISBN 978-94-6402-244-5

An electronic version of this dissertation is available at
<http://repository.tudelft.nl/>.

*To Moses Oluwabunmi Agbana, one out of the many that has departed as a result of untimely diagnosis of a treatable disease. To me this is more than a thesis.
Rest on bro till I see you again!*

Prov. 10:7

Contents

Summary	xi
Samenvatting	xv
1 Introduction	1
1.1 The devastating impact of Malaria & Schistosomiasis	2
1.2 Clinical diagnosis of malaria	2
1.3 WHO reference standard for malaria diagnosis.	3
1.3.1 Microscopic examination of malaria parasite.	4
1.3.2 Recognition of a malaria parasite	5
1.3.3 Estimation of parasitemia	5
1.3.4 Advantages of light microscopy	7
1.3.5 Limitations of light microscopy	7
1.4 The Motivation, Objective & Research goals	9
1.4.1 Motivation	9
1.4.2 Main objective	9
1.5 Dissertation layout	12
References	14
2 Overview of Malaria & Schistosomiasis	15
2.1 Malaria background information	16
2.1.1 Transmission	16
2.1.2 Existing state-of-the-art diagnostic methods	17
2.2 Urogenital Schistosomiasis	24
2.2.1 Transmission	24
2.2.2 State-of-the-art diagnostic methods	24
2.3 Conclusion	26
References	27
3 Light Microscopy With Extended Depth	33
3.1 Fundamental principle of optical microscopy	34
3.1.1 Theoretical principle	34
3.1.2 Coherent imaging.	36
3.1.3 Incoherent imaging	36
3.1.4 Depth of field.	37
3.2 Extending depth of field by wavefront coding	39
3.2.1 Basics of wavefront coding.	39
3.2.2 Experimental set-up and results	41

3.3	Aliasing, coherence and resolution in a lensless holographic microscope.	45
3.4	Theoretical basis	45
3.5	Defining Optimal system configuration.	48
3.6	Experimental validation and results.	50
3.7	Smart Optical Diagnostic Of Schistosomiasis (SODOS)	52
	References	63
4	Smart Optical Diagnosis of Urogenital Schistosomiasis	69
4.1	Introduction.	70
4.2	Experimental setup and method	71
4.2.1	Imaging <i>S. haematobium</i> eggs	71
4.3	The proposed method	73
4.4	Image classification using wavelet transform & statistical analysis	76
4.5	Image classification using a Support Vector Machine (SVM)	77
4.6	Statistical analysis	78
4.7	Experimental results & discussion	79
4.8	Discussion.	82
	References	85
5	Optimizing The Resolution of Cell-Phone Based Microscope	89
5.1	Introduction.	90
5.2	Design and performance	92
5.3	Experimental validation.	96
5.4	Practical detection of the malaria parasite	96
5.5	Discussion.	101
	References	103
6	Smart Optical Detection of Malaria Parasites	105
6.1	Statistics of the optical test	107
6.2	Experimental implementation.	109
6.3	Laboratory characterization.	109
6.4	Malaria detection in fresh patient samples	111
6.5	Discussion.	112
	References	116
7	From The Lab To The Field	119
7.1	Introduction.	120
7.2	Diagnostics gap.	120
7.3	Technological developments	121
7.3.1	Challenges and opportunities with digital handheld microscopes	121
7.4	Research setup	123
7.5	Field validation report.	125
7.5.1	First iteration.	125

7.6	Field research I	126
7.7	Second iteration	128
7.8	Field Research II	129
7.9	Discussion.	131
7.10	Conclusion	133
	References	134
8	Conclusion	137
	Acknowledgements	147
	Curriculum Vitæ	153
	List of Publications	157

Summary

Malaria remains an important cause of high morbidity and mortality worldwide. According to World Health Organisation (WHO) malaria report for 2017, malaria accounted for the death of 435,000 people. It is the leading cause of death among pregnant women and little children. 11% of maternal and 20% of under-five deaths are attributed to malaria every year. Malaria transmission is currently active in 95 countries putting the lives of 3.2 billion people at risk. 40% of the malaria related deaths are linked to Nigeria and the Democratic republic of the Congo.

Since malaria symptoms are generally non-specific and usually overlap with the symptoms of other febrile illnesses, clinical diagnosis are typically presumptive and often results into high number of false positives which potentially lead to the abuse of antimalarial drugs. The consistent abuse of antimalarial drugs has produced the consequent effect of drug resistance which is a major concern in the current global malaria control and elimination efforts. The WHO therefore recommends that an effective malaria case management plan must be predicated on a standard parasite-based confirmatory diagnostic test. Conventional Light Microscopy is the recommended reference diagnostic standard prescribed by the World Health Organisation. This method is particularly of interest because it allows parasite specie differentiation, quantification of the parasite density in a given blood smear, high accuracy (although this depends on the expertise of the microscopist), low direct cost, visualization of different stages of the parasite development etc. While well-equipped laboratories for malaria diagnosis are commonly available in developed urban and peri-urban areas, low-resource settings of malaria endemicity usually have very limited options.

The recommended standard microscopy is less accessible in resource-limited settings because of the following: lack of required technical skills, incessant power outages, lack of efficient maintenance capability, delayed diagnosis due to intense workload, inaccuracies due to manual counting of the parasites detected in the blood film etc. The inaccuracies of parasite density estimation eventually affects the accuracy and efficiency of the prescribed treatment which could have fatal consequences. A diagnostic process is termed inconclusive by the WHO until and unless a minimum of 100 measurement (microscopy examination of 100 high powered-fields) has been done on a prepared thick blood film. For a thin blood film which provides more details about the morphology of the parasite, an average of 800 measurement is required. This is an easy task for laboratory technologist in malaria non-endemic countries where an average of 120 malaria cases occur yearly. But for malaria endemic country where several thousand cases are reported daily, this is by no means a mean task as it demands full concentration, time, high expertise and experience.

To realize current global effort to reduce the heavy malaria burden, the need for a

reliable, efficient, accurate and automated point-of-care diagnostic tool cannot be overemphasized. The focus of this thesis work therefore, is to develop smart optical methods that alleviate the burden of manual microscopy by researching methods to optimise existing imaging modalities which can be integrated with smart algorithms for quick malaria parasite detection in infected patients.

Aside malaria, schistosomiasis is the second most common parasitic diseases. Although it falls into the category of a Neglected Tropical Disease (NTD), 220.8 million people required preventive treatment in the year 2017 according to the World Health Organisation report. It is a disease of the poor and it is prevalent in tropical and subtropical areas and particularly common in communities where there is no access to clean drinking water and proper sanitation. 779 million people are at risk of contracting this disease which results into impaired growth and development, diminished physical fitness, bladder cancer and decreased neurocognitive abilities. Although safe and effective medication is widely available for treatment, accurate diagnostic techniques for schistosomiasis is hugely underdeveloped and remains a critical challenge.

Intestinal and urogenital schistosomiasis are the two variants of this Neglected tropical disease but in this research, we focus on urogenital schistosomiasis (caused by *Schistosoma Haematobium*) because it is most prevalent among the population we worked with and also because it is easier to detect in urine.

The diagnostic protocol for *S. haematobium* prescribes urine filtration with WHO recommended standard membrane filters (with $12\mu\text{l}$ pore size). Several critical measurements by an expert must be done to detect the targeted foreign bodies (parasite eggs) in the urine samples before a reliable conclusion can be made. Also for a confirmatory diagnosis, it is standard practice to examine different samples collected from the patient at different specific intervals. This is particularly recommended to increase the amount of sample analysis per patient thereby increasing the sensitivity of the test. Since this process involves the microscopy examination of filtered urine samples, it is also limited by the challenges already described for standard malaria microscopy. Although several antigen and antibody based rapid diagnostic test kits have been developed for both malaria and schistosomiasis, the reliability of the performance of these diagnostic test is still a major concern. This thesis is aimed at the development of reliable, robust, accurate, cost effective and easy-to-use point-of-care optical devices for quick diagnosis of malaria and urogenital disease in human samples.

This thesis begins by looking at light microscopy with extended depth of field. Wavefront coding with adaptive optics and digital inline holography have been considered in this work. An optimal configuration that guarantees maximum resolution based on the coherence property of illuminating source and the specification of the imaging sensor is prescribed. In this system, interference of a plane and object wave at the detector plane generates a hologram from which the complex amplitude of the field in the object plane can be numerically reconstructed by solving an inverse source problem. This method is of practical interest particularly because unlike the conventional microscope, details in transparent biological samples can be retrieved since both

amplitude and the phase of the field is reconstructed. It provides potential solution towards label-free diagnosis of parasitic diseases. Combined with flow cytometry and data-driven algorithms we applied this methodology to the development of rapid detection of *Schistosoma haematobium*. A working prototype device with the potential to map the diseases has been developed and tested on the field.

The system design takes into consideration practical field conditions such as ease-of-use, cost, harsh environmental conditions, erratic power outages, system robustness against dust and other artifacts. Feedbacks and results from the field are very promising. Leveraging on recent advances in cellphone and 3-D printing technologies we developed an automated cellphone based microscope towards the realization of a rapid point-of-care diagnosis of malaria. The challenge here is to optimise the optical train of a low-cost commonly available cellphone to detect malaria parasite with sufficient resolution. It was found that existing cellphone based microscope could not resolve the $1\ \mu\text{m}$ size malaria parasites because of the system optical aberration and the numerical aperture limit of the phone objectives. Although this method demonstrate the capability of the cell phone based microscope to image malaria parasite, however the achievable field of view is limited to $150 \times 150\ \mu\text{m}$. This implies that over 600 measurement is needed for a conclusive diagnosis.

We circumvent this limitation by the novel implementation of computer-assisted dry fluorescent microscopy. Using computational analysis of image containing large number of blood cells, we establish a robust statistics which provides reliable diagnostic recommendation. The technique was tested with in vitro and in vivo samples and has demonstrated its suitability for highly sensitive, robust and automated diagnostics of malaria. It requires minimal human intervention, uses simple sample preparation, provides high degree of independence of expert judgement, and has a potential for massive community screening for malaria control and elimination programs.

The design specifications for the development of working prototypes presented in this thesis took into account feedbacks from diagnostic experts from the following non-governmental organisations: Doctors without Borders, Malaria Consortium, AMREF, Save the Children and Christian Aid (Nigeria). Also, our methodology was thoroughly validated by discussions and interactions with experts on the field (in Nigeria, Ivory Coast, Gabon, Uganda and Ghana) and with parasitologists, researchers and vaccine developers in the Netherlands, Spain, Ireland and Germany, leading to valuable new insights." It is our goal that the diagnostic methods and prototype presented in this thesis will be used to compliment the limitations of the existing diagnostic techniques.

Samenvatting

Malaria blijft een belangrijke oorzaak van een wereldwijd hoge morbiditeit en mortaliteit. Volgens een rapport van de Wereldgezondheidsorganisatie (WHO), werden er in 2017 alleen al 435.000 sterfgevallen aan malaria toegeschreven. Het is een van de voornaamste doodsoorzaken onder zwangere vrouwen en jonge kinderen. Malaria is jaarlijks verantwoordelijk voor 11% van de moedersterfte en 20% van de sterfgevallen van kinderen jonger dan 5 jaar. Momenteel is Malaria in 95 landen actief, wat het leven van 3.2 miljoen mensen in gevaar brengt. 40% van de aan malaria gerelateerde sterfgevallen vindt plaats in Nigeria en de Democratische Republiek Congo.

Aangezien malariasymptomen over het algemeen niet specifiek zijn, en regelmatig overlap vertonen met de symptomen van andere febriele ziekten, is de klinische diagnose meestal vermoedelijk. En resulteert dit vaak in een groot aantal fout-positieve resultaten die potentieel leiden tot onnodig gebruik van malaria medicatie. Om deze reden schrijft de WHO voor dat een effectief malaria behandelplan moet worden gebaseerd op een bevestigende, standaard, op parasieten gebaseerde diagnostische test. Conventionele lichtmicroscopie is de aanbevolen diagnostische referentiestandaard, voorgeschreven door de World Health Organisation. Deze methode is met name interessant, omdat het de mogelijkheid geeft tot de differentiatie van parasitaire soorten, de kwantificering van de parasitaire dichtheid in een gegeven bloeduitstrijkje, een grote accuratesse (hoewel dit afhankelijk is van de expertise van de microscopist), lage directe kosten, visualisatie van verschillende stadia van de ontwikkeling van de parasiet, enzovoort. Hoewel goed uitgeruste laboratoria voor malariadiagnostiek algemeen beschikbaar zijn in ontwikkelde stedelijke en peri-urbane gebieden, zijn de opties in low-resource settings van malaria endemische landen meestal zeer beperkt.

De aanbevolen standaard microscopie is minder toegankelijk in low-resource settings vanwege onder andere: tekort aan de vereiste technische vaardigheden, onberekenbare stroomuitval, gebrek aan efficiënte onderhoudsmogelijkheden, vertraagde diagnose vanwege hoge werkdruk, onnauwkeurigheden door handmatige telling van de gedetecteerde parasieten in de bloedfilm. De onnauwkeurigheden bij de schatting van de parasitaire dichtheid zijn van invloed op de juistheid en efficiëntie van de voorgeschreven behandeling en kunnen fatale gevolgen hebben. Een diagnostisch proces wordt door de WHO pas als overtuigend beschouwd wanneer een minimum van 100 metingen (microscopisch onderzoek van 100 high powered-fields) is uitgevoerd op een geprepareerde dikke bloedfilm. Voor een dunne bloedfilm, die meer details geeft over de morfologie van de parasiet, is een gemiddelde van 800 metingen vereist. Dit is een gemakkelijke taak voor laboranten in niet endemische landen waar jaarlijks gemiddeld 120 gevallen van malaria voorkomen. Maar voor malaria endemische landen, waar dagelijks duizenden gevallen worden gemeld, is dit geenszins een haalbare taak, aange-

zien zulke metingen volledige concentratie, tijd, een hoog expertiseniveau en ervaring vereisen.

Om de huidige wereldwijde inspanningen op het gebied van malaria reductie te realiseren, kan de behoefte aan een betrouwbaar, efficiënt, nauwkeurig en geautomatiseerd point-of-care diagnostisch hulpmiddel niet genoeg worden benadrukt. Vandaar dat de focus van dit proefschrift ligt op het ontwikkelen van slimme optische methoden die de last van handmatige microscopie verlichten door onderzoek te doen naar methoden om bestaande beeldvormingsmodaliteiten te optimaliseren, die kunnen worden geïntegreerd met slimme algoritmen voor snelle detectie van malariaparasieten bij geïnfecteerde patiënten.

Naast Malaria is Schistosomiasis de tweede meest voorkomende parasitaire ziekte. Alhoewel het in de categorie valt van de Neglected Tropical Diseases (NTD), ofwel verwaarloosde tropische ziekten, hadden er 220,8 miljoen mensen in 2017 een preventieve behandeling nodig, zo rapporteert de World Health Organisation. Het is een ziekte die is gerelateerd aan armoede, prevalent is in tropische en subtropische gebieden en met name voorkomt in gemeenschappen zonder toegang tot schoon drinkwater en goede sanitaire voorzieningen. 779 miljoen mensen lopen het risico besmet te raken met deze ziekte, wat leidt tot verstoorde groei en ontwikkeling, afnemende fysieke fitheid, blaaskanker en verminderde neurocognitieve vaardigheden. Hoewel veilige en effectieve medicatie op grote schaal beschikbaar is, zijn nauwkeurige diagnostische technieken voor Schistosomiasis zwaar onderontwikkeld en diagnostiek blijft een kritische uitdaging.

Intestinale en urogenitale Schistosomiasis zijn de twee varianten van deze verwaarloosde tropische ziekte, echter richten we ons in dit onderzoek enkel op de Urogenitale Schistosomiasis (veroorzaakt door de parasiet *Schistosoma haematobium*) aangezien deze variant aanwezig is in de populatie waarmee we werkten.

Het diagnostisch protocol voor *Schistosoma haematobium* schrijft urinefiltratie voor met de door de WHO aanbevolen standaard membraanfilters (met een poriëgrootte van $12\mu\text{l}$). Een expert moet verscheidene kritische metingen uitvoeren om de beoogde vreemde lichamen (de eieren van de parasiet) in urinemonsters te detecteren. En voor een optimale diagnose moeten er verschillende monsters worden onderzocht, die met tussenpozen bij eenzelfde patiënt zijn verzameld. Hierdoor neemt het aantal monster analyses per patiënt toe, alsmede de sensitiviteit van de test. Omdat in dit proces microscopisch onderzoek van gefilterde urinemonsters noodzakelijk is, wordt het evenals gelimiteerd door de eerder beschreven uitdagingen van de standaard malaria microscopie. Hoewel verschillende snelle, op antigeen- en antilichaam gebaseerde diagnostische testkits zijn ontwikkeld voor zowel malaria als schistosomiasis, is de betrouwbaarheid van deze diagnostische test nog altijd zorgelijk. Dit proefschrift richt zich op de ontwikkeling van betrouwbare, robuuste, nauwkeurige, kosteneffectieve en gebruiksvriendelijke point-of-care optische apparaten voor een snelle diagnose van malaria en urogenitale ziekten in menselijke monsters.

Dit proefschrift adresseert als eerste lichtmicroscopie met een grotere scherptediepte.

Wavefront-codering met adaptieve optica en digitale inline holografie zijn in dit werk overwogen. Een optimale configuratie, die maximale resolutie garandeert op basis van de coherentie-eigenschap van de lichtbron en de specificatie van de beeldsensor is voorgeschreven. In dit systeem, genereert de interferentie van een vlak en een object golf op het detector vlak een hologram waaruit de complexe amplitude van het veld in het object vlak numeriek kan worden gereconstrueerd door een inverse source probleem op te lossen. Deze methode is van belang omdat, in tegenstelling tot de conventionele microscoop, details in transparante biologische monsters kunnen worden opgehaald, doordat zowel de amplitude als de fase van het veld wordt gereconstrueerd. Het biedt een mogelijke oplossing voor labelvrije diagnose van parasitaire ziektes. In combinatie met flowcytometrie en datagestuurde algoritmen hebben we deze methodologie toegepast op de ontwikkeling van snelle schistosomiasis haematobium detectie. Een werkend prototype, met het potentieel om de ziekten in kaart te brengen, is ontwikkeld en getest in Sub-Sahara Afrika. Het ontworpen systeem houdt rekening met praktische voorwaarden zoals gebruiksgemak, kosten, extreme omgevingscondities, onberekenbare stroomuitval, robuustheid van het systeem tegen stof en artefacten. De feedback en resultaten van het veldonderzoek zijn veelbelovend.

Gebruikmakend van recente ontwikkelingen op het gebied van mobiele telefoons en 3D-print technologieën hebben we een geautomatiseerde microscoop ontwikkeld op basis van een mobiele telefoon, om snelle point-of-care diagnose van malaria te realiseren. De uitdaging hier ligt in de optimalisatie van de optical train van goedkope, algemeen verkrijgbare mobiele telefoons om de malariaparasiet met voldoende resolutie te detecteren. Het bleek dat de huidige, op mobiele telefoon gebaseerde microscoop, niet in staat was de 1-micron grote malariaparasieten te zien, vanwege de optische aberratie van het systeem en de numerieke openingslimiet van de telefoon. Hoewel deze methode aantoont dat een op mobiele telefoon gebaseerde microscoop de malariaparasiet kan afbeelden, is het bereikbare gezichtsveld echter beperkt tot 150 bij 150 mm. Dit betekent dat meer dan 600 metingen nodig zijn voor een doorslaggevende diagnose. We omzeilen deze beperking door de vernieuwende implementatie van computerondersteunde droge fluorescentiemicroscopie. Met behulp van computationele analyse van afbeeldingen met een groot aantal bloedcellen, stellen we robuuste statistieken op voor betrouwbare diagnostische aanbevelingen. De techniek is getest met in-vitro- en in-vivo-monsters en aangetoond geschikt te zijn voor zeer gevoelige, robuuste en geautomatiseerde malariadiagnostiek. Het vereist minimale menselijke tussenkomst, maakt gebruik van eenvoudige monstervoorbereiding, is in hoge mate onafhankelijk van deskundig oordeel en heeft een potentieel voor massale gemeenschap screening voor malaria controle- en eliminatieprogramma's.

De ontwerpspecificaties voor de ontwikkeling van de werkende prototypes zoals gepresenteerd in dit proefschrift, komen onder meer voort uit de feedback van diagnostische experts van de volgende niet-gouvernementele organisaties: Artsen zonder Grenzen, Malaria Consortium, AMREF, Save the Children en Christian Aid (Nigeria). Ook is de methodologie uitgebreid gevalideerd door middel van discussies en interacties met lokale experts (in Nigeria, Ivoorkust, Oeganda en Ghana) en met parasitologen, onder-

zoekers en vaccin ontwikkelaars in Nederland, Spanje, Ierland en Duitsland, resulterend in waardevolle nieuwe inzichten. Het is ons doel dat de in dit proefschrift gepresenteerde diagnostische methoden en prototypes zullen worden gebruikt ter aanvulling van de beperkingen van de bestaande diagnostische technieken.

1

Introduction

There is a spirit in man the inspiration of the Almighty giveth him understanding.

Job 32:8

Chapter Abstract

This chapter provides a quick overview of two main parasitic disease - Malaria & Urogenital Schistosomiasis considered in this research work. Malaria is a life threatening parasitic disease with high mortality rate and significant economic loss. The parasite is smart, constantly adapting to different environmental conditions thereby developing resistance to drugs. Limited access to quick and reliable diagnoses further amplifies its devastating impact on the populations at risk. We discuss the World Health Organisation reference diagnostic standard with specific focus on the advantages and limitations of the methods using Malaria as a case study. The objective, motivation and goals of this thesis concludes this chapter.

1.1. The devastating impact of Malaria & Schistosomiasis

Malaria: Malaria is one of the leading causes of high morbidity and mortality worldwide. According to World Health Organisation (WHO) malaria report for 2017, it accounted for the death of 435,000 people. Pregnant women and children are mostly affected. It causes miscarriage among pregnant women and kills one child every 2 minutes. Based on the WHO records, an approximate of 3.2 billion people are currently at risk of the disease [1]. Malaria is currently active in over 95 countries and more than 200 million cases are recorded yearly. Poor and disadvantaged people are disproportionately affected in malaria endemic countries particularly because they have limited access to functional health facilities and can barely pay for the required treatment.

Although malaria is endemic in all six WHO regions, its impact is severely felt in the WHO-African region [2]. The African region accounts for 90% of malaria death and two countries which reports 40% of these deaths are Nigeria and the Democratic Republic of the Congo.

“The WHO African Region carries a disproportionately high share of the global malaria burden. In 2017, the region was home to 92% of malaria cases and 93% of malaria deaths-WHO malaria report.”

The first of the five strategic pillars defined by WHO Global technical strategy for malaria elimination is focused on ensuring that malaria prevention, **diagnosis** and treatment is easily accessible to all. It is therefore an established fact that high morbidity and mortality can be significantly reduced by providing accurate and reliable diagnostic methods that affords quick testing and efficient treatment [1].

Schistosomiasis: Aside malaria, schistosomiasis ranks as the second most common parasitic disease. It is a neglected tropical disease and WHO report shows that preventive treatment was done for about 220.8 million people in the year 2017. It is a disease of the poor which is prevalent in tropical and subtropical areas, particularly in rural communities that lack access to clean drinking water and proper sanitation. Intestinal and urogenital Schistosomiasis are the two types of schistosomiasis but specific attention is devoted to urogenital schistosomiasis in this research because it is most prevalent in the population we worked with.

This section specifically focuses on the practical and optical techniques used for malaria diagnosis. Malaria is of choice particularly because of the size of the parasite (typically between 1-10 μ m) and the different developmental stages of the parasite. We briefly describe clinical diagnostic approach and further examine the WHO reference standard of malaria diagnosis. The parasitic lifecycle, transmission and state-of-the-art diagnostic methods for both malaria and schistosomiasis will be discussed in chapter 2.

1.2. Clinical diagnosis of malaria

Generally, clinical patients who complain of high fever, headache, profuse sweating-severe chills and general body pains are presumptively treated for malaria in endemic

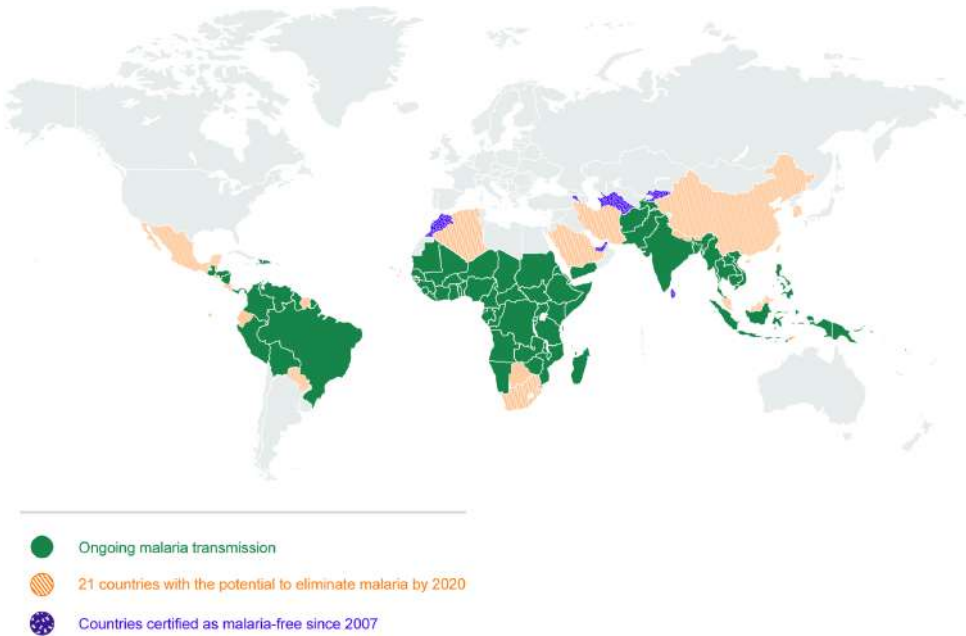


Figure 1.1: Map showing countries where transmission is currently ongoing. Some countries which have demonstrated strong capability to eliminate malaria by the year 2020 are also highlighted. (Image source: [2]).

communities. Unfortunately, cases of fever in such areas of high transmission are usually due to many diseases other than malaria [3, 4]. Clinical symptoms are generally nonspecific and usually overlap significantly with the symptoms of other febrile illnesses which often results in a high number of false positives results.

False positives leads to abuse of antimalarial drugs, exposure of malaria parasites to sub-therapeutic blood levels of the drugs and development of resistance to the drugs. Based on the current global efforts and plan to eliminate presumptive drug treatment of malaria, the WHO now recommends a standard diagnostic procedure which prescribes parasite-based confirmatory test prior to treatment [5]. The effectiveness of malaria case management can be greatly improved upon by implementing an efficient early and accurate diagnostic process. While well equipped standard laboratories for malaria diagnosis are commonly available in developed urban and peri-urban cities, low-resource settings of malaria endemicity usually have very limited options.

1.3. WHO reference standard for malaria diagnosis

According to WHO malaria diagnostic protocol, light microscopy remains the recommended reference diagnostic standard for the detection of malaria parasites. Microscopy examinations of Giemsa-stained blood smears is mostly and widely practised. Particular advantages that light microscopy offers include: specie differentiation, par-

asite quantification, accuracy, ability to distinguish asexual parasite stages from gametocytes (which enables effective treatment) and its low direct cost [6].

According to Payne et-al, "the size of the human malaria parasite ranges from $1\mu\text{m}$ (early trophozoite) in *Plasmodium falciparum* to $15\mu\text{m}$ or more in *P. vivax* or *P. ovale*; the larger gametocytes of *P. falciparum* only rarely exceed $10\mu\text{m}$ in the longer axis" [7]. To visualize the parasite stages in the appropriate detail for differential diagnosis, a microscope with magnification which ranges between 500 and 1000 \times is required. A typical laboratory microscopes combines a Huygenian eyepieces and a microscope objectives with high numerical aperture and magnification in the range of 50 to 100 \times . The microscopes are manually operated by highly skilled technical experts with precise visual and differential skills. For accurate and reliable morphological diagnosis, proper blood collection, good smear preparation and effective Giemsa staining must be ensured.

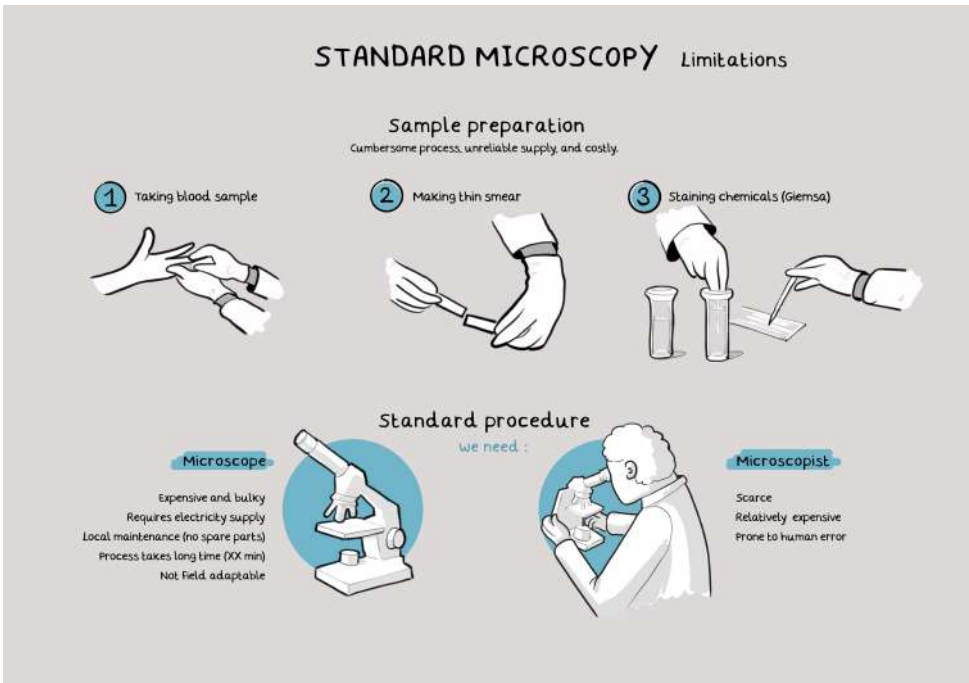


Figure 1.2: Depicts a complete overview of the WHO recommended malaria microscopy diagnostic protocol. The process starts with blood sample collection after which a thin or thick blood smear is prepared. The smears are subsequently stained with Giemsa to enable sufficient contrast for the visualization of the parasites by the microscopist.

1.3.1. Microscopic examination of malaria parasite

Malaria parasite detected in the blood specimen of a sick patient is the acceptable definitive confirmatory test. The blood is typically collected from the fingers or vein

of the patient and prepared either as a thick or thin blood film based on the need and urgency of the case. Thick blood films are typically prepared by dropping a volume of blood (approximately 6–10 μ l) which is carefully spread on clean microscope slide [8].

A thick blood film is air-dried and stained with a Giemsa stain [9]. The staining process takes an approximate of 10–30 minutes. The Giemsa stain causes the erythrocytes to lyse due to osmotic swelling. The residue left behind on the slide mostly consist white blood cells and the parasites present [6]. The advantage of the lysing of the erythrocytes is that it allows easy examination of more volume of blood. Under this condition, the limit of detection (LOD) of the parasite ranges between 4–20 parasites/ μ l [7]. This limit is observed to be higher (50–100 parasites/ μ l) under field conditions as reported by [10]. The thin blood film however is a monolayer of blood cells prepared from approximately 1 μ l of blood and estimated to be about 20–30 times less dense than the thick blood film. While the thick film provides high sensitivity the thin film provides better insight into parasite morphology and species identification.

The Giemsa stain enables a high contrast that allows the transparent malaria parasite nested in a red blood cell (erythrocytes) to become visible amidst other blood constituents such as white blood cells and blood platelets. In an examined thick blood film, the microscopist can only visualize the remains of a dehaemoglobinized red blood cells (layered in a thick mass), white blood cells and blood platelets.

1.3.2. Recognition of a malaria parasite

The skilled microscopist is trained to carefully look through thick and thin films using fine adjustment to focus as he moves through different fields. Consistent focusing and refocusing is required particularly to look through thick blood films to avoid the risk of missing a parasite. A parasite is confirmed by detecting the fine rings of the cytoplasm of some trophozoites or other stages of the infection. A minimum of 100 fields of a thick blood film must be examined before a diagnosis can be regarded as negative. For a thin blood film, at least 800 fields should be examined before declaring the slide as negative. A trained microscopist recognizes the malaria parasite and its different stage in a thin blood film. Considering the size of the parasite which is typically in the range of 1 μ m, this is an herculean task which demands lots of efforts, concentration, skills and focus. The early ring stage often called the trophozoite is the commonly seen stage of the malaria parasite. An early ring stage in an infected RBC and other stages which includes the Schizont and the gametocytes are shown in Fig.1.3. The images of the parasite stages are listed as visualized in a standard Giemsa stained form.

1.3.3. Estimation of parasitemia

The parasite density determines the severity of the infection and it provides useful insight into needed treatment and patient response to treatment. Parasite count may also be necessary in cross-sectional and epidemiological investigation and special studies. The microscopist can estimate the percentage of infected red blood cells using thin blood film only based on an estimate of the amount of parasites per white

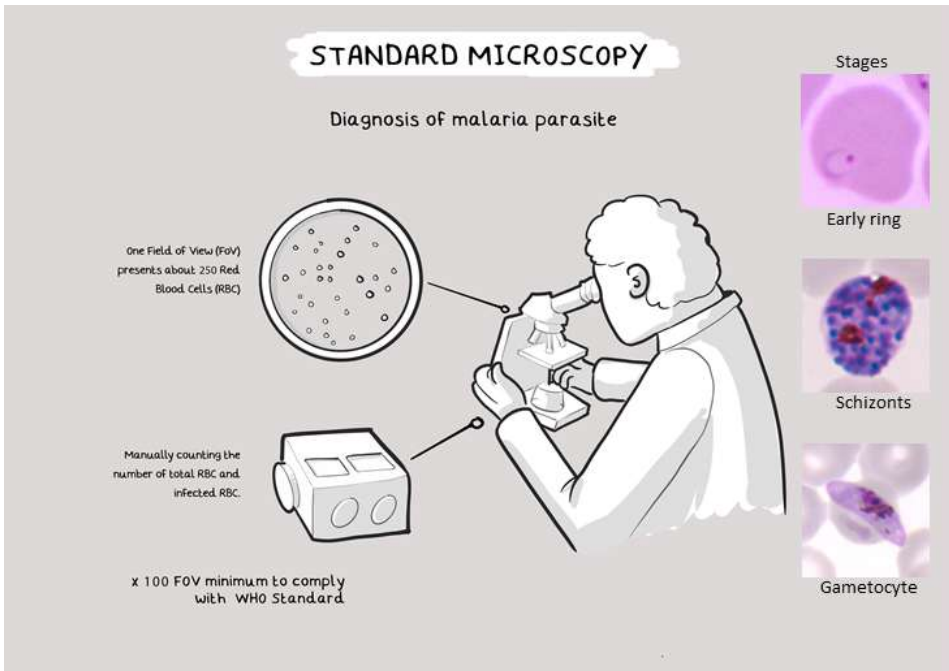


Figure 1.3: Represents the standard malaria microscopy. The sample is manually observed by an expert who examines hundreds of fields by intermittently focusing and refocusing the optical system. Amount of visualize parasites is manually counted using a manual counter shown in the image. Aligned to the right of the image are the different stages of the malaria parasite as visualized by the microscopist in a thin smear. These stages consist of the trophozoites (early ring), the Schizonts (sexual stage) and the Gametocytes (asexual stage) respectively.

blood cell or per microscope field. To finally derive the parasites per given volume of blood, certain standard approximations of the the amount of red & white blood cells in a microlitre of blood are required. In this case, we use 5×10^6 erythrocytes or 8000 white blood cells per microlitre of blood. In the case where microscope field is used, 400 microscope fields is a standard number for calculation. Using the defined values, the estimated parasitemia is based on the number of white blood cells counted and typically expressed as 'parasites per microliter of blood' with the following simple mathematical formula:

$$\text{Parasite}/\mu\text{l} = \frac{\text{Number of parasites} \times 8000}{\text{Number of WBC}} \quad (1.1)$$

Parasite quantification based on thin film however takes into consideration, the estimated number of infected red blood cells and expresses it as a percentage of the parasitemia based on the equation:

$$\text{Parasites} = \frac{\text{Infected RBC}}{\text{Total RBCs}} \times 100 \quad (1.2)$$

1.3.4. Advantages of light microscopy

The following features makes malaria microscopy an invaluable tool in the global malaria control and elimination effort.

- Cost effectiveness – has low direct cost
- High sensitivity for clinical malaria
- Easy differentiation of malaria species and parasite stages
- Easy quantification of parasite infection load in a blood sample
- High accuracy of diagnostic outcomes which determines the effectiveness of the recommended treatment.

1.3.5. Limitations of light microscopy

Despite the above listed advantages, the reliability of diagnostic results by light microscopy at the primary health care level is limited by many practical challenges. The most relevant limitations which motivates this research work are summarized below:

- **Required technical skills:** Primary health care facilities in resource limited settings suffer from the absence of effective, qualified and properly trained technical experts that will provide required expertise for sample analysis. This is mostly due to the lack of resources and sufficient quality assurance government programs that coordinates the recruitment, training and continuous assesment of the competence of microscopist. The accuracy and reliability of the result obtained through this diagnostic approach is highly dependent on the expertise of the microscopist [11, 12]. Therefore the accuracy and reliability of diagnosis is severely impacted particularly in rural areas .
- **Lack of maintainance capability:** The microscopes used in diagnostic centres in malaria endemic countries are designed, produced mostly in non-malaria infected countries and this reduces the available maintenance capabilities in endemic countries. Aside the low technical maintenance capacity available, lack of availability of required spare parts which also leads to significant amount of machine downtime is a common problem.
- **Power outages:** It is quite unfortunate that most of the rural areas of endemic countries lack consistent supply of electricity, which is critical for the operation of the microscope. This causes sudden interruptions during the diagnostic process resulting to long time delays in result interpretation, prescriptions and treatments.

- **Intense workload:** Since the sample analysis is manually done, a lot of human effort is required for the diagnostic process. Contrary to the amount of samples examined in non-malaria endemic countries where very limited amount of malaria cases occur in a year, endemic countries have enormous amount of samples to screen and diagnose on a daily basis. This heavy and very demanding workload requires intense focus, concentration and may result into fatigue, tiredness, which certainly causes delay in the provision of results to clinical staff. Above all, the intense manual demand can also result into error-prone diagnosis as infections are often missed particularly in cases of low to medium parasite density.
- **Manual counting and parasite estimation:** Manually counting the visualized parasites despite all the other mental demand on the microscopist is a huge set back to the accurate estimation of the parasite density. This is a problem that may translate to ineffective treatment and may have fatal consequences.
- **Lack of micro-precision mapping capabilities:** Data generated from manual microscopy are manually recorded and stored on paper in most of the rural areas of high disease prevalence. To successfully realize the WHO set goal of disease control and elimination, automation and digitalisation of mapping data is cogent. For instance, Merck is a pharmaceutical company that aims at providing an approximate of 250 million free tablets a year for the treatment of Schistosomiasis under the mass treatment program. Precision and target mapping will be useful in cutting down on wastage of both human and material resources. It will eliminate the treatment of too many uninfected people and probably reduce unnecessary cost. Furthermore, automating the data mapping process will contribute greatly to the elimination programs.

1.4. The Motivation, Objective & Research goals

1.4.1. Motivation

The previous sections discussed the WHO approved reference diagnostic test (light microscopy based test) for malaria and urogenital schistosomiasis. Despite the gains of this diagnostic approach several limiting factors which drastically reduces diagnostic performance were discussed in the preceding section. To realize current global effort or agenda to eliminate these parasitic diseases, the need for a reliable, efficient, accurate and automated diagnostic tool cannot be overemphasised. With this in mind, we decided to focus this research on the development of smart optical diagnosis of malaria and urogenital schistosomiasis.

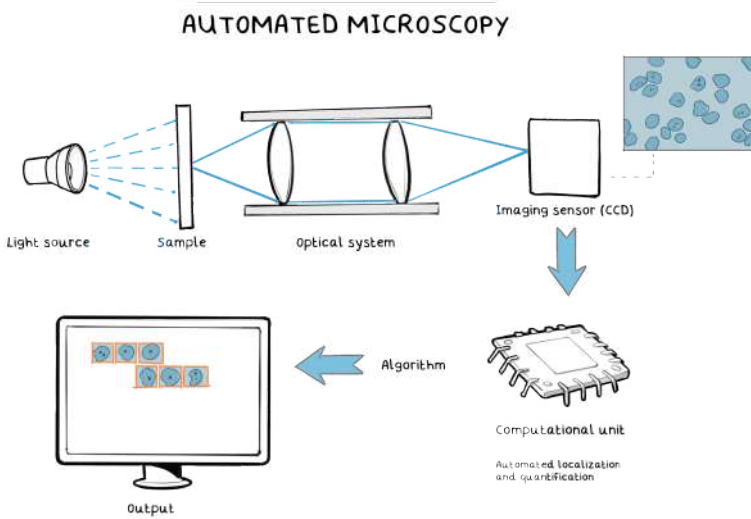


Figure 1.4: Illustration of a smart imaging system which combines optimised technical optics with integrated data driven algorithm. The system should consist of an appropriate illumination system, a robust imaging system and a computational unit that performs automated detection of the parasites.

1.4.2. Main objective

The main objective of this thesis is defined as follows:

“To research and develop robust, low-cost, easy-to-use, automated point-of-care diagnostic devices deployable in low-resource rural communities for quick, efficient, reliable and accurate optical screening of Malaria and Urogenital Schistosomiasis.”

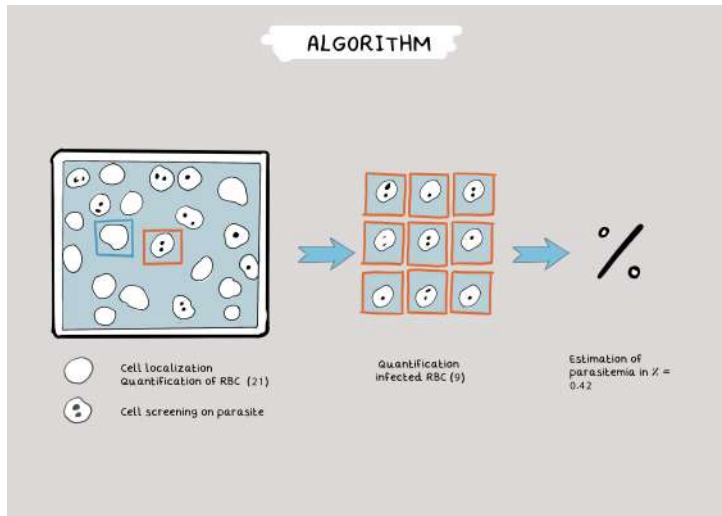


Figure 1.5: Developed algorithm should essentially perform the following critical task with minimal computational complexity: (i) cell localization, (ii) cell quantification & (iii) estimation of parasite density.

Research goals

Given the motivation described in the above, the goals of this thesis were to:

- Develop a single or multi-modal optical method based on the combination of standard imaging techniques and data-driven algorithms, to facilitate automated robust detection of malaria and urogenital schistosomiasis parasites in infected sample.
- Develop data-driven algorithms for automated parasite detection and quantification. Performance characteristics of the algorithm should include minimal computational complexity and should be implementable on low profile consumer grade electronics such as cellphones, raspberry pi etc.
- Optimise the optical train of commonly available consumer grade electronics such as cellphones, raspberry pi camera, for the imaging of parasitic diseases such as malaria and schistosomiasis.
- Develop proof-of-concept of diagnostic instrument which can be tested with field experts in endemic countries such as Nigeria.
- Explore the possibility of the development and integration of microprecision data mapping in developed point-of-care diagnostic devices.
- Gather standard system design requirement based on practical needs on the field and explore possibilities on how to further develop diagnostic methods beyond the lab towards practical application on the field.

Research Hypothesis

Although our technical research goals have been clearly enumerated, it is important to state the hypothesis that will be tested in this work particularly because of its' multi-disciplinary nature:

RH1: A combination of lensless imaging techniques with extended depth of field and artificial intelligence could achieve affordable, label free and easy-to-use smart detection of *Schistosoma haematobium* ova eggs in infected urine sample. Ch.3

RH2: The optical configuration for an alias-free, diffraction-limited resolution of an inline holographic microscope is dependent on the given coherence of the illumination and the pixel size of the imager. Ch.3

RH3: World Health Organisation recommended manual microscopy for the diagnosis of *Schistosoma haematobium* can be miniaturized and automated into an easy-to-use point of care diagnostic device using lowcost cellphone, simple binary classifier and locally sourced mesh filters for quick urine sample preparation. Ch.4

RH4: The cellphone optical train can be modified and optimised to realize a spatial resolution sufficient to resolve the *plasmodium falciparum* malaria parasite. Ch.5

RH5: A multimodal optical imaging platform integrated with data driven algorithm could provide automated widefield detection of *plasmodium falciparum* malaria parasite. Ch.6

RH6: User-context interaction is important for engineering design iterations that will realize appropriate and acceptable system design for point-of-care diagnostic device for field use. Ch.7

Impact on Global development

Prompt and accurate diagnosis as a result of diagnostic techniques developed in this thesis is important for the effective treatment of malaria and *Schistosoma haematobium* disease. This we envisage will lead to reduction in deaths, increase in economic growth and improvement of the overall quality of life of affected people in sub-Saharan Africa and other target countries. With simple diagnosis, an instant prescription of appropriate medicine for the patient may become possible. Cost of training personnel will be reduced as the device will require minimal technical training for smooth and reliable operation. It is the ultimate goal of this research to set up a start-up company in Nigeria and other African countries for serial production of working diagnostic devices, which will also create extra employment opportunities for the locals.

1.5. Dissertation layout

This thesis is organised and documented to cover this research in the following order:

Quick overview of malaria & schistosomiasis: Chapter 2 specifically focuses on presenting a quick background information on Malaria and Schistosomiasis with respect to their history, transmission and parasitic cycle. A quick review of existing state-of-the-art diagnostic method is also presented in this chapter. Pros and cons of each of the diagnostic method is briefly highlighted to provide sufficient insight into the diagnostic gaps in the current global control and elimination effort.

Light microscopy with extended depth: Chapter 3 specifically focuses on the optimal system design configuration that guarantees maximum resolution and performance of lensless imaging system. The chapter explores the design of digital inline holographic microscope and its application to the detection of *S. haemtobium* eggs in urine samples. To validate the theoretical methodology described, a novel label-free diagnostic method of *S. haemtobium* was developed for field use.

This chapter is written based on the published work of the author:

Aliasing, coherence, and resolution in a lensless holographic microscope, **TE. Agbana**, H.Gong, AS. Amoah, V. Bezzubik, M. Verhaegen, G.Vdovin, Optics Letters. 42, 2271-2274 (2017)

Smart optical diagnosis of urogenital schistosomiasis - Chapter 4 covers the automated detection of urogenital schistosomiasis eggs in filtered urine sample. Simple and widely available low-cost urine filtration method was explored. Integrated with egg detection algorithms, we present the first offline detection of *S. haemtobium* in urine sample using cellphone-based microscope to the best of our knowledge. With minimal computational complexity, proposed method can be implemented in low-cost consumer grade electronics.

The content of this chapter is based on the submitted manuscript which is currently being peer reviewed:

Discrete wavelet transform detection of Schistosoma haematobium using a cellphone microscope, **TE. Agbana**, S. Jujjavarapu, JC. Diehl, AS. Amoah, M. Yazdanbakhsh, W. Oyibo, O. Oladimeji, M. Verhaegen, G.Vdovin. Submitted(2019)

Optimizing the resolution limit of cell-phone based microscope - In chapter 5 , we present the limits of the achievable maximum resolution of the cell phone based microscope based on the inherent aberration of the imaging system. Parasite detection capability of optimised system is tested with cultured malaria samples in the laboratory. In this chapter, we report developed methodology for the first cellphone-based imaging of malaria parasites using cultured samples.

The results presented in this chapter is based on the published work of the author in the following article:

Imaging & identification of malaria parasites using cellphone microscope with a ball lens, **TE. Agbana**, JC. Diehl, F. van Pul, SM.Khan , V. Patlan, M. Verhaegen,

G.Vdovin, PloS one. 13 (10),(2018).

Smart optical detection of malaria parasites - Detection of malaria parasites using fluorescent based method is common. However, wide adoptability of this diagnostic technique has been restrained due to specific challenges. In this chapter we present a multimodal imaging method which combines fluorescent imaging with data-driven algorithm to realize easy, low-cost and smart detection of malaria parasites in infected blood sample. Promising results obtained from laboratory tests performed in WHO approved ANDI malaria research center, Lagos, Nigeria, are also presented in this chapter. This chapter is based on written manuscript ready for submission to a peer review journal :

From lab to the field - It is part of the goal of this project to explore possible development of developed proof-of-concept into viable functional prototypes. In this chapter we provide a quick overview of developed working prototype based on close collaboration with the Faculty of Industrial Design Engineering, TUDelft, the Netherlands. Developed prototypes are validated within the local context. Using the Schistoscope as a case study, we present insightful results based on expert inputs from the field. Furthermore, we report the adaptive design approach followed to facilitate the rapid development and deployment of point-of-care diagnostic devices for use in low-resource settings.

This chapter is based on the published work of the author as indicated as follows:

Schistoscope: Towards a locally producible smart diagnostic device for Schistosomiasis in Nigeria, **TE. Agbana**, GY Van, O. Oladimeji, G.Vdovine, W. Oyibo, JC. Diehl, Proc. IEEE GHTC, IEEE Global Humanitarian Technology (2019).

References

- [1] W. H. Organization, *Global technical strategy for malaria 2016-2030* (World Health Organization, 2015).
- [2] R. N. Rabinovich, C. Drakeley, A. A. Djimde, B. F. Hall, S. I. Hay, J. Hemingway, D. C. Kaslow, A. Noor, F. Okumu, R. Steketee, *et al.*, *malera: An updated research agenda for malaria elimination and eradication*, *PLoS medicine* **14**, e1002456 (2017).
- [3] S. C. Murphy, J. P. Shott, S. Parikh, P. Etter, W. R. Prescott, and V. A. Stewart, *Malaria diagnostics in clinical trials*, *The American journal of tropical medicine and hygiene* **89**, 824 (2013).
- [4] V. D'Acromont, C. Lengeler, H. Mshinda, D. Mtasiwa, M. Tanner, and B. Genton, *Time to move from presumptive malaria treatment to laboratory-confirmed diagnosis and treatment in african children with fever*, *PLoS medicine* **6**, e252 (2009).
- [5] W. H. Organization, *Guidelines for the treatment of malaria* (World Health Organization, 2015).
- [6] P. B. Bloland, W. H. Organization, *et al.*, *Drug resistance in malaria*, Tech. Rep. (Geneva: World Health Organization, 2001).
- [7] D. Payne, *Use and limitations of light microscopy for diagnosing malaria at the primary health care level*, *Bulletin of the World Health Organization* **66**, 621 (1988).
- [8] L. Siahaan, *Laboratory diagnostics of malaria*, in *IOP Conference Series: Earth and Environmental Science*, Vol. 125 (IOP Publishing, 2018) p. 012090.
- [9] W. H. Organization, *Malaria microscopy quality assurance manual-version 2* (World Health Organization, 2016).
- [10] C. Wongsrichanalai, M. J. Barcus, S. Muth, A. Sutamihardja, and W. H. Wernsdorfer, *A review of malaria diagnostic tools: microscopy and rapid diagnostic test (rdt)*, *The American journal of tropical medicine and hygiene* **77**, 119 (2007).
- [11] F. Odhiambo, A. M. Buff, C. Moranga, C. M. Moseti, J. O. Wesongah, S. A. Lowther, W. Arvelo, T. Galgalo, T. O. Achia, Z. G. Roka, *et al.*, *Factors associated with malaria microscopy diagnostic performance following a pilot quality-assurance programme in health facilities in malaria low-transmission areas of kenya, 2014*, *Malaria journal* **16**, 371 (2017).
- [12] P. Alonso and A. M. Noor, *The global fight against malaria is at crossroads*, *The Lancet* **390**, 2532 (2017).

2

Overview of Malaria & Schistosomiasis

*You light a lamp for me. The LORD, my God,
lights up my darkness.*

Psalm 18:28

Development of robust, affordable, field-compatible and functional optical diagnostic instrument to combat the impact of two devastating parasitic diseases in low-income countries is the primary objective of this research. This chapter provides a quick overview and general background information on the history, transmission and parasitic life-cycle of the parasites under consideration. This chapter also serves as a quick review of the existing state-of-the-art diagnostic techniques. The gains, limitations and diagnostic gaps of these methods are briefly described.

2.1. Malaria background information

"Malaria" means bad air in the Italian language and for over 2500 years, it was generally accepted that malaria fevers were due to bad air. Scientific studies on malaria however became possible after the discovery of the parasites by Charles Louis Alphonse Laveran in 1880 [1, 2]. Malaria is a vector-borne parasitic tropical disease transmitted by the bite of the female Anopheles mosquito in over 91 nations [3]. Six common plasmodium species that infect human beings include: *Plasmodium falciparum*, *Plasmodium malariae*, *Plasmodium ovale curtisi* and *Plasmodium ovale wallikeri*, *Plasmodium vivax* and *Plasmodium knowlesi* [3–7]. Most of the malaria deaths recorded in sub-Saharan Africa is attributed to *Plasmodium falciparum*. *Plasmodium falciparum* is the most deadly species and it produces high levels of blood-stage parasites in its human host. *Plasmodium knowlesi* also causes malaria but its impact is most prevalent in Southeast Asia.

Despite the fact that malaria is preventable and treatable, an estimated 225 million cases is recorded every year with approximately half a million deaths. The fact that the symptoms of malaria (fever, headache, fatigue, etc) are similar to those of other common illness necessitate the need for effective and reliable diagnostic tests to guide proper treatment.

A common assumption in rural areas, where malaria diagnostic tests are often lacking, is that most fevers are malaria and as a result, the health workers provide presumptive treatment based on clinical symptoms. Presumptive treatment often results in massive misuse or overuse of antimalarial medicines for non-malaria diseases. An Effective malaria case management should involve disease diagnosis and appropriate treatment. Early stage detection of the parasite allows for rapid patient recovery if immediate treatment is effected. Delayed or ineffective treatment however may progress to severe malaria which could become fatal if left unattended to.

2.1.1. Transmission

The transmission life cycle between infected female Anopheles mosquito and humans is shown in Fig.2.1. Humans are infected by the deposition of sporozoites due to bites of an infected mosquito. Injected sporozoites develops in the liver within a typical time frame of 1-2 weeks. At this stage, a tangible amount of parasites are replicated and this causes the malaria disease in humans. As the parasite develops in the red blood cells, male and female gametocytes are produced [8–10]. The gametocytes is picked up by mosquito through a blood meal. The male and female gametes fuse in the mosquito to form a zygote and the zygote develops into a mobile ookinete. Released sporozoites migrate to the mosquito's salivary glands where the lifecycle is completed.

Symptoms of malaria develops as soon as the erythrocytic cycle produces a parasitaemia above a determined threshold of approximately 100 parasites per μl . Common symptoms of uncomplicated malaria includes fever, body-aches, headache, cough, diarrhoea, chills etc. At a very severe stage, cerebral malaria with neurological signs and symptoms such as seizure, coma, etc can be experienced. Typical incubation periods

for *Plasmodium falciparum* ranges between 10-14 days.

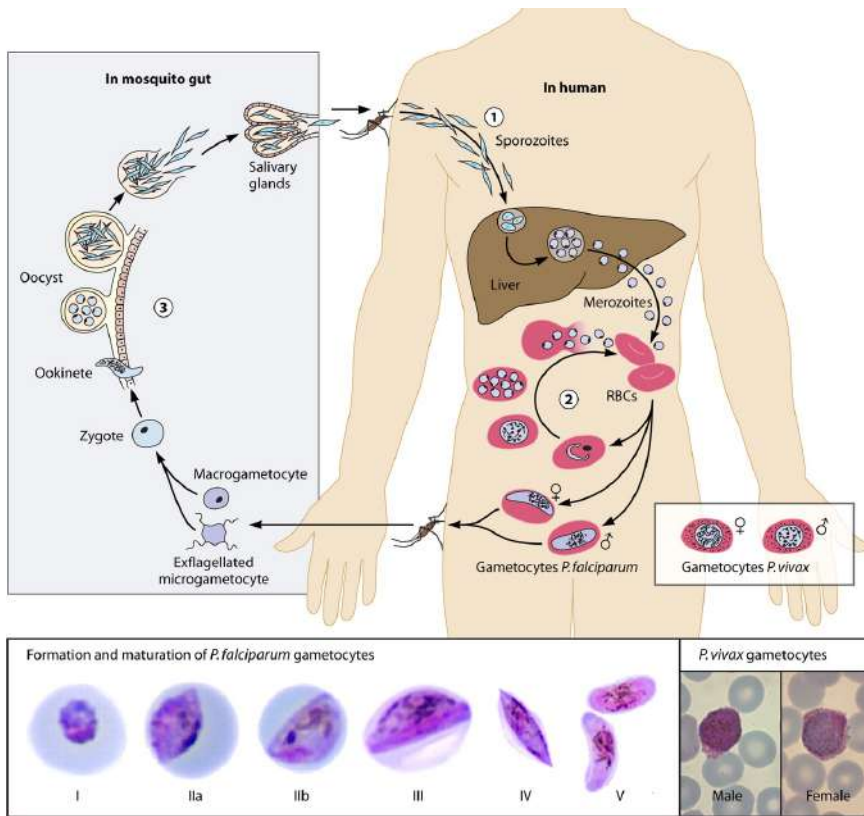


Figure 2.1: Life cycle of malaria parasite developmental stages in humans showing the development of the parasite from early trophozoites to gametocyte. (Malaria Reference Laboratory, London School of Hygiene and Tropical Medicine, United Kingdom.)

Generally, malaria diagnostic tests are aimed at establishing the presence of malaria in sick patients who show clinical symptoms consistent with malaria. Aside the qualitative result which may be positive or negative, information on the parasite density and the species present in the given sample can also be provided. The parasite density provides insight to severity of infection and how urgent the treatment should be. The response of the patient to treatment can also be monitored by the diagnostic test. A decrease in parasite density will correlate to a positive patient response to treatment and vice versa.

2.1.2. Existing state-of-the-art diagnostic methods

Malaria diagnostic landscape has experienced significant advancement and development in recent times. Developed diagnostic methods are aimed at detecting in a very timely manner, the malaria disease in sick patients. The performance metrics typically



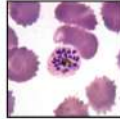
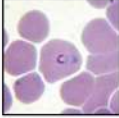
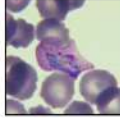
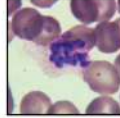
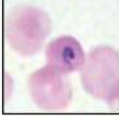



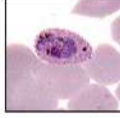
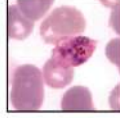
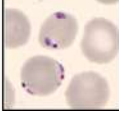


Human malaria				
	Rings	Trophozoites	Schizonts	
<i>P. falciparum</i>				<ul style="list-style-type: none"> Parasitised red cells (pRBCs) not enlarged RBCs containing mature trophozoites sequestered in deep vessels Total parasite biomass = circulating parasites + sequestered parasites
<i>P. vivax</i>				<ul style="list-style-type: none"> Parasites prefer young red cells pRBCs enlarged Trophozoites are amoeboid in shape All stages present in peripheral blood
<i>P. malariae</i>				<ul style="list-style-type: none"> Parasites prefer old red cells pRBCs not enlarged Trophozoites tend to have a band shape All stages present in peripheral blood
<i>P. ovale</i>				<ul style="list-style-type: none"> pRBCs slightly enlarged and have an oval shape, with tufted ends All stages present in peripheral blood
<i>P. knowlesi</i>				<ul style="list-style-type: none"> pRBCs not enlarged Trophozoites, pigment spreads inside cytoplasm; like <i>P. malariae</i>, band forms may be seen Multiple invasion and high parasitaemia can be seen like <i>P. falciparum</i> All stages present in peripheral blood

Figure 2.2: The visualized parasite stages in thin blood films is shown. Different developmental stages of the parasite ranging from early trophozoites through the schizonts in infected red blood cells is presented. The blood film is examined using standard light microscope with an high numerical aperture oil immersion objective lens at 1000 \times magnification.

used to characterize the efficacy of these techniques are sensitivity, specificity and limit of detection (LOD). Sensitivity is the probability of an infected patient to actually test positive when the result is compared to the reference standard test. Increase in sensitivity results into a consequent decrease in false negatives which is quite important in malaria diagnosis as low sensitivity could result into missed diagnosis. Specificity of the test refers to the probability that an uninfected patient actually tests negative accordingly. The amount of false positives decreases as the specificity increases. A lot of emphasis is now laid on the specificity of the test particularly because of the general concerns of the increasing drug resistance and the absolute desire to improve the quality of care of malaria patients. The detectable parasite threshold in a given blood sample is expressed as the limit of detection. The standard sensitivity performance threshold defined by the WHO guidelines for malaria diagnostics is 95% at 100 parasites/ μ l of blood.

A quick overview of the existing state-of-the-art malaria diagnostic techniques is discussed below:

- **Conventional Light Microscopy:** A quick overview of conventional light mi-

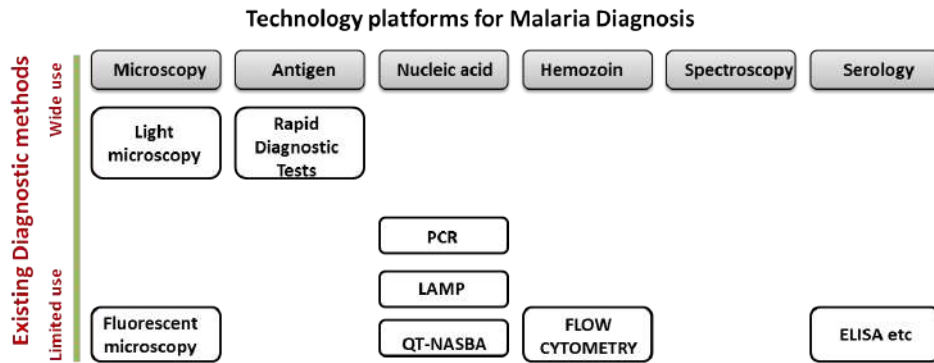


Figure 2.3: Technology platforms for malaria diagnosis depicting existing diagnostic methods and their usage.

croscopy has been discussed in chapter one, this section provides additional information on this diagnostic method. It is interesting to note that Giemsa staining protocol for malaria microscopy has been in existence for over 130 years [2, 11, 12] yet it remains the WHO approved reference standard for malaria diagnosis.

The diagnostic method affords the thorough examination of a thick or thin blood film by an expert microscopist who detects, quantifies and ascertains the various stages of the parasites. The variation in parasite developmental stages determines the severity of the infection. Accuracy of the results depends on the experience of the microscopist.

In optimal laboratory conditions for instance, microscopic diagnosis is highly sensitive and specific with a parasite detection limit as low as 12 parasites/ $1\mu\text{l}$ of blood. In field settings however, the performance of microscopy could be limited as a result of points highlighted in the chapter 1 of this thesis [13, 14]. Other limitations could be due to erratic power outages, insufficient time to stain & examine slides, lack of effective quality assurance and regulation system [15, 16]. Furthermore, staining and result analysis are very labour intensive (approximately 35 minutes per slide) as already highlighted in chapter 1. Although the technology is quite simple, sustained financial and human resource investment to upgrade skills of microscopist through participation in accredited quality assurance and skills upgrade training program is lacking. As a result, the reliability of the test result vary from one operator to another.

- Fluorescence Microscopy:** The use of fluorochrome as a diagnostic method became popular with Hagemann's technique for detecting mycobacterium tuberculosis [17]. Application of this technique for avian and human malaria detection was reported by Patton & Metcalf [18, 19]. Rapid malaria detection in thick blood films from patient with low density infection using acridine orange (AO)

stains with Fluorescence microscopy has been reported in [20–22].

The complexity of detection is minimized by the use of fluorochrome staining which creates sufficient contrast and enhances easy identification of the parasite in stained blood films. Reduced diagnostic time is also an advantage derived from this staining method because the parasites appear like bright stars in the sky at night. The quantified buffy coat method is also applied to fluorescence malaria microscopy. The method employs the use of specific capillary tubes which are pre-coated with acridine orange. About $50\mu\text{l}$ of blood is centrifuged at $14,400\times\text{g}$ ($12,000\text{RPM}$) for 5 minutes [23]. The separated blood constituents is examined and parasite which are present appear green at emission wavelength of about $410\text{--}415\mu\text{m}$. Although this method is more sensitive and specific for malaria diagnosis, it has however not been widely adopted because of the cost, complexity (need for extra equipment) and technical skills required for accurate diagnosis. Species differentiation is also difficult to ascertain. Microscopy quality control which relies on storing slides for re-reading by a supervisor is a challenge with the fluorescent method with acridine orange as prepared samples must be instantly analysed since the AO stains can fade with time.

- **Antigen Detection (Rapid Diagnostic Tests):** Antigen based tests uses antibodies to detect antigens produced by the pathogen through lateral flow immunochromatograph. Malaria rapid diagnostic test kits detect malaria specific antigens present in infected blood samples. Typical test procedures involves the capillary diffusion of a sample through a membrane to which reagents are attached. The blood sample interacts with reagents and produces reactions that can be observed with the human eye in 10-30 minutes. The rapid diagnostic test kits are generally available in various formats such as dipstick [24], card or cassette. In optimal conditions, some of the RDT products can attain a sensitivity performance limit similar to good field microscopy.

Malaria RDTs are relatively inexpensive and the most basic *P. falciparum* tests cost approximately \$0.40 – \$ 0.60. They are of specific interest in the fight against malaria because they require no laboratory infrastructure, power supply, or special equipment [25]. With minimal training, they are useable by community health workers in rural areas.

Although widely adopted for quick screening and detection of malaria, antigen based detection methods are limited due to the following [26]:

1. Quality Control: The quality of the test performed with RDT is difficult to validate on the field since there are no existing practical technologies to measure the quality of the test results.
2. Robustness of Rapid Diagnostic Test: No sufficiently concrete data has been provided to show the robustness of RDTs against harsh environmental conditions such as temperature and humidity. Field results have shown that overexposure of the RDTs to heat and humidity deteriorates the sensitivity of the test kits.

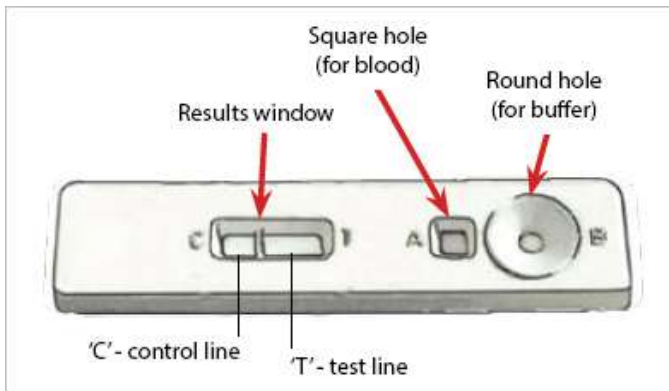


Figure 2.4: A commonly available RDT cassette which consist of a sample well through which the blood is added and a buffer well by which drops of buffer are added.

3. Limit of Detection: RDTs have shown high sensitivity for malaria patient with intense clinical symptoms. In many cases however, the detection limit may not be sufficient to detect low infection loads. For effective control and elimination programs, high sensitivity is a critical requirement.
 4. Differentiating between Current and Previous Infections: RDTs which detect Histidine rich protein-II may find it difficult to distinguish between active and previous infection since the HRP-II antigens continues to circulate in the blood for approximately six weeks after successful treatment [27–29]. This is a current challenge and it seriously reduces the specificity of RDTs.
- **Nucleic Acid Detection: Polymerase Chain Reaction (PCR):** Nucleic acid detection is based on the detection of parasite genes (DNA/RNA). It provides rapid diagnosis with high sensitivity [30–32]. Polymerase Chain Reaction – based technique detects malaria parasites by a process called amplification. The nucleic acid present in the blood is multiplied and analysed for the presence of malaria. PCR can detect low level of parasitemia and this makes it more sensitive and specific than microscopy and other antigen or antibody based test. The limit of detection is typically in the range of 1-5 parasite per μl of blood [33]. Although this specialised intricate process is time consuming, the development of Real-Time PCR (RT-PCR) however allows real-time parasite gene amplification and detection. RT-PCR has been reported to provide semi-quantitative result, differentiates between species [34–36] and can be done in 90 minutes as compared to ≥ 6 hours required for conventional PCR. RT-PCR is less prone to contamination error and the automation process reduces human labour requirements.

PCR based methods requires very well established laboratories as well as highly skilled technical laboratory technologist with sufficient experience in molecular biology. It is mostly used as a reference standard or for research and surveillance purposes due to its high cost per test. Because of the complexity of the procedure, results are not immediately available to the clinicians. Hence they are not commonly used for diagnosis. They can be used to investigate complex cases such as specie determination after diagnosis or patients response to a particular drug treatment.

PCR is particularly reserved for specialized uses and not currently deployed for field use for some reasons among which are (i) Lack of standardization. (ii) Cost of setting up a laboratory. (iii) Careful sample handling is needed to avoid sample contamination and this is not realizable in most rural areas. (iv) Constant electricity to provide stable power source. (v) Need for highly trained and skilled laboratory technicians. (vi) Need for a cold-chain for proper storage of the reagents needed to perform PCR. (vii) Diagnostic time for conventional and nested PCR methods are time consuming requiring an average of ≥ 6 hours.

- **Loop-mediated isothermal amplification (LAMP):** LAMP was recently developed to overcome the limitations of PCR [37–39]. Similar to the PCR technique, extracted DNA is amplified under isothermal conditions [40]. LAMP amplification generates large amount of amplified product. Detection can be enhanced by adding a fluorescent dye accordingly. When sufficient by-product of the LAMP reaction has been formed, the dye fluoresce and can be read with either or without an ultraviolet light. Simpler sample preparation methods are achievable in LAMP as compared to PCR based techniques. LAMP operates a more stable temperature, does not require thermal cycling and provides diagnostic test results in less than an hour. LAMP is also less technically complex and more cost effective as compared to PCR. Despite its many advantages over PCR, LAMP is also a laboratory based test requiring, stable power, and several reagents and consumables for sample collection, preparation and testing. Despite the promise of LAMP for malaria diagnosis, challenges standing in the way of field implementation include: lack of standardized methodology regarding sample collection, DNA extraction and amplification or detection [41]. False positive LAMP reactions can occur from contamination with small amount of DNA [37].
- **Quantitative nucleic acid sequence-based amplification (QT-NASBA):** Produces RNA amplification by the use of enzymatic reaction and thus requires no thermal temperature cycling. Its detection limit, sensitivity and specificity compares directly with PCR performance. It is mostly used for HIV testing and not for Malaria testing. Its capability to discriminate between the sexual and asexual stages of the parasite makes it superior in performance to PCR and LAMP for malaria diagnosis.

- **Hemozoin based detection:** Hemozoin is a malaria pigment synthesized by plasmodium. Hemozoin helps the parasite to avoid a toxic substance called free heme which is produced when the haemoglobin in the erythrocytes is digested. Although hemozoin has been linked to malaria disease in the early 1800s, its use for the diagnosis of malaria still remains a subject of discussion. Moreso a traditional microscope must be modified to clearly visualize hemozoin in blood films. Haematology analysers primarily used to conduct full blood counts have been investigated for use in hemozoin-based malaria diagnosis [42, 43]. The CD 3500 is the first automated method based on this principle that allows detection of malaria during routine analysis of full blood-count. Since hemozoin produces a unique light scattering pattern, this technique count flowing cells containing haemozoin in a flow cytometer channel. These method has been reported to have between 49–98% sensitivity and 82–97% specificity. However, validation and uptake of malaria diagnosis using haematology analysers has been limited due to variability in performance, cost of automated analysers, size, complexity of operating the instruments and need for algorithms to detect and classify abnormalities indicative of malaria disease.
- **Serology:** In response to infections, the human bodies produces specific antibodies which provide some protection from disease. Antibodies are boosted in infected patients and this confirms the patients exposure to malaria. Serologic based tests are not used for diagnosing malaria because it cannot detect between current and past infections. This method finds more relevance in malaria surveillance, control and elimination programs.
ELISA, indirect fluorescent antibody test (IFAT), microarrays, RDTs are several techniques used for malaria serology. Enzyme-linked immunosorbent Assay (ELISA) is however a commonly used diagnostic platform familiar to many laboratories in developing countries due to its widespread use in diagnosing HIV. It is a laboratory based test procedure and it requires standard laboratory settings with highly skilled technicians.
Typical sample testing procedure involves, sample preparation from a few drops of fingerprick blood (typically $\geq 10 \mu\text{l}$ of blood). Sample can be collected as serum or dried blood spots collected on filter paper. Reaction procedures involves the antigens coated onto the bottom of each well of a 96-well plate. Antibodies to the antigen present in the incubated serum samples added to the wells bind to the antigen in the plate and unbound matters are removed from the wells after a series of buffer rinsing. The detection process is followed by the addition of a second antibody which has an enzyme attached to it. The antibody binds to any human antibodies present in the well and excess matter is washed away after incubation. The addition of a final enzyme substrate causes the production of a coloured product in wells containing a malaria antibody/antigen which indicates a positive for malaria antibodies. The colour change is detected using an ELISA plate reader (a spectrophotometer) which measures the amount of colour produced. The amount of colour produced is proportional to the amount of an-

tibody present. Common challenges with the diagnostic procedure includes, high requirement of standard laboratory equipment. with protocols requiring use of an incubator. Reagents require cold storage and for long-term storage, freezing of samples is required. Diagnostic time depends on the number of samples to be tested and potentially leads to long delays in diagnostic outcomes. Training and technical support is required for laboratory staff.

2.2. Urogenital Schistosomiasis

Next to malaria, schistosomiasis is the most prevalent parasitic disease. Its a neglected tropical disease which causes about 240,000 deaths per year, infects about 240 million people and available records shows that over 800 million people are at risk. It is a disease of poverty which is mostly caused by access to limited sanitary facilities and majority of the death cases is linked with Africa [44, 45]. Three major species that causes severe damage of internal organs are *Schistosoma mansoni*, *S. japonicum* and *S.haematobium* [46, 47].

Urogenital schistosomiasis is caused by *S.haematobium* and if left untreated can result into severe bladder and kidney health related problems. As a matter of fact, chronic infection of *S.haematobium* has recently been connected with bladder cancer.

2.2.1. Transmission

Fresh water snail are intermediate host which host the schistosome life cycle. The infectious cercariae deposited in water sources enters the human body through penetration of the skin. It enters circulation in the human body through capillaries and lymphatics. (Fig.2.5)¹ Infectious cercariae deposited in water sources penetrate mammalian skin and causes infection in humans when it enters the circulation of its host through the capillaries and lymphatics.

The disease status is typically classified into three stages: acute, chronic or advanced schistosomiasis [48]. Tourists or travellers infected for the first time however show symptoms which includes fever, headache, malaise, abdominal pain and eosinophilia [49]. Egg deposition in the urinary bladder wall particularly, is an indication of the advanced or chronic phase of the infection [50]. Typical symptoms includes hematuria, and dysuria, bladder calcification [51–53].

2.2.2. State-of-the-art diagnostic methods

Diagnosis of schistosomiasis is important for effective treatment and monitoring control programs, as well as evaluating existing control programs to limit the wastage of resources. Asides logistics and cost limitations, the other major constraint of current diagnostic tools for urogenital schistosomiasis is low sensitivity, especially for individuals with low-intensity infections and areas with low endemicity. Below, we review the standard diagnostic techniques for urogenital schistosomiasis and we aim to highlights

¹Fig. 2.5 Copyright 2002 Massachusetts Medical Society.

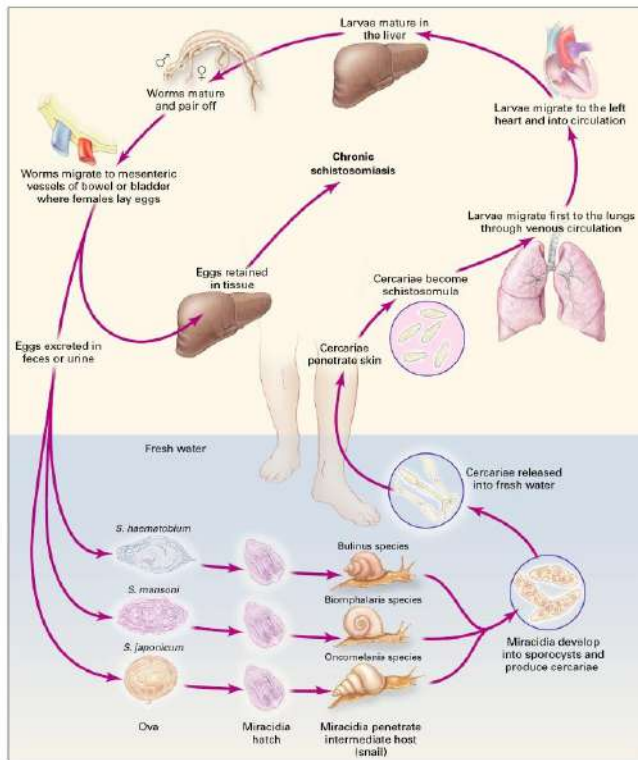


Figure 2.5: Figure, depicts the life cycle of the human schistosome parasite.

the advantages and drawbacks of each method discussed.

- The 'Gold Standard' Microscopy:** Microscopy which is the reference standard for the diagnosis of urogenital schistosomiasis involves the filtration of 10ml of patient urine with a recommended polycarbonate membrane of $12\mu m$ pore size [54]. The filtered residue is stained with lugoz iodine and examined under a standard light microscope by an expert for the presence of eggs. The simplicity of the diagnostic procedure makes it widely acceptable. Also the low personnel training requirements, minimal equipment need, minimal laboratory space requirement, quantification of secreted eggs for morbidity assessment and reuse & recycling of filter materials makes it more attractive and suitable for field use. A major limitation to the accuracy of the test results however is the variation in the day to day secretion of eggs in the infected patients [55]. Increasing sensitivity of diagnostic technique therefore will require repeated collection, pooling and analysis of larger samples which is time, labour and cost intensive.

- **Urine Reagent Strip test kits:** In many rural areas where laboratory facilities are not readily available, reagent strips are commonly used to identify micro-haematuria in urine [56, 57]. The advantages of such reagent strips include quick screening, low-cost and ease-of-use amidst many others [58, 59]. It provides a sensitivity of $\geq 79\%$ [58] but the specificity is however subjective.
- **Antibody-Based Detection:** Enzyme-linked immunosorbent assay (ELISA) is widely used for antibody based diagnosis and it detects the soluble antigens of the eggs [59]. It has high sensitivity and can detect very low-intensity infection which can be easily missed by microscopy or reagent strip tests. It can also be useful for the diagnosis of patients with light worm burdens where egg excretion may not have occurred. A major challenge with the anti-body based test is their low specificity and also cases of cross reaction with other trematode diseases has been reported. The greatest limitation is their inability to distinguish past from active infection [60].
- **CCA & CAA:** A live adult schistosome worm excretes glycoprotein (antigens) into the circulating system of its host. The detected circulating cathodic antigen (CCA) has been observed to correlate with active infection in patient. They are deployable as point-of-care diagnostic devices and are commonly packaged in a similar format as dipsticks [61]. While CCA based test have shown a moderate sensitivity for *S.mansoni* [62, 63], its performance in detecting *S.haematobium* is significantly poor. Although this product might be promising for control and elimination program, the efficacy and accuracy of test results still requires more validation. Moreso, the product is currently being developed.
- **PCR & LAMP** – These diagnostic methods are also used for the detection of urinary schistosomiasis. The procedures, protocols, sensitivity, specificity and limitations are similar to the description made in the malaria section.

2.3. Conclusion

The limitations of the described diagnostic methods reveals the fact that the global burden of both malaria and urogenital schistosomiasis disease is significantly underestimated. Some of the current state-of-the-art diagnostic techniques (such as the antigen and antibody based tests) reviewed herein are not sufficiently accurate in terms of sensitivity and specificity. The sensitive DNA-based methods, are not only cost intensive but are also not easily deployable to rural areas where they are mostly needed. To realize the current elimination and control effort, the need for the development of robust, efficient, reliable and very sensitive diagnostic methods is very critical. This thesis aims at developing such tools to complement the diagnostic gap.

References

- [1] F. E. Cox, *History of the discovery of the malaria parasites and their vectors*, *Parasites & vectors* **3**, 5 (2010).
- [2] L. J. Bruce-Chwatt, *Alphonse laveran's discovery 100 years ago and today's global fight against malaria*, *Journal of the Royal Society of Medicine* **74**, 531 (1981).
- [3] A. Elizabeth, P. P. Aung, and W. Charles, *Malaria*, *Lancet* **391**, 1608 (2018).
- [4] N. Tangpukdee, C. Duangdee, P. Wilairatana, and S. Krudsood, *Malaria diagnosis: a brief review*, *The Korean journal of parasitology* **47**, 93 (2009).
- [5] B. Singh and C. Daneshvar, *Human infections and detection of plasmodium knowlesi*, *Clinical microbiology reviews* **26**, 165 (2013).
- [6] A. F. Cowman, J. Healer, D. Marapana, and K. Marsh, *Malaria: biology and disease*, *Cell* **167**, 610 (2016).
- [7] M. Ahmed and J. Cox-Singh, *P lasmodium knowlesi—an emerging pathogen*, *ISBT science series* **10**, 134 (2015).
- [8] G. A. Josling and M. Llinas, *Sexual development in plasmodium parasites: knowing when it's time to commit*, *Nature Reviews Microbiology* **13**, 573 (2015).
- [9] T. Bousema and C. Drakeley, *Epidemiology and infectivity of plasmodium falciparum and plasmodium vivax gametocytes in relation to malaria control and elimination*, *Clinical microbiology reviews* **24**, 377 (2011).
- [10] J. Farrar, P. J. Hotez, T. Junghanss, G. Kang, D. Laloo, and N. J. White, *Manson's Tropical Diseases E-Book: Expert Consult-Online and Print* (Elsevier Health Sciences, 2013).
- [11] K. Torres, C. M. Bachman, C. B. Delahunt, J. A. Baldeon, F. Alava, D. G. Vilela, S. Proux, C. Mehanian, S. K. McGuire, C. M. Thompson, *et al.*, *Automated microscopy for routine malaria diagnosis: a field comparison on giemsa-stained blood films in peru*, *Malaria journal* **17**, 339 (2018).
- [12] D. Zurovac, B. Midia, S. Ochola, M. English, and R. Snow, *Microscopy and outpatient malaria case management among older children and adults in kenya*, *Tropical Medicine & International Health* **11**, 432 (2006).
- [13] C. Wongsrichanalai, M. J. Barcus, S. Muth, A. Sutamihardja, and W. H. Wernsdorfer, *A review of malaria diagnostic tools: microscopy and rapid diagnostic test (rdt)*, *The American journal of tropical medicine and hygiene* **77**, 119 (2007).
- [14] W. H. Organization, *Malaria microscopy quality assurance manual-version 2* (World Health Organization, 2016).

- [15] J. D. Maguire, E. R. Lederman, M. J. Barcus, W. A. P. O'Meara, R. G. Jordon, S. Duong, S. Muth, P. Sismadi, M. J. Bangs, W. R. Prescott, *et al.*, *Production and validation of durable, high quality standardized malaria microscopy slides for teaching, testing and quality assurance during an era of declining diagnostic proficiency*, *Malaria Journal* **5**, 92 (2006).
- [16] P. Mukadi, V. Lejon, B. Barbé, P. Gillet, C. Nyembo, A. Lukuka, J. Likwela, C. Lumbala, J. Mbaruku, W. Vander Veken, *et al.*, *Performance of microscopy for the diagnosis of malaria and human african trypanosomiasis by diagnostic laboratories in the democratic republic of the congo: results of a nation-wide external quality assessment*, *PLoS One* **11**, e0146450 (2016).
- [17] P. Hagemann, *Fluoreszenzfärbung von tuberkelbakterien mit auramin*, *Munich Med Wschr* **85**, 1066 (1938).
- [18] R. L. Patton, R. L. Metcalf, *et al.*, *The demonstration of the protozoan parasite of quail malaria by fluorescence microscopy*. *Science* (Washington) (1943).
- [19] R. Metcalf *et al.*, *The detection of the plasmodia of human malaria in blood films by fluorescence microscopy*. *Journal of the National Malaria Society* **4**, 223 (1945).
- [20] T. M. Sodeman, *The use of fluorochromes for the detection of malaria parasites*, *The American journal of tropical medicine and hygiene* **19**, 40 (1970).
- [21] A. Spielman, J. B. Perrone, A. Teklehaimanot, F. Balcha, S. C. Wardlaw, and R. A. Levine, *Malaria diagnosis by direct observation of centrifuged samples of blood*, *The American journal of tropical medicine and hygiene* **39**, 337 (1988).
- [22] I. Bosch, C. Bracho, and H. A. Pérez, *Diagnosis of malaria by acridine orange fluorescent microscopy in an endemic area of venezuela*, *Memorias do Instituto Oswaldo Cruz* **91**, 83 (1996).
- [23] C. Wongsrichanalai and F. Kawamoto, *Fluorescent microscopy and fluorescent labelling for malaria diagnosis*, *Encyclopedia of Malaria* , 1 (2014).
- [24] C. J. Shiff, J. Minjas, and Z. Premji, *The parasight-rf test: A simple rapid manual dipstick test to detect plasmodium falciparum infection*, *Parasitology Today* **10**, 494 (1994).
- [25] P. L. Chiodini, *Malaria diagnostics: now and the future*, *Parasitology* **141**, 1873 (2014).
- [26] D. Bell and R. W. Peeling, *Evaluation of rapid diagnostic tests: malaria*, *Nature Reviews Microbiology* **4**, S34 (2006).
- [27] P. A. Ndour, S. Larréché, O. Mouri, N. Argy, F. Gay, C. Roussel, S. Jauréguiberry, C. Perillaud, D. Langui, S. Biligui, *et al.*, *Measuring the plasmodium falciparum*

- hrp2* protein in blood from artesunate-treated malaria patients predicts post-artesunate delayed hemolysis, *Science translational medicine* **9**, eaaf9377 (2017).
- [28] D. Gamboa, M.-F. Ho, J. Bendezu, K. Torres, P. L. Chiodini, J. W. Barnwell, S. Incardona, M. Perkins, D. Bell, J. McCarthy, *et al.*, *A large proportion of p. falciparum isolates in the amazon region of peru lack pfhrp2 and pfhrp3: implications for malaria rapid diagnostic tests*, *PloS one* **5**, e8091 (2010).
- [29] A. Berhane, M. Russom, I. Bahta, F. Hagos, M. Ghirmai, and S. Uqubay, *Rapid diagnostic tests failing to detect plasmodium falciparum infections in eritrea: an investigation of reported false negative rdt results*, *Malaria journal* **16**, 105 (2017).
- [30] L. Milne, M. Kyi, P. Chiodini, and D. Warhurst, *Accuracy of routine laboratory diagnosis of malaria in the united kingdom*. *Journal of clinical pathology* **47**, 740 (1994).
- [31] G. Snounou, S. Viriyakosol, X. Zhu, W. Jarra, L. Pinheiro, and V. do Rosario, *469 thaithong s, brown kn. 1993. high sensitivity of detection of human malaria parasites by the use of nested polymerase chain reaction*, *Mol Biochem Parasitol* **61**, 315.
- [32] C. C. Hermsen, D. Telgt, E. Linders, L. Van De Locht, W. Eling, E. Mensink, and R. W. Sauerwein, *Detection of plasmodium falciparum malaria parasites in vivo by real-time quantitative pcr*. *Molecular and biochemical parasitology* **118**, 247 (2001).
- [33] B. A. Mathison and B. S. Pritt, *Update on malaria diagnostics and test utilization*, *Journal of clinical microbiology* **55**, 2009 (2017).
- [34] O. Sethabutr, A. E. Brown, S. Panyim, K. C. Kain, H. K. Webster, and P. Echeverria, *Detection of plasmodium falciparum by polymerase chain reaction in a field study*, *Journal of Infectious Diseases* **166**, 145 (1992).
- [35] G. Snounou, S. Viriyakosol, W. Jarra, S. Thaithong, and K. N. Brown, *Identification of the four human malaria parasite species in field samples by the polymerase chain reaction and detection of a high prevalence of mixed infections*, *Molecular and biochemical parasitology* **58**, 283 (1993).
- [36] J. M. Tham, S. H. Lee, T. M. Tan, R. C. Ting, and U. A. Kara, *Detection and species determination of malaria parasites by pcr: comparison with microscopy and with parasight-f and ict malaria pf tests in a clinical environment*, *Journal of clinical microbiology* **37**, 1269 (1999).
- [37] M. S. Hsiang, B. Greenhouse, and P. J. Rosenthal, *Point of care testing for malaria using lamp, loop mediated isothermal amplification*, (2014).

- [38] M. Tambo, M. Mwinga, and D. R. Mumbengegwi, *Loop-mediated isothermal amplification (lamp) and polymerase chain reaction (pcr) as quality assurance tools for rapid diagnostic test (rdt) malaria diagnosis in northern namibia*, *PLoS one* **13**, e0206848 (2018).
- [39] R. Ocker, Y. Prompunjai, S. Chutipongvivate, and P. Karanis, *Malaria diagnosis by loop-mediated isothermal amplification (lamp) in thailand*, *Revista do Instituto de Medicina Tropical de São Paulo* **58** (2016).
- [40] T. Notomi, H. Okayama, H. Masubuchi, T. Yonekawa, K. Watanabe, N. Amino, and T. Hase, *Loop-mediated isothermal amplification of dna*, *Nucleic acids research* **28**, e63 (2000).
- [41] E.-T. Han, *Loop-mediated isothermal amplification test for the molecular diagnosis of malaria*, *Expert review of molecular diagnostics* **13**, 205 (2013).
- [42] G. Campuzano-Zuluaga, T. Hänscheid, and M. P. Grobusch, *Automated haematology analysis to diagnose malaria*, *Malaria Journal* **9**, 346 (2010).
- [43] M. P. Grobusch, T. Hänscheid, B. Krämer, J. Neukammer, J. May, J. Seybold, J. F. Kun, and N. Suttrop, *Sensitivity of hemozoin detection by automated flow cytometry in non-and semi-immune malaria patients*, *Cytometry Part B: Clinical Cytometry: The Journal of the International Society for Analytical Cytology* **55**, 46 (2003).
- [44] P. J. Hotez and A. Fenwick, *Schistosomiasis in africa: an emerging tragedy in our new global health decade*, (2009).
- [45] M. J. van der Werf, S. J. de Vlas, S. Brooker, C. W. Looman, N. J. Nagelkerke, J. D. F. Habbema, and D. Engels, *Quantification of clinical morbidity associated with schistosome infection in sub-saharan africa*, *Acta tropica* **86**, 125 (2003).
- [46] G. Raso, P. Vounatsou, D. P. McManus, E. K. N'Goran, and J. Utzinger, *A bayesian approach to estimate the age-specific prevalence of schistosoma mansoni and implications for schistosomiasis control*, *International journal for parasitology* **37**, 1491 (2007).
- [47] W. H. Organization et al., *Schistosomiasis: progress report 2001-2011, strategic plan 2012-2020*, (2013).
- [48] D. J. Gray, A. G. Ross, Y.-S. Li, and D. P. McManus, *Diagnosis and management of schistosomiasis*, *Bmj* **342**, d2651 (2011).
- [49] A. G. Ross, G. R. Olds, A. W. Cripps, J. J. Farrar, and D. P. McManus, *Enteropathogens and chronic illness in returning travelers*, *New England Journal of Medicine* **368**, 1817 (2013).

- [50] A. N. Wamachi, J. S. Mayadev, P. L. Mungai, P. L. Magak, J. H. Ouma, J. K. Magambo, E. M. Muchiri, D. K. Koech, C. H. King, and C. King, *Increased ratio of tumor necrosis factor- α to interleukin-10 production is associated with schistosoma haematobium-induced urinary-tract morbidity*, The Journal of infectious diseases **190**, 2020 (2004).
- [51] C. Hatz, B. Vennervald, T. Nkulila, P. Vounatsou, Y. Kombe, C. Mayombana, H. Mshinda, and M. Tanner, *Evolution of schistosoma haematobium-related pathology over 24 months after treatment with praziquantel among school children in southeastern tanzania*. The American journal of tropical medicine and hygiene **59**, 775 (1998).
- [52] J. M. Correia da Costa, N. Vale, M. J. Gouveia, M. C. Botelho, B. Sripa, L. L. Santos, J. H. Santos, G. Rinaldi, and P. J. Brindley, *Schistosome and liver fluke derived catechol-estrogens and helminth associated cancers*, Frontiers in genetics **5**, 444 (2014).
- [53] E. F. Kjetland, I. E. Hegertun, M. F. Baay, M. Onsrud, P. D. Ndhlovu, and M. Taylor, *Genital schistosomiasis and its unacknowledged role on hiv transmission in the std intervention studies*, International journal of STD & AIDS **25**, 705 (2014).
- [54] F. Mutapi, *Changing policy and practice in the control of pediatric schistosomiasis*, Pediatrics **135**, 536 (2015).
- [55] M. A. Raslich, R. J. Markert, and S. A. Stutes, *Selecting and interpreting diagnostic tests*, Biochemia medica: Biochemia medica **17**, 151 (2007).
- [56] A. G. Lalkhen and A. McCluskey, *Clinical tests: sensitivity and specificity*, Continuing Education in Anaesthesia Critical Care & Pain **8**, 221 (2008).
- [57] H. Feldmeier and G. Poggensee, *Diagnostic techniques in schistosomiasis control. a review*, Acta tropica **52**, 205 (1993).
- [58] Y.-C. Zhu, *Immunodiagnosis and its role in schistosomiasis control in china: a review*, Acta tropica **96**, 130 (2005).
- [59] M. J. Doenhoff, P. L. Chiodini, and J. V. Hamilton, *Specific and sensitive diagnosis of schistosome infection: can it be done with antibodies?* Trends in parasitology **20**, 35 (2004).
- [60] S. Sayasone, J. Utzinger, K. Akkhavong, and P. Odermatt, *Repeated stool sampling and use of multiple techniques enhance the sensitivity of helminth diagnosis: a cross-sectional survey in southern lao people's democratic republic*, Acta tropica **141**, 315 (2015).
- [61] A. Polderman, U. G. Panday, S. Ramkisoen, L. Van Lieshout, and B. Oostburg, *A sedimentation-selective filtration method for the diagnosis of light infections with schistosoma mansoni*, Acta tropica **58**, 221 (1994).

- [62] A. Ebrahim, H. El-Morshedy, E. Omer, S. El-Daly, and R. Barakat, *Evaluation of the kato-katz thick smear and formal ether sedimentation techniques for quantitative diagnosis of schistosoma mansoni infection*, *The American journal of tropical medicine and hygiene* **57**, 706 (1997).
- [63] I. I. Bogoch, J. R. Andrews, R. K. Dadzie Ephraim, and J. Utzinger, *Simple questionnaire and urine reagent strips compared to microscopy for the diagnosis of schistosoma haematobium in a community in northern ghana*, *Tropical medicine & international health* **17**, 1217 (2012).

3

Light Microscopy With Extended Depth

*Darkness covered the earth and;
God said 'Let light be!' and all was light.*

Genesis 1:1

In diagnostic applications where sample scanning is cogent, improving the axial resolving power of the imaging system is crucial. In this chapter, we explore practical methodologies that potentially extends the Depth of Field of a microscope for potential use in label free imaging of parasitic disease. Such a system will alleviate the cost and complexity of sample preparation techniques and allows for easy field use. We have also shown in this chapter that the maximum achievable resolution of in-line lensless holographic microscope is limited by aliasing and, for collimated illumination, can not exceed the camera pixel size. This limit can be achieved only when the optimal conditions on spatial and temporal coherence state of the illumination are satisfied. The expressions defining the configuration, delivering maximum resolution with given spatial and temporal coherence of the illumination are obtained. The validity of these conditions is confirmed experimentally.

Parts of this chapter have been published in "Aliasing, coherence, and resolution in a lensless holographic microscope," *Optics Letters* **42**,12 (2017) [1] & in "Wavefront coding with adaptive optics," *Proc. SPIE 9335, Adaptive Optics and Wavefront Control for Biological Systems*, 93350Q (2015); **324**, 289 (1906) [2]

3.1. Fundamental principle of optical microscopy

Fourier series provides useful insight into how well an optical system can reproduce an object in its image space by decomposing the object and considering it as a summation of spatial sinusoidal waves at unique frequencies [3]. The smallest feature of an object that can be resolved by an optical microscope is defined by its spatial resolution. The smaller the value of the spatial resolution the more the resolvable details of the object. Ernst Abbe in 1873 defined the spatial resolution of a microscope by considering the observed object as a periodic diffraction element [4, 5]. Based on quantitative mathematical analysis, he showed that a minimum of two orders of a diffraction grating should be collected by the objective lens in order to resolve the smallest features of the grating. He described in words, the first definition of the spatial resolution $\Delta_{x,y}$ of an optical microscope which is mathematically expressed as :

$$\Delta_{x,y} = \frac{\lambda}{n \sin \theta} = \frac{\lambda}{NA} \quad (3.1)$$

λ is the wavelength of the light source, n the refractive index, θ is the diffraction angle and NA the numerical aperture [6]. Based on Abbe theory, the maximum resolvable features of an object under examination is defined by the numerical aperture of the microscope objective used. Only diffracted features of the object with a spatial period higher than $\Delta_{x,y}$ are intercepted by the finite pupil of the objective lens. Taking into consideration the illumination design where the NA of the condenser lens is matched with the NA of the objective lens, Equation 3.1 can be written as:

$$\Delta_{x,y} = \frac{\lambda}{2NA} \quad (3.2)$$

The result of a more rigorous mathematical work of Hermann von Helmholtz shows that equation 3.1 is not only valid for coherent illumination but for incoherent illumination also [7, 8].

A generalized definition of spatial resolution is based on Rayleigh criterion. Lord Rayleigh, considered microscopic objects as a sum of point sources [9] and proposed that two close-lying points are considered resolved if the first intensity maximum of one diffraction pattern coincides with the first intensity minimum of the other [10]. His definition leads to a spatial resolution which is mathematically expressed as

$$\Delta_{x,y} = 0.61 \frac{f\lambda}{R} \quad (3.3)$$

where f is the focal length and R , the radius of the finite pupil of the lens. Although Abbe's resolution criterion is more rigorous, Rayleigh criterion is a more commonly known formulation of the resolution for imaging instruments.

3.1.1. Theoretical principle

In an imaging system, the light intensity distribution in the object plane is collected by an optical system and propagated through the system to produce its conjugate in

a different plane along the optical axis [11, 12]. Fig.3.1 is a simple optical system. It consists of an illumination source, the optical train and an image plane.

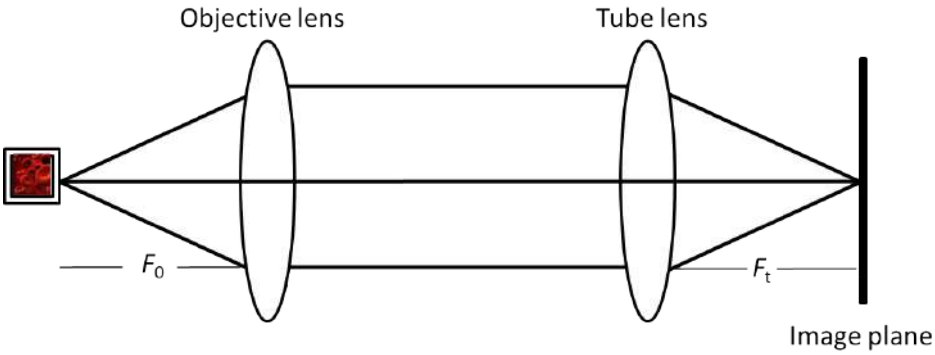


Figure 3.1: A schematic diagram of a simple optical train of a microscope. The object is placed at the focal distance F_0 of the objective lens. Collected and collimated light from the lens is focused by the tube lens which is placed at its focal distance F_t from the image plane. The magnification of the optical system is the ratio of the focal lengths expressed as $\frac{F_t}{F_0}$.

The object is placed at a distance f_o from the objective lens and the image plane is at a distance f_t from the exit pupil of the tube lens. The circular pupil function $P(x, y)$ of the imaging system has a diameter D which is unity inside and zero outside the defined aperture. Assuming that the imaging system is diffraction-limited, the location of the ideal image point is related to the location of the original object through a scaling factor M (magnification of the optical system) [12]. The propagated 2-D distribution of the complex amplitude impinging at the image plane can therefore be expressed as:

$$\iint_{-\infty}^{\infty} h(u, v; \xi, \eta) \times U_o(\xi, \eta) d\xi d\eta \quad (3.4)$$

where $U_o(\xi, \eta)$ is the complex field of the source, u and v are the coordinates at the object space. Equation 3.4 can be rewritten using the convolution theorem as:

$$U_i(u, v) = h(u, v; \xi, \eta) \otimes U_o(\xi, \eta) \quad (3.5)$$

where $h(u, v; \xi, \eta)$ is the amplitude point spread function of the imaging system defined by the Fourier transform of the pupil function ($P(x, y)$) as:

$$h(u, v; \xi, \eta) = \frac{A}{\lambda z_i} \iint_{-\infty}^{\infty} P(x, y) \times e^{\left\{-j \frac{2\pi}{\lambda z_i} [(u-M\xi)x + (v-M\eta)y]\right\}} dx dy \quad (3.6)$$

The irradiance $I_i(u, v)$ registered by a CCD sensor placed at the image plane is determined by estimating the square of the time-averaged image amplitude and it's mathematically expressed as:

$$I_i(u, v) = \langle |U_i(u, v)|^2 \rangle \quad (3.7)$$

3.1.2. Coherent imaging

A coherent imaging system is linear in complex amplitude [13, 14]. Combining equation 3.5 and 3.7, the expression of the image intensity can therefore be defined by convolving the object amplitude $U_o(\xi, \eta)$ with the point spread function $h(u, v; \xi, \eta)$.

$$I_i(u, v) = \langle |h(u, v; \xi, \eta) \otimes U_o(\xi, \eta)|^2 \rangle \quad (3.8)$$

Using convolution theorem and equation 3.5, the electric field in the image plane in the frequency-space is given as:

$$\mathcal{F}\{U_i(u, v)\} = \mathcal{F}\{h(u, v; \xi, \eta)\} \times \mathcal{F}\{U_o(\xi, \eta)\} \quad (3.9)$$

Then the frequency-domain irradiance is mathematically defined as:

$$I_i(f_x, f_y) \propto |P(x, y) \times \mathcal{F}\{U_o(\xi, \eta)\}|^2 \quad (3.10)$$

For a coherent imaging system, the cut-off frequency f_c is calculated using the expression:

$$f_c = \frac{D}{\lambda z_i} = \frac{NA}{\lambda} \quad (3.11)$$

3.1.3. Incoherent imaging

For a spatially incoherent light source, the registered intensity distribution at the image plane is the convolution of the square amplitude spread function $h(u, v; \xi, \eta)$ with the object irradiance and it is mathematically expressed as:

$$I_i = ||h(u, v; \xi, \eta) \otimes U_o(\xi, \eta)|^2|^2 \quad (3.12)$$

The intensity point spread function (IPSF) is derived from the amplitude spread function ($h(u, v; \xi, \eta)$) and commonly referred to as the Airy disk. Applying the convolution theorem as previously done in the coherent case, we obtain:

$$\mathcal{F}\{I_i(u, v)\} = \mathcal{F}\{|h(u, v; \xi, \eta)|^2\} \times \mathcal{F}\{|U_o(\xi, \eta)|^2\} \quad (3.13)$$

Using equation 3.13, the optical transfer function $OTF(f_x, f_y)$ can be derived as:

$$OTF(f_x, f_y) = \mathcal{F}\{|h(u, v; \xi, \eta)|^2\} \propto \mathcal{F}\{|\mathcal{F}\{P(x, y)\}|^2\} \quad (3.14)$$

From the Optical transfer function, the modulation transfer function and phase transfer function are derived from the real and imaginary parts of the fourier transform operation. The modulation transfer function represents the contrast distribution ratio between the image M_{image} and the object M_{object} at a given spatial frequency f_x, f_y . The phase transfer function provides useful information for the transversal shift of the

image.

$$MTF(f_x, f_y) = \frac{M_{image}}{M_{object}}(f_x, f_y) \quad (3.15)$$

The contrast $M(f_x, f_y)$ expresses the intensity modulation depth of the signal and it's expressed as:

$$M(f_x, f_y) = \frac{I_{max} - I_{min}}{I_{max} + I_{min}}(f_x, f_y) \quad (3.16)$$

In an incoherent imaging system, the cut-off frequency f_c of the transfer function is defined as:

$$f_c = 2 \frac{NA}{\lambda_0} \quad (3.17)$$

3.1.4. Depth of field

Equation 3.17 provides an estimate of point-to-point lateral resolution and ofcourse a lot of emphasis is placed on the lateral resolution in optical microscopy particularly in the examination of parasites in prepared thin or thick blood film. In diagnostic application where samples scanning (e.g scanning through volume of urine samples for detection of *Schistosomia haematobium* eggs) is required however, lateral resolution is not enough, axial resolving power of the imaging system must also be taken into consideration. The axial resolution is measured parallel to the optical axis and often referred to as the depth of field.

Aside spatial resolution, depth of field also defines the performance of an optical imaging system. Depth of field determines the amount of information obtainable from a single registered image and it is dependent on the numerical aperture of the optical system. A greater depth of field is observed as the numerical aperture of the optical system decreases [15]. Hence, high resolution microscopes usually have limited DOF [16, 17].

Low-cost optical system with increased depth of field and sufficient resolution is considered in this research particularly because of its application for the development of point-of-care diagnostic instruments. An optical system with extended DOF is of interest for the development of label-free imaging of *Schistosomia haematobium* eggs in a urine sample. Such a robust system will alleviate the cost and complexity of sample preparation and enable ease-of-use in remote areas where standard laboratory facilities are not readily available.

A mathematical expression for the total depth of field of an imaging system is given as:

$$D_{tot} = \frac{\lambda \times n}{NA^2} + \frac{n}{M.NA}e \quad (3.18)$$

It is the summation of both the wave and geometrical optical depths of field shown in equation 3.18. D_{tot} is the depth of field, λ the wavelength, n is the refractive index, NA is the numerical aperture of the objective lens and e is the smallest resolvable

distance by a detector placed in the image plane where M is the lateral magnification of the microscope.

3.2. Extending depth of field by wavefront coding

Control of the DOF of optical imaging system has been an active research topic for many years. A conventional method of extending the DOF involves stopping the lens, and — in a more sophisticated approach — manipulating the pupil function by inserting shade masks or apodizers in the pupil [18, 19]. This method increases DOF at the expense of light power at the image plane, lower resolution and reduced SNR. The use of axicons is another technique used for increasing the DOF [20]. This technique is usable mostly for on-axis images, as a wider field of view suffers from strong aberrations. Hausler *et al* [21] proposed a method which involves a continuous change in focus during the exposure time, superimposing the modulation transfer function for different foci in a single image. This technique produces a depth invariant point spread function (PSF), but it requires the use of quick controllable focus change, which can be cumbersome. Spectral focal sweep [22] alleviates the problem of moving parts by exploiting the chromatic aberration. The efficiency of this approach however depends on the illumination and reflection spectra of objects being imaged. Objects that are not sufficiently broadband cannot produce a large spectral focus range. Taking multiple images at different focus level and synthesizing them via image processing was also proposed for DOF extension [23].

Finally, a distinct method for extending the DOF was proposed by Dowski and Cathey [24–26]. This technique called 'Wavefront coding' involves the use of cubic phase plate at the pupil plane, to form and store intermediate coded images. Digital processing of inverse filtration is then used to restore the coded images. It is a hybrid optical/digital technique that reduces the system complexity, improves imaging capabilities and provides a good performance [27].

3.2.1. Basics of wavefront coding

A family of cubic phase pupil functions produce defocus-invariant PSFs [24, 28–30]. Usually these functions are implemented with cubic phase plates. The cubic phase plates have a two-dimensional phase delay [29, 30] as a function of spatial coordinates, described by:

$$P(x, y) = a_{3,0}x^3 + a_{2,1}x^2y + a_{1,2}xy^2 + a_{0,3}y^3 \quad (3.19)$$

where the coefficients $a_{i,j}$ define the form and the amplitude of the pupil function. The DOF achievable by the coded imaging system is directly proportional to the strength of the phase element. Since the implementation of the optical system could be based on diverse application and different circumstances, the requirements to the wavelengths, NA, required DOF and the resolution of the imaging system could also vary. With this variation in application, it is extremely useful to find a dynamic method to control the cubic phase in real time. In this section, we investigate wavefront coding with adaptive optics.

Adaptive optics allows for quick switching between zero pupil modulation, corresponding to an ideal optical system, to dynamically controlled extended DOF system with cubic element in the pupil. This approach provides a flexible *ad hoc* DOF exten-

sion.

The intensity pattern $u_i(x, y)$ in an image plane at distance z from the pupil can be described as a convolution of the object intensity $u_o(x, y)$ and the corresponding incoherent point spread function [11, 12] $h(x, y, z)$:

$$u_i(x, y) = u_o(x, y) * h(x, y). \quad (3.20)$$

For a mis-focused optical system, the shape of PSF depends on the defocus amount $W_{2,0}$:

$$h(x, y) \propto \left| \int_{A \neq 0} e^{ikA(\xi, \eta)} e^{ikW_{2,0}(\xi^2 + \eta^2)} e^{i\frac{k}{z}(x\xi + y\eta)} d\xi d\eta \right|^2, \quad (3.21)$$

$A(\xi, \eta)$ is the pupil function, ξ, η are the coordinates in the exit pupil, $W_{2,0}$ is the defocus parameter, and k is the wave number.

Implementing wavefront coding techniques implies adding a phase element with a cubic phase function to the exit pupil of the optical system.

The PSF of a wavefront-coded aberration free optical system can be written as:

$$h_c(x, y) \propto \left| \int_{A \neq 0} e^{ikA(\xi, \eta)} e^{ikW_{2,0}(\xi^2 + \eta^2)} e^{ikP(\xi, \eta)} e^{i\frac{k}{z}(x\xi + y\eta)} d\xi d\eta \right|^2, \quad (3.22)$$

where $P(\xi, \eta)$ is given by Eq. (3.19). With a careful choice of coefficients a_{ij} , the obtained PSF h_c is approximately invariant for a range of defocus values $W_{2,0}$ (with accuracy to shifts in the image plane) [24, 28, 29]. Thus the coded images

$$u_c(x, y) = u_o(x, y) * h_c(x, y) \quad (3.23)$$

are also little dependent on the defocus value, and can be deconvolved using defocus-independent Wiener filter [31, 32]:

$$W(\xi, \eta) = \frac{H_c^*(\xi, \eta)}{|H_c(\xi, \eta)|^2 + C}, \quad (3.24)$$

where $H_c = \mathcal{F} h_c$ is the Fourier transform of the coded PSF and C is a parameter related to the image SNR, which is interactively adjusted to provide a good reconstruction result. To obtain the diffraction limited quality image, an inverse Fourier transform operation \mathcal{F}^{-1} must be performed on the filtered image:

$$\mathcal{F}^{-1}[U_c(\xi, \eta) \cdot W(\xi, \eta)] \quad (3.25)$$

where $U_c(\xi, \eta)$ is the Fourier transform of $u_c(x, y)$.

3.2.2. Experimental set-up and results

An experimental setup shown in Fig. 3.2 has been developed to verify our proposed methodology. Low-cost 15-mm 19-ch (17 deformable modes plus tip-tilt) Micromachined Membrane Deformable Mirror (MMDM) from OKO Tech, Delft, the Netherlands was used as the adaptive phase element. This device can be used for fast dynamic correction of low-order optical aberrations such as defocus, astigmatism, coma, trefoil etc. [33].

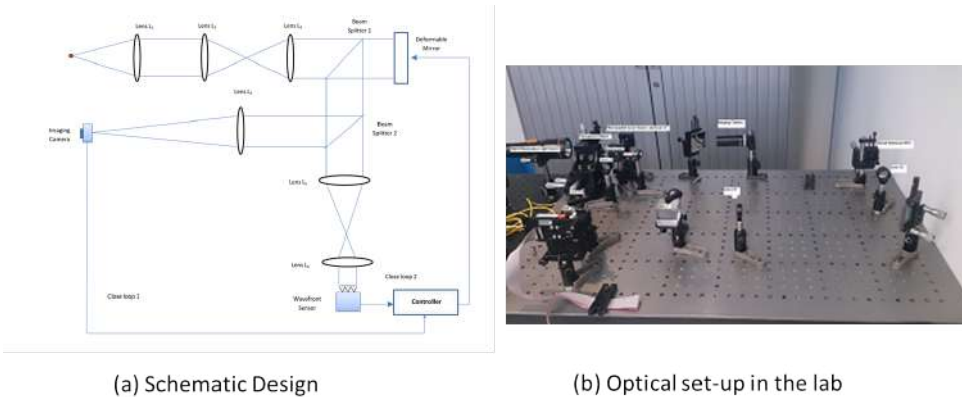


Figure 3.2: The configuration of the optical arrangement of the proposed system.

Light from a single-mode fiber ($\lambda = 632nm$) is collimated by lens L1. The telescope formed by lenses L2 and L3 reimages the system pupil, scaling it to the diameter of 10mm centered on the MMDM. The beam reflected from the MMDM is split into two arms: one towards the imaging camera and the other to the wavefront sensor. Relay optics formed with L5 and L6 conjugates the Shack Hartman WFS with the system pupil and the deformable mirror, while the lens L4 focuses the beam to the CCD. The control includes two closed loop system:

1. to enable the adaptive compensation of the aberrations in the optical system, including the non-common path aberration;
2. to control the deformable mirror, for extended DOF WF coding.

The adaptive system was calibrated in the following order:

- At the first stage the Nelder-Mead simplex optimisation algorithm was used to control the MMDM shape, to minimize the spot size of the focused image of the single-mode fiber tip on the CCD. As a result of this optimization, with the help of a deformable mirror, we obtained a virtually aberration free optical system that imaged the fiber tip plane to the CCD plane.
- A reference pattern was registered in the Shack-Hartmann sensor, that corresponds to the aberration free system. Starting from this system state, the

FrontSurfer software (OKO Tech, Delft, the Netherlands) was used for the calibration of the MMDM. The FrontSurfer uses a set of measured influence functions of the mirror for fitting of the desired phase aberration [33]. This aberration is defined as a combination of Zernike polynomials [34] which can be manually controlled. To create a cubic phase function, a combination of two 3rd-order Zernike terms (coma+trefoil) was formed by the DM in the system pupil. The strength of this target function can be dynamically controlled, however we found that the maximum amplitude of the cubic function is limited by the DM.

- After the desired PSF was obtained, it was registered by the CCD. A special care was taken to register the PSF at the linear shoulder of the CCD response, avoiding oversaturation that would cause information loss at the reconstruction phase.
- In the calibrated system with coded pupil, a transparency showing a house tower was used as an object. The object was illuminated with extended incoherent white LED source.
- A number of images of both the PSF and the object have been registered for different in and out of focus positions for ideal optical system and for coded system. Fig. 3.3 shows the recorded experimental PSF of our conventional and coded imaging system.

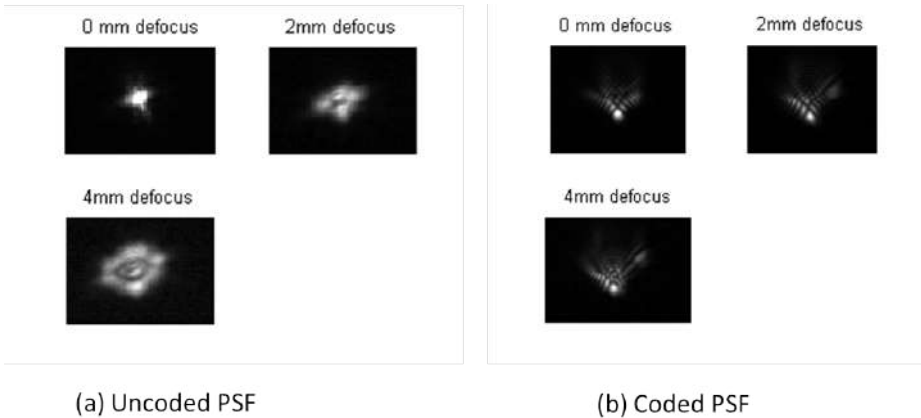


Figure 3.3: Experimental PSFs. The cubic function formed by the MMDM has maximum amplitude of 1λ .

The MTFs, estimated from the measured PSFs are depicted in Fig. 3.4 and 3.5 respectively. Fig. 3.4 shows that as the conventional system becomes more and more defocused, the size of the PSF increases causing loss of the high frequency terms in the image. With the coded system, the invariance of the MTFs at higher spatial

frequencies decreases only slightly, and digital restoration of the image with simple filtering is possible. The restoration process operates on the coded MTF with the goal to retrieve the diffraction limited features of the image. Comparing the conventional system to the coded system, it can be observed that defocus alleviation by the coded system results in increase of DOF. When the defocus is increased beyond a certain limit however, coding cannot provide sufficient invariance. This drops the performance of the coded MTF resulting to loss of spatial resolution on the restored image. For visual illustration, our object was imaged with the conventional and coded imaging systems respectively. Fig. 3.6-(top) shows the recorded image of the object in focus as shown in (a). Moving the object through a defocus range of 4mm in steps of 2mm produced blurry images as shown in (b) and (c) respectively. Coded images recorded under similar conditions are depicted in Fig.3.6-(bottom). All coded images are restored using the in-focus cubic PSF and Wiener Filtering and the restored images are presented in Fig.3.7. The DOF extension is clearly visible, in spite of limited range of cubic function that could be created with MMDM.

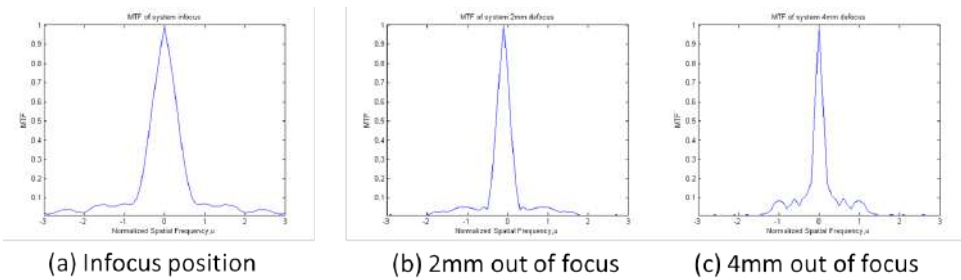


Figure 3.4: Modulation Transfer Functions for three focus positions in aberration-free optical system.

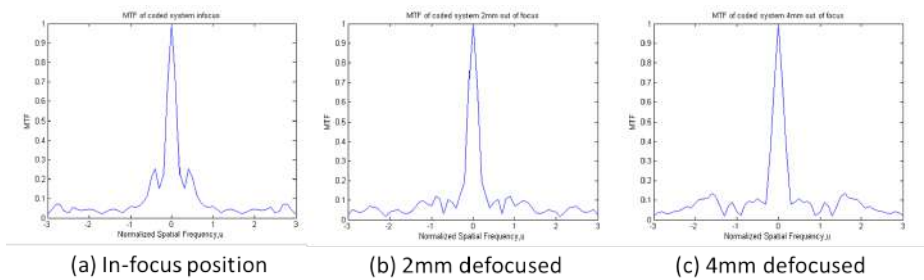


Figure 3.5: Modulation Transfer Function from a dynamic cubic phase element focus-invariant system

In summary, the experimental verification proves that the deformable mirror in an imaging optical system is not only efficient in improving the dynamic image quality and correcting the system aberrations, but can also be used for static and dynamic

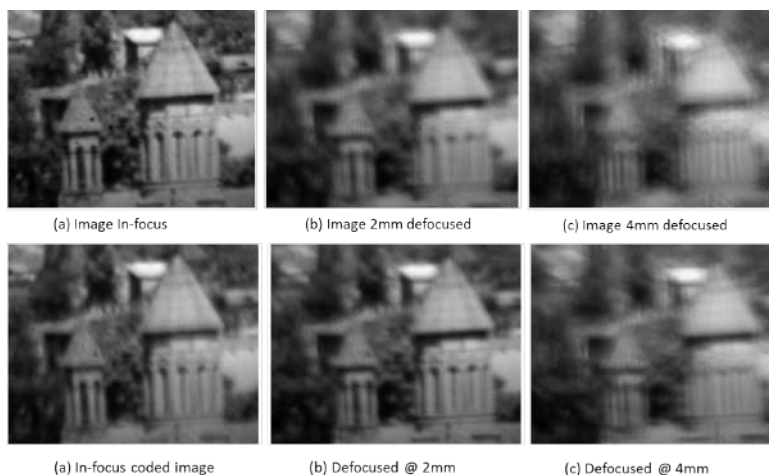


Figure 3.6: Recorded Images with conventional imaging system depicting image registered with object in-focus and at two different defocus plane is shown at the top. The intermediate coded images at the bottom are registered with the object in-focus and also at defocused range of 2 mm and 4 mm from ideal focal positions respectively.

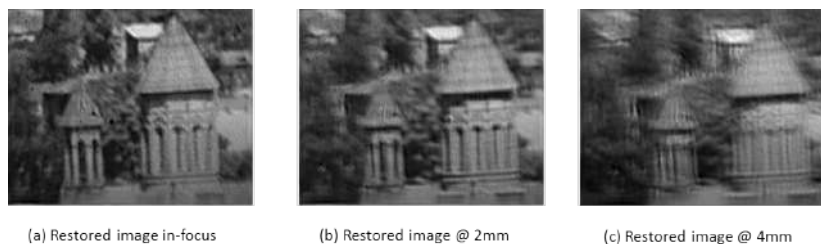


Figure 3.7: Restored images with signal processing. Restored coded images demonstrates visible increase in depth of field.

wavefront coding by forming a pre-defined phase mask in the system pupil. Although this method is not cost effective and as such may not find relevant application for low-cost point of care diagnostic devices, the experimental results obtained for extended DOF clearly demonstrate the applicability and the usability of the method for laboratory based diagnostic instruments. The extended DOF range can be further improved by using a deformable mirror with larger number of actuators and larger range of deformations, compared to the 19-ch MMDM. For this particular DM, the maximum amplitude of the cubic function was limited to about 1λ , which is sufficient to demonstrate the positive effect, but not enough for a wide practical application.

3.3. Aliasing, coherence and resolution in a lensless holographic microscope

Rapid advancement in computational microscopy has opened new possibilities in the design of miniaturized lensless imaging devices and systems with wide applications in biological imaging, especially when simple robust and low-cost solutions are required [35–37]. Lens-less digital in-line holographic microscope (DIHM) represents the simplest possible configuration, as it requires only three components: a light source, sample, and an image sensor [38, 39]. In this system, an object wave interferes with a plane reference wave at the detector plane to form an interferogram as shown in Fig.3.8. The complex amplitude of the field in the object plane is numerically reconstructed by solving the inverse source problem, applying back-propagation from the sensor to the sample plane [40, 41]. Unlike the conventional microscope, the instrument can provide details in transparent biological samples since both amplitude and the phase of the field is reconstructed [39, 42–47].

The maximum achievable resolution in lensless in-line holographic microscope is limited by:

- The signal to noise ratio, which depends on the sample size, the diffracted intensity and the detectability of the interference fringes formed at the detector plane [48].
- Spatial aliasing, occurring when the intensity fringes are undersampled by the sensor. Reconstructed images exhibit distortions and fake features, not present in the object.
- Limited spatial and temporal coherence of the source, limiting the maximum observable fringe frequency, limiting the maximum system resolution [49].

Noises originating from experimental conditions strengthened by the coherence properties of the illumination source in DIHM has been investigated in [50]. Engineering the optical system geometry with respect to the coherence properties of the source and detector specifications to reduce aliasing has not been considered. This however forms a major difference with our work. Coherence requirement for different holographic setups has been compared by Daniel et-al. [49], again this has not been discussed with respect to spatial aliasing.

In this chapter we derive the system configuration and illumination properties for achieving the highest possible resolution with alias-free imaging.

3.4. Theoretical basis

Consider a DIHM with the object illuminated by a plane wave with wavelength λ and the coherent properties described by the spatial coherence length ρ_s , and temporal coherence length ρ_t . As shown in Fig. 3.8, the light diffracted by the object interferes

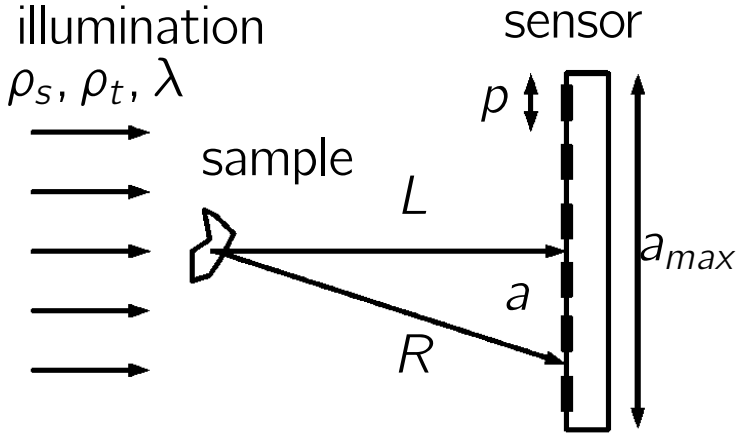


Figure 3.8: Schematic of a holographic microscope. The sample is illuminated with a plane wave with wavelength λ , having spatial coherence size of ρ_s and the temporal coherence length of ρ_t . The diffraction pattern is registered by a sensor with pitch p at a distance L .

with the illumination to form a hologram at the distance L on the detector with pixel pitch p [51, 52].

For alias-free imaging, the minimum period of the fringe pattern, created by the interference between the illumination and the scattered waves, should be at least twice larger than the pitch of the sensor p . To satisfy to this condition, using the notations of Fig. 3.8, we state:

$$a = \frac{\lambda L}{2p} \quad (3.26)$$

This relation sets the resolution limit for the microscope. Indeed, since the resolution $r = \lambda/(2A)$ depends on the numerical aperture $A = a/L$, combining these expressions with 3.26 we obtain the expression for the resolution, as limited by aliasing:

$$r = p. \quad (3.27)$$

Consider an object with a circular cross section of radius r . As shown by [48, 53], the intensity distribution of the interferogram, obtained with spatially and temporally coherent light, measured at the detector at a distance L from the object is given by:

$$I(a) \approx 1 - \frac{kr^2}{L} \sin\left(\frac{ka^2}{2L}\right) \frac{2J_1(kar/L)}{(kar/L)} \quad (3.28)$$

where $k = 2\pi/\lambda$. Using the asymptotic approximation for Bessel function $J_1(x) \approx \sqrt{\frac{2}{\pi x}} \cos(x - 0.75\pi)$ and neglecting the fast oscillating term $\sin\left(\frac{ka^2}{2L}\right)$, we obtain the expression for the asymptotic envelope of the fringe intensity:

$$I(a)_{env1} \approx 1 - \frac{2}{\pi} \sqrt{\frac{\lambda L r}{a^3}} \cos\left(\frac{k a r}{L} - 0.75\pi\right). \quad (3.29)$$

By neglecting the cos oscillation term in Eq. 3.29, we obtain the smoothly decaying envelope of the fringe intensity:

$$I_{min} \approx 1 - \frac{2}{\pi} \sqrt{\frac{\lambda L r}{a^3}}; \quad I_{max} \approx 1 + \frac{2}{\pi} \sqrt{\frac{\lambda L r}{a^3}}; \quad (3.30)$$

Then the fringe visibility as defined in [53, 54], can be estimated with a formula:

$$V(a) = \frac{I_{max} - I_{min}}{I_{max} + I_{min}} \approx \frac{2}{\pi} \sqrt{\frac{\lambda L r}{a^3}}. \quad (3.31)$$

Since we are interested in the fringe visibility at the edges of our field, the condition of validity of Eq. 3.31, $\frac{k a r}{L} > 1$, is satisfied. Fig. 3.9 illustrates the fringe intensity calculated for $r = 25 \mu\text{m}$, $L = 0.05 \text{ m}$ and $\lambda = 0.65 \mu\text{m}$ according to the exact formula Eq. 3.28, and using asymptotic approximations 3.29 and 3.30.

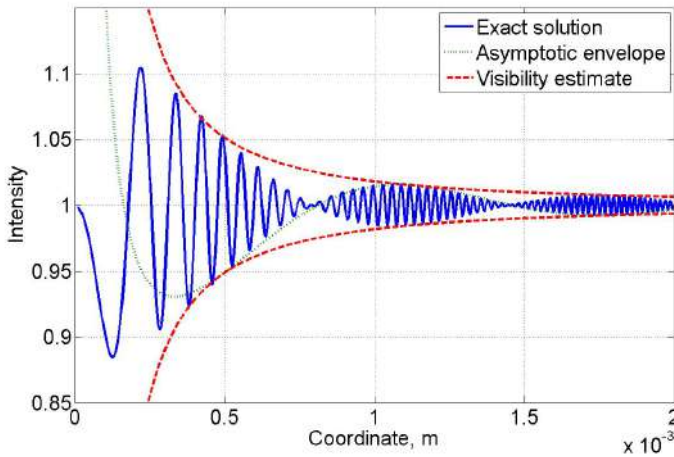


Figure 3.9: Fringe intensity calculated for $r = 25 \mu\text{m}$, $L = 0.05 \text{ m}$ and $\lambda = 0.65 \mu\text{m}$ according to the exact formula Eq. 3.28, and using the asymptotic approximations 3.29 and 3.30.

To avoid aliasing, the fringe visibility should decay to zero at a distance defined by expression 3.26. In practice, we can consider the fringe to be invisible, when its visibility equals to the inverse of the signal-to noise ratio of the camera:

$$V(a) = S^{-1}. \quad (3.32)$$

The solution of this equation produces the estimate for the distance providing aliasing-

free hologram registration with spatially and temporally coherent illumination:

$$L = \frac{4S}{\pi} \sqrt{\frac{2\rho^3 r_{max}}{\lambda^2}}. \quad (3.33)$$

According to 3.31 the fringe visibility is proportional to the square root of the feature size r , therefore, if the object has a range of features, the maximum feature size r_{max} should be used in 3.33, as then all fringes created by features with $r < r_{max}$ will have lower visibility at $a = \frac{\lambda L}{2\rho}$. This secures alias-free fringe registration, but causes loss of the fringe patterns created by smaller features, leading to resolution loss.

If the parameters of the sample are unknown, we can require the condition 3.26 to be satisfied for any place in the sensor, setting the aliasing cutoff size a equal to the sensor size $a = a_{max}$ as shown in Fig. 3.8, to obtain a condition:

$$L = \frac{2\rho a_{max}}{\lambda}. \quad (3.34)$$

If Eq. 3.34 is satisfied, then the optimal resolution is not achieved for all features of the sample. From the coherent case we can draw conclusions, that will be useful in the further analysis:

- The best achievable resolution of an in-line holographic microscope, limited by aliasing, is in the order of its pixel size. Configuration described by Eq. 3.34 provides an alias-free compromise with the resolution loss for all feature sizes.
- It is impossible to derive a configuration that provides the optimal fringe visibility for all feature sizes with a coherent illumination. If the smallest feature is optimally resolved without aliasing or loss of fringes due to low visibility, then the larger features will cause aliasing due to higher visibility of high-frequency fringes. If the largest features are imaged free of aliasing, then the smaller features will be imaged with loss of resolution, as the fringe visibility is lost far below the aliasing limit.

So it is of a great interest to control the fringe aliasing by tuning the coherent properties of the illumination.

3.5. Defining Optimal system configuration

Without any loss of generality, we can assume that, in accordance with the definition of the spatial coherence length ρ_s all fringes with $a > \rho_s$, as shown in Fig. 3.8, have zero fringe visibility. Then, in the assumption of complete temporal coherence $\rho_t = \infty$, we can define the optimal spatial coherence length for alias-free holographic imaging in the setup shown in Fig. 3.8:

$$\rho_s = \frac{\lambda L}{2\rho} \quad (3.35)$$

This condition provides optimal imaging: larger values of ρ_s result in aliasing, while smaller values cause resolution loss. Optimal imaging in this context refers to a system

configuration that delivers maximum resolution which satisfies to Nyquist Shannon criterion without aliasing.

Using the Van Cittert-Zernike theorem [55] to express the ρ_s via the numerical aperture of the illumination source A_s and the wavelength: $\rho_s = \lambda/2A_s$, we obtain the expression for the numerical aperture of incoherent illumination, securing alias-free imaging:

$$L = \frac{p}{A_s} \quad (3.36)$$

For alias-free imaging with extended monochromatic source, the angular size of the camera pixel, as observed from the sample plane, should be equal to the numerical aperture of the illumination source.

In a similar way, in the assumption of absolute spatial coherence $\rho_s = \infty$ of the illumination, expression 3.26 can be used to derive the limitation to temporal coherence, securing alias-free imaging. The path difference between the illumination and scattered waves should be equal to the coherence length: $R - L = \rho_t$ and accounting for 3.26 and introducing practical approximation $\rho_t = \frac{\lambda^2}{\Delta\lambda}$ where $\Delta\lambda$ is the illumination linewidth, we solve equation

$$R - L = \sqrt{a^2 + L^2} - L = \frac{\lambda^2}{\Delta\lambda}, \quad (3.37)$$

to obtain the expression for the illumination linewidth, securing the alias-free registration of interference fringes by the sensor:

$$\begin{aligned} \Delta\lambda &= \lambda^2 \left(\sqrt{\frac{L^2(\lambda^2 + 4p^2)}{p^2}} - 2L \right)^{-1} \approx \frac{4p^2}{L} \\ L &\approx \frac{4p^2}{\Delta\lambda} \end{aligned} \quad (3.38)$$

where the approximation in the right side of 3.38 is valid only for $p \gg \lambda$

Expressions 3.33, 3.34, 3.36, 3.38 define the optimum microscope configuration for different coherence states of illumination. Obviously, these expressions represent rather simplified approximations, derived from physical considerations, that can not replace an in-depth analysis, taking into account the exact distributions of spatio-temporal coherence functions. On the other hand, in practice the coherence functions frequently adhere to simple models, while in more complex practical cases these functions are frequently unknown. Expressions 3.36 and 3.38 provide physical insight and guidance for the designing of an optimally-configured instrument, avoiding resolution loss and undersampling.

The configuration with diverging illumination, shown in Fig. 3.10 is of a great practical interest, as it allows to obtain magnified images with magnification $M = \frac{L^*+Z}{Z}$ and resolution $r = p$ in the plane of registration. The configuration with plane wave illumination, shown in Fig. 3.8 can be made equivalent to the configuration Fig. 3.10

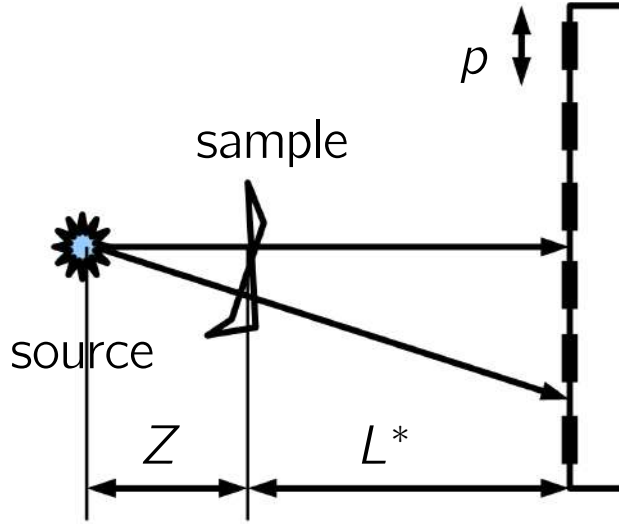


Figure 3.10: Microscope configuration with divergent beam, providing sample magnification.

by satisfying the condition $L = ML^*$:

$$L^* = 0.5(\sqrt{4LZ + Z^2} - Z). \quad (3.39)$$

Formula 3.39 is obtained by geometrical analysis, in the paraxial approximation, similar to described in [56]. It is easy to see that $\lim_{Z \rightarrow \infty} L^* = L$.

3.6. Experimental validation and results

We have conducted a simple experiment, that demonstrates the practical usefulness of the derived models. We designed a microscope using Thorlabs light source S1FC635 Thorlabs with a central wavelength of 635nm and $\Delta\lambda = 0.8nm$. Since a single-mode fiber was used, a complete spatial coherence and limited temporal coherence was assumed. A commercial CMOS sensor UI-1942LE (3840×2748), with pixel pitch $p = 1.67\mu m$ was used to register the hologram.

We have implemented both configurations: with plane wave, as shown in Fig. 3.8 and with divergent wave with $Z = 16$ mm, as shown in Fig. 3.10. Both configurations were tested in three modes: - undersampling, causing strong aliasing, optimal mode described by Eq. 3.38 and 3.39, and mode with a too large L , when the high-frequency fringes are lost due to low temporal coherence of the source. The experimental results, shown in Fig. 3.11, are in good agreement with our expectations, as we have observed undersampling and resolution loss at the expected parameter ranges, with best resolution obtained in a good agreement with our theoretical predictions. Our digital in-line microscope, based on the configuration shown in Fig. 3.10, resolves element 5 of group 7, with feature width of $2.5\mu m$.

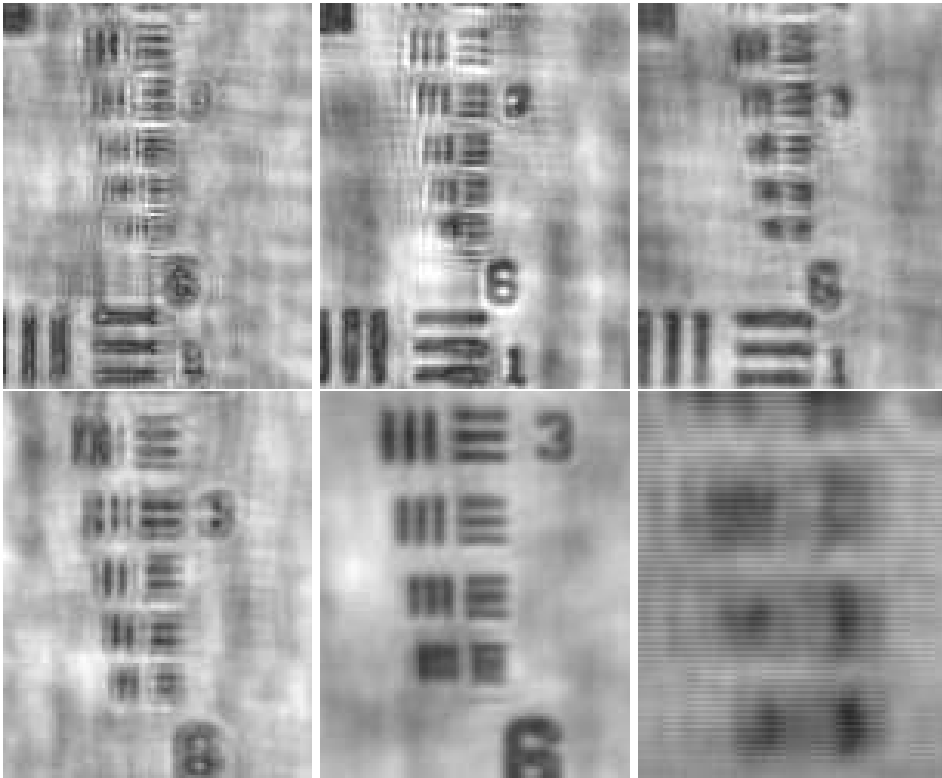


Figure 3.11: Test image of group 7 of the USAF resolution chart. Top row registered in the configuration as shown in Fig. 3.8 with $L = 2$ mm, corresponding to undersampling (left), $L = 13$ mm, corresponding to optimal case described by Eq. 3.38 (middle), and $L=26$ mm, corresponding to resolution loss due to low coherence (right). The bottom row is registered in configuration shown in Fig. 3.10 with $Z = 16$ mm, $L^* = 2$ mm, corresponding to undersampling (left), $L^* = 8.5$ mm, corresponding to optimal case described by Eq. 3.38 and 3.39 (middle), and $L^* = 26$ mm, corresponding to resolution loss due to low coherence (right).

The optimized lensless digital microscope has been further tested with biological samples. Schistosomiasis haematobium eggs ($120 \times 40 \mu\text{m}$) in a saline solution prepared on a wet glass slide was imaged using optimized lensless microscope. From the hologram registered by the detector, a high fidelity image showing the eggs with their clearly visible terminal spine was reconstructed as shown in Fig. 3.12.

In this section, we have shown that the maximum achievable resolution of a coherent in-line lensless holographic microscope is limited by aliasing and, for a plane-wave illumination, can not exceed the camera pixel size. Moreover, illumination with coherent light does not allow to achieve optimal aliasing-free imaging for a wide range of feature scales, as the aliasing conditions are significantly different for waves scattered by features with different scales. However, alias-free imaging with resolution equal

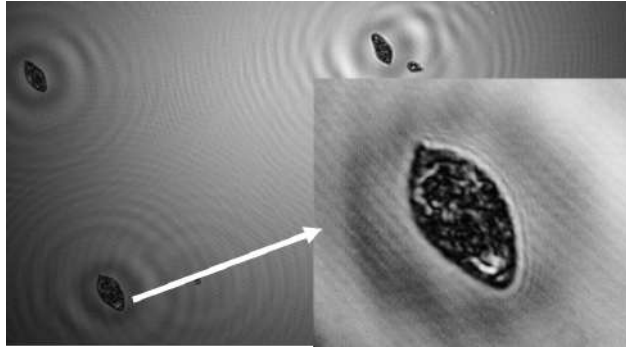


Figure 3.12: Reconstructed image of *Schistosoma haematobium* eggs in a saline solution obtained with optimal configuration of a lensless microscope.

to the diffraction limit, can be achieved, if we apply special requirements to spatial and temporal coherence of the illumination. The expressions defining the configuration delivering maximum resolution with given coherence state of the illumination are obtained for spatially and temporally incoherent, or partly coherent, light. Matching the microscope parameters to the coherence of illumination is similar to focusing the imaging lens, though the physics and tolerances of these adjustments can not be compared. Experiments, conducted by us, demonstrate clear advantage of instruments, designed with parameters, matched to the coherence of illumination.

3.7. Smart Optical Diagnostic Of Schistosomiasis (SODOS)

S. haematobium, *S. mansoni*, and *S. japonicum* are three well-known species, in this research work however, we focus on the rapid diagnosis of *S. haematobium* in urine samples. The choice is due to the fact that a urine sample is a more simple material to obtain and process [57]. Also, developing an algorithm for the detection of relatively large structures that are typically not present in normal urine is easily achievable. Compared to feces in which the eggs from the other species can be detected, urine is a more cleaner sample to work with.

Microscopic examination of *S. haematobium* eggs in urine sample using filtration, sedimentation or centrifugation techniques is the traditional method used for the diagnosis of an infected individual. The use of hand-held microscopes and cellphone-based microscopes for the diagnosis of *S. haematobium* and other parasitic diseases in field settings has been widely reported in literature [57–62]. The portability, ease-of-use and relatively low cost make this diagnostic technique attractive for the application in resource poor settings. The performance of these lens-based imaging techniques is however limited by two critical factors : (i) robustness of the imaging system, (ii) the required manual demand of sample preparation, analysis and documentation of test results. Possible misalignment of the optics, system complexity and required technical expertise for system repairs and maintenance constitute potential limitations to the

robustness of the imaging system. Cost, wide availability of recommended urine filters, power requirement of centrifuge on the field, need for sample staining and delays due to sedimentation are common factors that increase the complexity of conventional sample preparation procedures on the field.

In this work, we propose a simple, robust, easy-to-use and automated image based technique that could potentially address the above limitations using the combination of lens-less imaging and flow cytometry. The proposed method completely alleviates the burden, cost and complexity of the sample preparation methods. Automated detection, classification and counting of eggs has been achieved by use of deep learning classification routines combined with simple image processing methods. Due to the achieved minimal computational complexity the developed AI model runs smoothly on simple, low-cost general computers such as Raspberry Pi. The developed model could enable automated diagnosis which can potentially reduce manual labour. Design considerations and steps for a functional, robust and interactive prototype with mapping potentials for field test is also reported. To the best of our knowledge, no similar diagnostic method for urinary schistosomiasis has been reported in literature.

Theoretical details

Lensless imaging is a good option for the design and development of point-of-care devices for global health application [63–65]. It uses a digital sensor to directly sample the light transmitted through a specimen without the use of any imaging lenses [66, 67]. Its relative advantages over conventional lens-based microscopes include a larger field of view (FoV), decoupling of FoV from achievable spatial resolution, increased robustness and cost-effectiveness. Bright-field lens-free microscopes are largely categorized into contact-mode shadow imaging-based microscopes and diffraction-based lens-free microscopes. In the contact-mode shadow imaging-based technique, diffraction is reduced by minimizing the sample to sensor distance (typically less than $1\mu\text{m}$). Linder et al. [68] applied this on-chip imaging method for the detection of *S. haematobium* eggs by simply placing residue of centrifuged urine directly on CMOS sensors and applying computer vision to detect *S. haematobium* eggs present. The method achieves a spatial resolution that is sufficient for egg detection. However, modifying the hardware and replacing the camera sensor after every measurement increases the cost and technical requirement for maintaining such a system. Also, the need to centrifuge or sediment the urine sample increases the complexity of the sample preparation method on the field.

Our approach is based on diffraction-based lens-free Digital Inline Holography Microscopes (DIHMs). In in-line holography a spherical wave of wavelength λ , emanating from a monochromatic point source illuminates a sample as shown in Fig. 3.13.

As a result of the coherent optical field impinging on the sample plane, the shadows registered by the CCD exhibit interference fringe patterns. The fringe pattern is as a result of the interference between light scattered from an object on the sample and a reference wave that passes undisturbed through a transparent glass slide. The electric

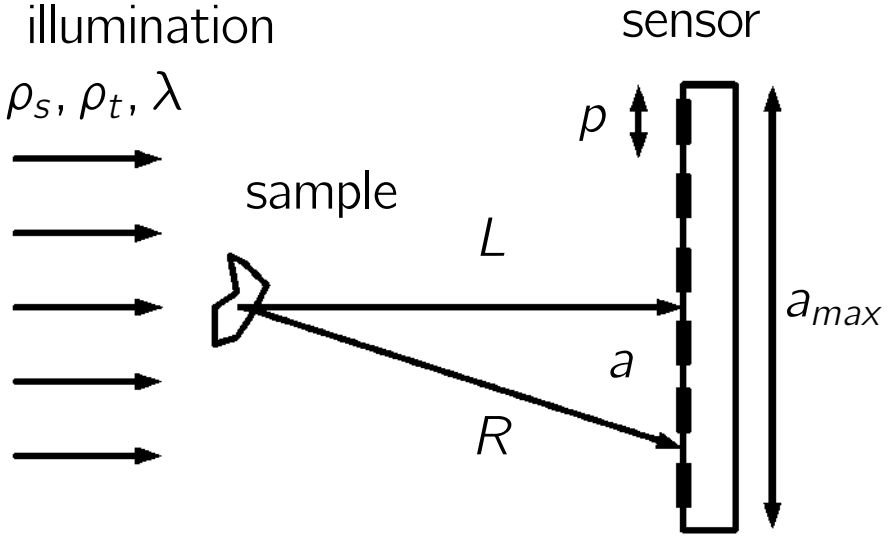


Figure 3.13: Schematic of a lensless in-line holographic microscope. The sample is illuminated with a plane wave with wavelength λ , having spatial coherence size of ρ_s and the temporal coherence length of ρ_t . The diffraction pattern is registered by a sensor with pitch p at a distance L .

field at the plane where the reference and object light waves interact can be described as the sum of the reference wave, $E_{R,s}$, and the object wave $E_{O,s}$ as shown in equation below,

$$E_s = E_{R,s} + E_{O,s} = \psi_R + \psi_O(x_s, y_s) e^{i\phi_O(x_s, y_s)}, \quad (3.40)$$

where ψ_R is the amplitude of the reference wave, $\psi_O(x_s, y_s)$ is the spatially varying amplitude (transmittance) of the object, and $\phi_O(x_s, y_s)$ is the spatially varying phase (optical thickness) of the object. The complex amplitude of the field in the object plane is numerically reconstructed from the recorded hologram by solving the inverse source problem, applying backpropagation from the sensor to the sample plane. Mathematically expressed as,

$$\begin{aligned} \psi_{rec}(x, y) &= \mathcal{F}^{-1}\{\mathcal{F}\{\psi(x, y; z)\} \times \mathcal{H}(k_x, k_y; -z)\} \\ \text{Where} & \\ \mathcal{H} &= \exp[-jk_0 z] \exp\left[\frac{j(k_x^2 + k_y^2)z}{2k_0}\right] \end{aligned} \quad (3.41)$$

where ψ_{rec} is the reconstructed optical field of the object, $\psi(x, y; z)$ is the captured hologram, and \mathcal{H} is the transfer function of free space. Our previous published work [1], defined the optimal configuration that delivers maximum resolution to a

digital inline holographic microscope. These configuration can be realized by tuning the following controlling parameters : (i) pixel size (p) of the recording sensor, (ii) linewidth $\Delta\lambda$ of the coherent illumination cone (iii) distance L between the source and the sensor plane represented by the equation below:

$$L = \frac{4p^2}{\Delta\lambda} \quad (3.42)$$

Flow cytometry

Flow cytometry is a technique that employs an optical-electronic detection device to analyze the physical and chemical properties of microscopic particles suspended in a liquid medium [69]. Modern micromachining methods have allowed even low-cost construction of microfluidic devices and flow channels that have had significant effect on the development of novel biomedical instrumentation in recent times. To avoid the complexity and cost of sample preparation, we investigated the possibility of detecting *S. haematobium* eggs by flowing infected patient urine without any staining protocol directly through a microchannel flow cell. Since microfluid flow is generally a low-Reynolds-number we expect a simple laminar flow and reduced system complexity.

In this work, we combine DIHM with flow cytometry to capture and detect eggs in the urine flow with a good spatial resolution and a depth of field not achievable by conventional optical microscopy. Because of its large depth of field, DIHM is ideally suited for capturing the 3-D motion of the target *S. haematobium* eggs with spatial resolution at micrometer level. To capture the stream lines of urine moving across the defined window (the recording area of the sensor), 10 ml of urine as required by World Health Organisation diagnostic protocol, was calibrated and pumped through the channel with an injection syringe. Holograms were precisely recorded by synchronizing the urine flow rate with the frame rate of the CMOS sensor. Using developed AI models, the reconstructed images were automatically screened for the presence of *S. haematobium* eggs.

Experimental set-up

Ethics Statement

Eggs were obtained from gut tissue of hamsters infected with *S. haematobium* in accordance with the project license that was approved by the Dutch Central Authority for Scientific Procedures on Animals (CCD) (animal license number AVD116002017106). Hamsters were sacrificed prior and eggs were obtained after ON digestion of the gut tissue with collagenase B followed by extensive washing. The morphology and size of these gut-derived eggs represent those normally seen in urine of infected humans. Anonymized urine samples provided by willing donors who gave informed oral consent were collected and spiked with approximately 200 *S. haematobium* eggs per 10 ml of urine. Although the eggs were harboured from the gut of infected hamsters, they adequately represents the eggs normally seen in the urine of infected humans both in size and in morphology. This makes them suitable for the experimental validation of

our proposed method.

The experimental setup for DIHM is designed based on the configurations presented in [1], following the schematic diagram of Fig. 1. A spherical wave of wavelength $\lambda = 635$ nm from a coherent point source (A S1FC635 Fiber-Coupled Laser Source from Thorlabs) illuminates the defined area of interest (AOI) of the microchannel flow. A geometrically magnified diffraction pattern at the sensor plane placed at distance L from the source is formed on a CMOS sensor with resolution of 3840×2748 pixels at a framerate of 3.2 fps.

To efficiently record objects moving through the defined trajectory, the sensor recording area of dimension ($6.119 \text{ mm} \times 4.589 \text{ mm}$) was aligned and matched with the defined AOI of the microchannel cell. The microflow cells used in this experiment were obtained from Ibidi (a microchannel cell manufacturing company) and has a channel width of 5 mm with a depth of 0.2 mm . The channel width of 5 mm was deliberately chosen to be of smaller dimension than the recording area of the sensor. Channel depth is not a concern in this case since DIHM allows for the digital sectioning of the microchannel through image reconstruction at different planes. Given the channel depth $d(\text{mm})$, examined volume \mathcal{V} , and the imaging area A and neglecting the effects of viscosity and friction for simplicity, urine flow time T_f can be approximated as:

$$T_f = \frac{\mathcal{V}}{A \times d * fps} = \frac{10^{-5}}{7.3424 \times 10^5 \times d} \quad (3.43)$$

Since the hologram video recording of the urine flow is memory intensive, we captured singular frames based on the exact measurement of the flow across the defined sensor window. To achieve this, we ensured a controlled flow of urine by the systematic control of the piston of the syringe with a stepper motor. This was done in such a way that the kinematics of the targets in the urine sample for example the egg (particle) motion and position can be followed at the capture rate of the image-acquisition system. Synchronizing the flow and the sensor's frame rate allows automated flow of 0.016 ml per frame. This allows the recording of 669 holographic images per urine sample of 10.7 ml , reducing the error of multiple measurements and intensive memory requirements as compared to the memory demand of video recording. The acquired holographic image frames are pre-processed and backpropagated into different planes to ensure sectioning and visualization of the whole depth of the microchannel.

Below is the summary of the procedures to obtain high-resolution DIHM reconstruction images of the target *S. haematobium* injected through the microchannels:

- Recording of holograms using a CMOS sensor. A frame rate of 0.8 frames per second which includes syringe movement, image compression and storage using the Pi 3B+ was used in the designed system.
- Recording of the microflow channel without flowing urine. The recorded image is stored as the reference image h_{ref} . The reference image contains possible manufacturing defects, dents, stains or damages on the microchannel and it is removed from subsequent hologram recordings by pixel-wise subtraction i.e., h_1

- h_{ref} , etc. Resultant image contains only object-related information (flowing eggs and other urine contaminants) required for processing.
- Foreground object detection by using simple algorithm to detect all moving objects recorded in the flow. The algorithm aims at detecting moving *S. haematobium* eggs and other fringe particles in the flow. The blob detection algorithm identifies potential areas of interest and thus reduces the dimension of reconstructed image.
- Backpropagation of the pre-processed hologram from the sensor to the sample plane. Different focusing distances are sampled to scan the entire microchannel depth.
- Reconstructed cropped region of interest is fed into a trained classifier for classification as *S. haematobium* eggs or not.

The complex amplitude of the field in the object plane is numerically reconstructed by backpropagating the recorded hologram from the sensor to the sample plane through a propagation distance of 3 mm. As a result of the depth of the microchannel flow cell of ($800\mu m$), egg flow is observed at different depths making reconstruction at different planes a critical factor to realize a sharp image. Since the dimensions of the *S. haematobium* eggs varies between $110 - 170 \mu m$ in length and $40 - 70 \mu m$ in width, we scanned the entire depth of the micro-channel using defined reconstruction distances of $400, 200, 100$ and $50 \mu m$. Acquired images are shown in Fig.(3.14 & 3.15).

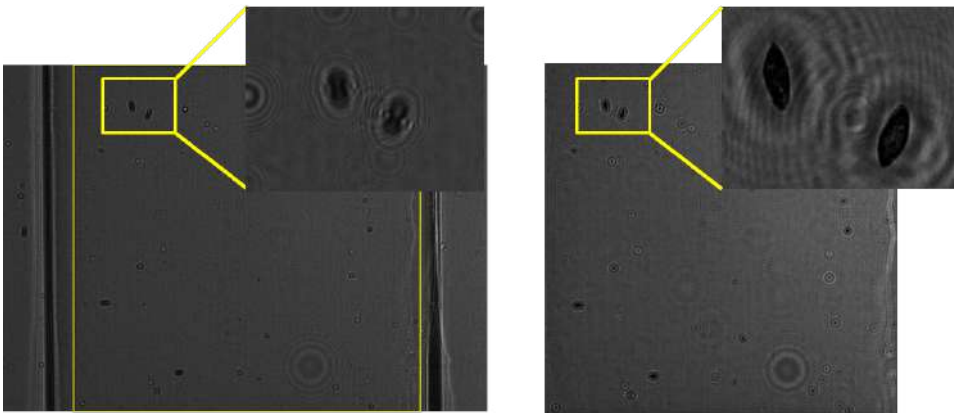


Figure 3.14: Registered hologram of the microchannel cell with flowing cultured sample shown on the left. The registered hologram consists of *S. haematobium* eggs flowing through the channel. The inset on the image on the left shows the registered fringe patterns of two eggs. The image at the right shows the reconstructed holographic image with the inset depicting the reconstructed images shown in the left image.

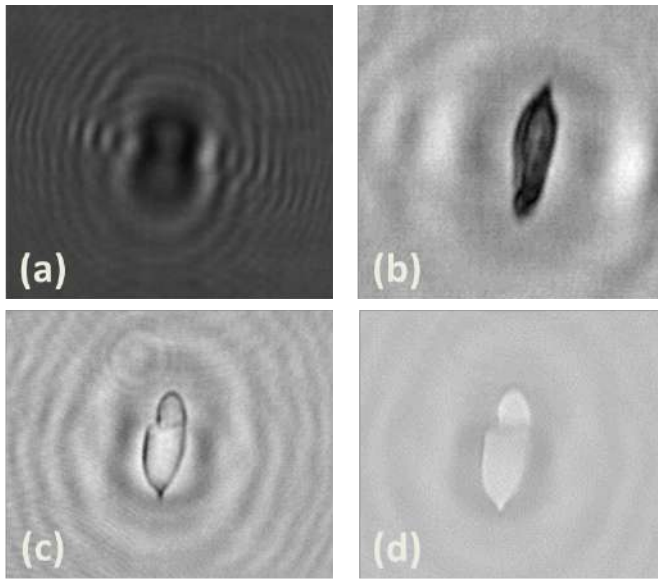


Figure 3.15: (a) Is the recorded hologram, (b) shows a reconstructed *S. haematobium* egg, (c) is the reconstruction image of an egg shell and (d) is the phase reconstruction of the egg shell.

Image analysis and detection of eggs

The developed algorithm utilizes machine learning-based methods to create AI models for detection, analysis and classification of egg image features in the reconstructed image. The training set used for the development of our classification algorithm consisted of 3,000 randomly selected reconstructed images of *S. haematobium* eggs registered from urine spiked with eggs. The second class consists of patches or sub-images of background noise, and other particles presents in urine. The images in this class are classified as "Noise". To train the classification algorithm, we performed data augmentation to create synthetic variations of the images in the training data. Specifically, we used rotations (by 90° 180° and 270°) and flips of all the four orientations. By this intermediate steps, we increased the dataset size by four times, from 3000 images to 12,208 images in each class. To reduce the variation in illumination, we normalized all the pixel values from $[0, 255]$ to $[0, 1]$. The dataset was split into a training set and a test set, with 70% and 30% of the images respectively. While the *S. haematobium* eggs are assigned a class label of 1, the background noise and particles were assigned a class label of 0. For the classifier, we specifically chose to implement and report on the Support Vector Machine classifier for it's less computational demand. Specifically, we used the C-Support Vector Classification (C-SVC) [70, 71] with a linear kernel. The normalized pixel data are the features' input for the classification model. The used training functionality for the SVM classifier is from the *Scikit-learn* [72]. On a

desktop machine with an Intel Intel i7 7700HQ (@ 2.80 GHz) processor and 16GB memory, the average training time is 4.5 seconds. The trained model demonstrated a validation accuracy of 94% after only 10 epochs. In the detection pipeline, after obtaining the coordinates of the potential ova from the localisation step, the procedure is programmed to vectorise the 64×64 sized blobs detected in the reconstructed image. The vectorized 64×64 matrices are transformed to a 4096×1 vector by concatenating the rows and therefore fed into the SVM classification model. The output of the classifier is either a zero (0) or a one (1) which represents the classes of S.H egg or not an S.H egg respectively.

The SVM classifier outperforms the 2D-DWT coupled with LDA procedure. The SVM classifier was used to demonstrate a simple classification model for the system. Convolutional neural networks (CNN) is an alternative model that can be used to replace the SVM. Also, the entire detection pipeline can be replaced with a deep-learning based object detectors but this will consequently increase the computational time as well. This work report on the proof-of-concept study and the SVM model that was used to verify the methodology, further details of the image processing algorithm and the Convolutional Neural Network models developed and tested for the classification of *S. haematobium* eggs can be found in the master thesis report [73].

Performance metrics of algorithm & result

For quantitative evaluation of our classification models, we calculated the sensitivity for *S. haematobium* egg detection at the object level as the percentage of true positive (TP) divided by true positives and false negatives (FN). The specificity on an object level was estimated as the percentage of true negatives (TN) divided by the summation of true negatives and false positives (FP). In the case of true positives, the egg detected by the algorithm is confirmed as egg after comparison with a ground truth. The ground truth corresponds to eggs manually identified in the acquired image by a medical expert. For true negatives, a non-egg detected, is actually confirmed not an egg. For false positives, what is predicted as an egg by the algorithm is actually not an egg and false negatives occurs when a detected egg is reported as a non-egg by the algorithm.

- Sensitivity provides the proportion of actual positives (eggs) that were identified correctly as eggs in a reconstructed image by the algorithm,

$$\text{Sensitivity} = \frac{\text{TP}}{\text{TP} + \text{FN}} \quad (3.44)$$

- Specificity measures the proportion of non-eggs that are correctly identified by the algorithm as non-eggs in the reconstructed image,

$$\text{Specificity} = \frac{\text{TN}}{\text{TN} + \text{FP}} \quad (3.45)$$

- The accuracy is the measure of the number of correct predictions made by the

model and is defined as:

$$\text{Accuracy} = \frac{\text{TP} + \text{TN}}{\text{TP} + \text{FP} + \text{FN} + \text{TN}} \quad (3.46)$$

According to WHO recommendation, the required competence levels for peripheral-level malaria microscopist is a sensitivity of 90%, specificity of 80% and an accuracy of 95% [74]. These standard values will be used as the benchmark in this work. Based on the defined performance metrics, the trained model demonstrated a sensitivity of 50.6%, a specificity of 98.6% and an accuracy of 96.8%. The sensitivity and specificity tests were measured by comparing the output of our detection algorithm with the result obtained from direct expert visualization and manual counting of eggs in the reconstructed images. The sensitivity and specificity of the detection algorithm can be significantly improved with a larger training data set. This proof-of-principle study was designed to validate this methodology and estimate the performance of the detection algorithm. Diagnostic sensitivity and specificity of this technique will be measured and validated with both cultured and human samples in subsequent planned study.

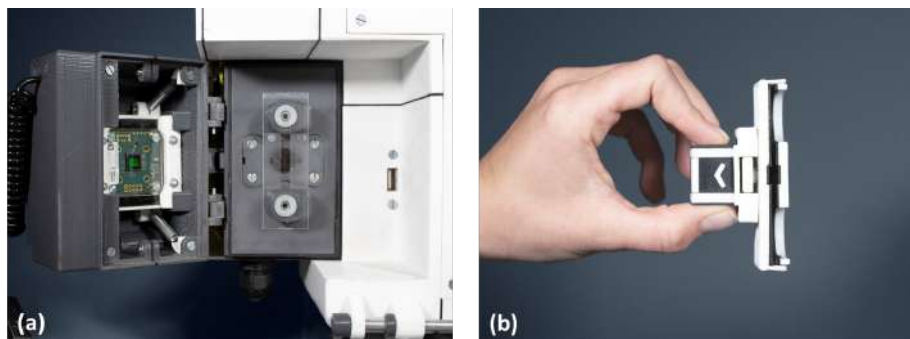


Figure 3.16: (a) Is the assembled parts of the imaging sensor & the micro-channel flow cell, and (b) the placement tool designed to allow for easy mounting and de-mounting of the micro-channel flow cells without damage. The prototypes were created using 3D printed laser cut parts in combination with standard off-the-shelf components.

System fabrication and assembly

Design challenges to realize the first prototype of the envisioned diagnostic device include designing an appropriate embodiment of the diagnostic system and providing a suitable enclosure to mount the imaging sensor, microchannel flow cell and the monochromatic source. The three main components were aligned on the same optical axis and mounted on 3D printed enclosures as shown in Fig 3.16(a). This assembly prevents stray lights and therefore reduces noise in the recorded hologram. To flow the urine sample through the microchannel flow cell, we designed an automated sample injection system shown in Fig. 3.17(b). The sample injection system uses a syringe to systematically discharge the urine sample through the cells and the outflowing urine is



Figure 3.17: (a) Is the complete diagnostic device and (b) shows the sample injection chamber where the syringe containing 12 ml of infected urine sample is mounted. The urine is pumped through the micro-channel flow-cell by an attached stepper motor to provide accurate and consistent flow. 1.3 ml of the sample is used to flush out particles from the micro-channel flow cell.

collected with a cup placed beneath the outlet of the flow cell. Since the position of the syringe is critical for system calibration, we placed a calibration sensor at the initial starting point (rest position) of the syringe. Persistent air bubbles in the microchannel flow cells reduced the diagnostic accuracy. To eliminate the air bubbles, we repeatedly pushed and retracted fluids back to the syringe and thus eliminate the air bubbles by allowing them to rise into the syringe without wasting the urine sample. Also, we created an algorithm to automatically detect these bubbles and trigger this mechanism until all bubbles are completely removed. Based on the frame rate of the imaging sensor we implemented a trigger-based mode system to enable exact acquisition of the hologram at the defined area of interest. Since the image acquisition window captures approximately 0.016 ml of the sample, the stepper motor is automated and controlled to dispel the same volume of urine accordingly. After every image acquisition, the laser diode is turned-off to reduce the power consumption and to prevent overheating. To avoid low contrast holograms, we set the exposure time of the sensor at 20 ms. A complete system is shown in Fig.3.17(a).

Major advantage of this method would be that it can be faster, high throughput (and therefore, cheaper), less labor-intensive, and maybe more sensitive if the method allows bigger volumes of urine to be tested.

Discussion

Compared to conventional lens-based microscopes, lensless computational imaging platforms are in general simpler in hardware, compact in system design and lightweight. The essential advantage of this imaging technique is that it provides complex field information of the examined biological specimen in a wide field-of-view. In this proof

of concept study, we have demonstrated a simple, less labor-intensive diagnosis of *S.haematobium* infection using a combination of a lensless in-line holographic microscope with flow cytometry technique. Our proposed method requires no sample preparation method and can therefore potentially alleviate the cost and complexity associated with conventional sample preparation technique. Computer-assisted diagnosis is achieved using low computationally expensive feature extraction binary classifier combined with simple image processing technique. The automated egg detection algorithm could potentially reduce the intensive manual labour, and the usual need for human expert associated with the conventional diagnostic methods. However, the current limitation of this technique is that over 650 holographic images are registered per sample. Required computational effort and time required to process this large amount of data is critical. For example, an average of 3.5 hours is required for the processing of 650 images registered from the flow of one 12 ml sample. The reported diagnostic time per sample is too high as compared to the current standard manual microscopy diagnostic methods that requires less than 15 minutes per test. For this method to find contributory relevance as -a point-of-care diagnostics in a resource-poor setting, the image reconstruction and egg detection algorithm must be optimized for improved time efficiency and accuracy. Current effort is ongoing in our laboratory to speed up the reconstruction and egg detection time. System performance in terms of sensitivity and specificity is also being improved. Preliminary results obtained are promising and a larger field study is being planned to validate the developed methods with human samples. We hope that our proposed methodology will complement existing point-of-need diagnostic devices for the detection of *S. haematobium* eggs in urine samples collected in resource limited settings.

References

- [1] T. E. Agbana, H. Gong, A. S. Amoah, V. Bezzubik, M. Verhaegen, and G. Vdovin, *Aliasing, coherence, and resolution in a lensless holographic microscope*, Optics letters **42**, 2271 (2017).
- [2] T. E. Agbana, O. Soloviev, V. Bezzubik, V. Patlan, M. Verhaegen, and G. Vdovin, *Wavefront coding with adaptive optics*, in *Adaptive Optics and Wavefront Control for Biological Systems*, Vol. 9335 (International Society for Optics and Photonics, 2015) p. 93350Q.
- [3] J. W. Goodman, *Introduction to Fourier optics* (Roberts and Company Publishers, 2005).
- [4] E. Verdet, *Leçons d'optique physique publiées par a*, Levisal, Victor Masson et fils, Paris **1** (1869).
- [5] E. Abbe, *A contribution to the theory of the microscope and the nature of microscopic vision*, in *Proceedings of the Bristol Naturalists' Society*, Vol. 1 (1874) pp. 200–261.
- [6] A. Ernst, *On the estimation of aperture in the microscope*, JR Microsc. Soc **1**, 388 (1881).
- [7] H. Fripp, *On the limits of the optical capacity of the microscope*, The Monthly microscopical journal **16**, 15 (1876).
- [8] M. A. Lauterbach, *Finding, defining and breaking the diffraction barrier in microscopy—a historical perspective*, Optical nanoscopy **1**, 8 (2012).
- [9] L. Rayleigh, *Xii. on the manufacture and theory of diffraction-gratings*, The London, Edinburgh, and Dublin Philosophical Magazine and Journal of Science **47**, 81 (1874).
- [10] G. B. Airy, *On the diffraction of an object-glass with circular aperture*, Transactions of the Cambridge Philosophical Society **5**, 283 (1835).
- [11] M. Born and E. Wolf, *Principles of Optics*.
- [12] J. W. Goodman, *Introduction to Fourier Optics, 3rd ed.*
- [13] J. D. Schmidt, *Numerical simulation of optical wave propagation with examples in matlab*, (SPIE Bellingham, Washington, USA, 2010).
- [14] G. Zheng, *Fourier ptychographic imaging: a MATLAB tutorial* (Morgan & Claypool Publishers, 2016).
- [15] R.E.Fisher, B.Tadic-Galeb, and P.R.Yoder, *Optical System Design*.

- [16] K.Kubala, E. R. Dowski, and W. T. Cathey, *Reducing complexity in computational imaging systems*, Optics Express **18**, 2102 (2003).
- [17] J.N.Mait, R.Athale, and J. Gracht, *Evolutionary paths in imaging and recent trends*, Optics Express **11**, 2093 (2003).
- [18] M. Mino and Y. Okano, *Improvement in the of_t of a defocused optical system through the use of shaded apertures*, Applied Optics **10**, 2219 (1971).
- [19] J. Ojeda-Castaneda, E.Tepichin, and A.Diaz, *Annular apodizers for low sensitivity to defocus and spherical aberration*, Optics Letter **11**, 487 (1986).
- [20] Z. Zhai, S. Ding, Q.Lv, X. Wang, and Y. Zhong, *Extended depth of field through an axicon*, Journal of Modern Optics. **56**, 1304 (2009), [doi:10.1080/09500340903082689].
- [21] G. Hausler, *“a method to increase the depth of focus by two step image processing,”* Optics Communication **6**, 38 (1972).
- [22] O. Cossairt and S. Nayar, *Spectral focal sweep: Extended depth of field from chromatic aberrations*, in *Computational Photography (ICCP), 2010 IEEE International Conference on* (2010) pp. 1–8.
- [23] I.De, B.Chanda, and B.Chattopadhyay, *Enhancing effective depth-of-field by image fusion using mathematical morphology*, Image Vision Comput **24**, 1278 (2006).
- [24] E. Dowski,Jr. and W. T. Cathey, *Extended depth of field through wave-front coding*, APPLIED OPTICS. **34**, 1859 (1995), [doi:10.1117/1.2338565].
- [25] J. Gracht, E. R. Dowski, M. G. Taylor, and D. Deaver, *Broadband behaviour of an optical-digital focus-invariant system*, Optics Letter **21**, 919 (1996).
- [26] P.Zammit, R.Harvey, and G.Carles, *Extended depth-of-field imaging and ranging in a snapshot*, Optica **1**, 209 (2014).
- [27] E. R. Dowski and G. Johnson, *Wavefront coding: A modern method of achieving high performance and / or low cost imaging systems*, SPIE **3779**, 137 (1999).
- [28] W. T. Cathey and E. Dowski,Jr., *New paradigm for imaging systems*, APPLIED OPTICS. **41**, 6080 (2002), [doi:10.1117/1.2338565].
- [29] S. Bradburn, W. T. Cathey, and E. R. Dowski, *Realizations of focus invariance in optical-digital systems with wave-front coding*, Appl.Opt. **36**, 9157 (1997).
- [30] A. B. Samokhin, A. N. Simonov, and M. C. Rombach, *Optical system invariant to second-order aberrations*, J. Opt. Soc. Am. A **26**, 977 (2009).

- [31] C.Ferran and S.Bosch.A.Carnicer, *Design of optical systems with extended depth of field:an educational approach to wavefront coding techniques*, IEE Transactions on education .
- [32] R.C.Gonzalez and R.E.Wood, *Digital Image Processing*.
- [33] G.Vdovin, O.Soloviev, M.Loktev, and V.Patlan, *OKO Guide to Adaptive Optics, 4th ed.*
- [34] J.Antonello, *Optimisation-based wavefront sensorless adaptive optics for microscopy*.
- [35] O. Mundanyali, D.Tsend, C.Oh, S.O.Isikman, I.Sencan, W. Bishara, C.Oztoprak, S.Seo, B. Khademhosseini, and A. Ozcan, *Compact, light-weight and cost-effective microscope based on lensless incoherent holography for telemedicine applications*, Lab Chip **10**, 1417 (2010).
- [36] S.O.Isikman, A.Greenbaum, M.Lee, W. Bishara, O.Mundayali, T.Su, and A. Ozcan, *Lensfree computational microscopy tools for cell and tissue imaging at the point-of-care and in low-resource settings*, Analytical Cellular Pathology **35**, 229 (2012).
- [37] M.Lee, O.Yaglidere, and A.Ozcan, *Field-portable reflection and transmission microscopy based on lensless holography*, Biomed. Opt.Express **2**, 2721 (2011).
- [38] A. Ozcan and E.Mcleod, *Lensless imaging and sensing*, Annu. Rev. Biomed. Eng **18**, 77 (2016).
- [39] J. B.J.Thompson and W.R.Zinky, *Application of hologram techniques for particle size analysis*, Appl. Opt. **6**, 519 (1967).
- [40] E.Mcleod and A.Ozcan, *Unconventional methods of imaging: computational microscopy and compact implementations*, Rep.Prog.Phys **79** (2016).
- [41] L.Orzo, *High speed phase retrieval of in-line holograms by the assistance of corresponding off-axis holograms*, Opt. Express **23**, 16638 (2015).
- [42] D. Gabor, *A new microscopiic principle*, Nature **161**, 777 (1948).
- [43] W.Xu, M.H.Jericho, I. Meinertzhagen, and H.J.Kreuzer, *Digital in-line holography for biological applications*, PNAS **98**, 11601 (2001).
- [44] E.Serabyn, K.Liewer, C.Lindensmith, K. Wallace, and J.Nadeau, *Compact, lensless digital holographic microscope for remote microbiology*, Opt. Express **24**, 28540 (2016).
- [45] U. Schnars and W. P. Juptner, *Digital recording and numerical reconstruction of holograms*, Measurement Science and Technology **13**, R85 (2002).

- [46] C. M.Kanka, A.Wuttig and R.Riesenberg, *Fast exact scalar propagation for an in-line holographic microscopy on the diffraction limit*, Opt.Lett. **35**, 217 (2010).
- [47] M. H. J.Garcia-Sucerquia, Wenbo Xu, *Immersion digital in-line holographic microscopy*, Opt.Lett. **31**, 1211 (2006).
- [48] P. Dunn and B.J.Thompson, *Object shape, fringe visibility and resolution in far-field holography*, Optical Engineering **21**, 327 (1982).
- [49] D.Claus, D.Iliescu, and J.M.Rodenburg, *Coherence requirement in digital holography*, Appl.Opt. **52**, A326 (2013).
- [50] J. Garcia-Sucerquia, *Noise reduction in digital lensless holographic microscopy by engineering the light from a light-emitting diode*, Appl.Opt. **52**.
- [51] U. Schnars and W. Jueptner, *Digital Holography: Digital Hologram Recording, Numerical Reconstruction and Related Techniques* (Springer, 20051957).
- [52] V. de Hulst H.C, *Light scattering by small particles* (John Wiley and Sons, 1957).
- [53] G.A.Tyler and B.J.Thompson, *Fraunhofer holography applied to particle size analysis a reassessment*, Optica Acta: International Journal of Optics **23**, 685 (1976).
- [54] F. Pedrotti, Leno.M.Pedrotti, and Leno.s.Pedrotti, *Introduction to Optics* (Pearson Education Limited, 2002).
- [55] M.Born and E.Wolf, *Principle of Optics, 7th ed.* (Cambridge University, 2002).
- [56] E. A. Sziklas and A. E. Siegman, *Mode calculations in unstable resonators with flowing saturable gain. 2: Fast fourier transform method*, Appl. Opt. **14**, 1874 (1975).
- [57] I. I. Bogoch, J. T. Coulibaly, J. R. Andrews, B. Speich, J. Keiser, J. R. Stothard, E. K. N'goran, and J. Utzinger, *Evaluation of portable microscopic devices for the diagnosis of schistosoma and soil-transmitted helminth infection*, Parasitology **141**, 1811 (2014).
- [58] J. Rajchgot, J. T. Coulibaly, J. Keiser, J. Utzinger, N. C. Lo, M. K. Mondry, J. R. Andrews, and I. I. Bogoch, *Mobile-phone and handheld microscopy for neglected tropical diseases*, PLoS neglected tropical diseases **11**, e0005550 (2017).
- [59] J. T. Coulibaly, M. Ouattara, M. V. D'Ambrosio, D. A. Fletcher, J. Keiser, J. Utzinger, E. K. N'Goran, J. R. Andrews, and I. I. Bogoch, *Accuracy of mobile phone and handheld light microscopy for the diagnosis of schistosomiasis and intestinal protozoa infections in côte d'ivoire*, PLoS neglected tropical diseases **10**, e0004768 (2016).

- [60] R. K. Ephraim, E. Duah, J. S. Cybulski, M. Prakash, M. V. D'Ambrosio, D. A. Fletcher, J. Keiser, J. R. Andrews, and I. I. Bogoch, *Diagnosis of schistosoma haematobium infection with a mobile phone-mounted foldscope and a reversed-lens cellscope in ghana*, *The American journal of tropical medicine and hygiene* **92**, 1253 (2015).
- [61] T. E. Agbana, J.-C. Diehl, F. van Pul, S. M. Khan, V. Patlan, M. Verhaegen, and G. Vdovin, *Imaging & identification of malaria parasites using cellphone microscope with a ball lens*, *PLoS one* **13**, e0205020 (2018).
- [62] N. A. Switz, M. V. D'Ambrosio, and D. A. Fletcher, *Low-cost mobile phone microscopy with a reversed mobile phone camera lens*, *PLoS one* **9**, e95330 (2014).
- [63] O. Mudanyali, D. Tseng, C. Oh, S. O. Isikman, I. Sencan, W. Bishara, C. Oztoprak, S. Seo, B. Khademhosseini, and A. Ozcan, *Compact, light-weight and cost-effective microscope based on lensless incoherent holography for telemedicine applications*, *Lab on a Chip* **10**, 1417 (2010).
- [64] M. Lee, O. Yaglidere, and A. Ozcan, *Field-portable reflection and transmission microscopy based on lensless holography*, *Biomedical optics express* **2**, 2721 (2011).
- [65] W. Xu, M. Jericho, I. Meinertzhagen, and H. Kreuzer, *Digital in-line holography for biological applications*, *Proceedings of the National Academy of Sciences* **98**, 11301 (2001).
- [66] A. Ozcan and E. McLeod, *Lensless imaging and sensing*, *Annual review of biomedical engineering* **18**, 77 (2016).
- [67] J. Garcia-Sucerquia, W. Xu, S. K. Jericho, P. Klages, M. H. Jericho, and H. J. Kreuzer, *Digital in-line holographic microscopy*, *Applied optics* **45**, 836 (2006).
- [68] E. Linder, A. Grote, S. Varjo, N. Linder, M. Lebbad, M. Lundin, V. Diwan, J. Hannuksela, and J. Lundin, *On-chip imaging of schistosoma haematobium eggs in urine for diagnosis by computer vision*, *PLoS neglected tropical diseases* **7**, e2547 (2013).
- [69] H. M. Shapiro, *Practical flow cytometry* (John Wiley & Sons, 2005).
- [70] B. E. Boser, I. M. Guyon, and V. N. Vapnik, *A training algorithm for optimal margin classifiers*, in *Proceedings of the fifth annual workshop on Computational learning theory* (ACM, 1992) pp. 144–152.
- [71] C. Cortes and V. Vapnik, *Support-vector networks*, *Machine learning* **20**, 273 (1995).
- [72] F. Pedregosa, G. Varoquaux, A. Gramfort, V. Michel, B. Thirion, O. Grisel, M. Blondel, P. Prettenhofer, R. Weiss, V. Dubourg, et al., *Scikit-learn: Machine learning in python*, *Journal of machine learning research* **12**, 2825 (2011).

- [73] P. Nijman, *Digital holography integrated with flow cytometry for detection of urinary schistosomiasis*, (2019).
- [74] W. H. Organization, *Malaria microscopy quality assurance manual-version 2* (World Health Organization, 2016).

4

Smart Optical Diagnosis of Urogenital Schistosomiasis

In Him was life, and the life was the light of men.

John 1:4

We present a simple offline method for the diagnosis of urinary schistosomiasis using a cellphone-based microscope and an inexpensive urine filtration procedure for sample preparation. Microscopic examination of the filtered urine residue is done in a single field of view (FOV), over an area of $4\text{ mm} \times 4\text{ mm}$, as compared to the manual examination of multiple fields performed using the standard diagnostic method. Using simple image processing in the spatial and spectral domains and a binary image classifier, we have shown that *Schistosoma haematobium* eggs in a registered digital image are detectable and quantifiable. We have tested the algorithm on a simple cellphone and a Raspberry Pi and achieved processing times of 5 s and 6.2 s respectively. The resulting system is robust, inexpensive and can be used for the point-of-care diagnosis of urinary schistosomiasis in low-resource settings.

Parts of this chapter is under review in Discrete wavelet transform detection of *Schistosoma haematobium* using a cellphone microscope.

4.1. Introduction

Schistosomiasis, a parasitic disease caused by blood dwelling flukes of the genus *Schistosoma*, remains a challenging neglected tropical disease (NTD). About 80% of the estimated 207 million infections are among the rural dwellers in tropical sub-Saharan countries where access to clinical diagnostic instruments is practically limited [1, 2]. Microscopic examination of the urine sample using filtration or sedimentation techniques is the traditional method used for the detection of *S. haematobium* [3–6]. Hand-held microscopes and cellphone-based microscopes have been used in field settings for diagnosis of schistosomiasis and soil-transmitted helminths in recent times mainly because they offer portability, simplicity and are inexpensive. Results from the work of Bogoch et al. [7] show that portable light microscopes provide sufficient diagnostic yield of *Schistosoma* infections, however, clear images of *S. haematobium* are difficult to obtain with the cellphone. Furthermore, although there are portable microscopes that demonstrate exceptional performance, they are expensive (approximately \$ 950) for use in low-resource settings.

On-chip imaging of *S. haematobium* eggs in urine samples for diagnosis by computer vision has been presented by Linder et al. [8]. The method achieves a spatial resolution that is sufficient for egg detection. However, modifying the hardware and replacing the camera sensor after every measurement increases the cost and technical requirement for maintaining such a system. The developed algorithms were implemented on a laptop computer, and such a system will not be practical for use in a field setting.

A summary of the results of recent field studies, which evaluated the accuracy of cellphone-based microscopes for the detection of NTDs in clinical settings has been reviewed in [9]. Cellphone microscopy using a glass ball lens has shown to be cumbersome due to the small field of View (FOV). The small FOV requires the movement of the sample which results in poor image quality, resulting in the need for multiple measurements and leading to reduced diagnostic sensitivity and specificity. The reversed-lens cell-scope has demonstrated a modest sensitivity of 67% and specificity of 100%. However, it also requires manually moving the phone over the sample for the registration of multiple FOVs as reported by Ephraim et al. [10].

According to Rajchgot et al [9], comparatively little work done has been done on realizing a simple low-cost sample preparation method which will enable the use of mobile microscopy in remote settings without laboratory infrastructure. An efficient diagnostic instrument for use in rural areas should be easily usable by community health-workers. Such diagnostic process should consist of simplified sample preparation procedure and an integrated detection algorithm that should provide simple point-of-care diagnosis of urinary schistosomiasis with reduced human intervention.

In this chapter, we propose a simple methodology that uses a low-cost chiffon filter and a cellphone-based microscope integrated with an egg detection algorithm. Urine filtration with the locally available filter is examined with the cellphone microscope in

one FOV. The registered image is immediately analysed by the algorithm to detect and quantify the number of *S. haematobium* eggs. To the best of our knowledge, this work reports the first off-line automated detection of *S. haematobium* eggs on cellphone-based microscope. We believe that this point-of-care device will complement existing diagnostic techniques for rapid diagnosis of urinary schistosomiasis particularly in rural areas.

4.2. Experimental setup and method

Ethics Statement

Eggs were obtained from gut tissue of hamsters infected with *S. haematobium* in accordance with the project license that was approved by the Dutch Central Authority for Scientific Procedures on Animals (CCD) (animal license number AVD116002017106). Hamsters were sacrificed prior to worm and egg isolation. Anonymized urine samples provided by willing donors who gave informed oral consent were collected and spiked with the obtained *S. haematobium* eggs. These samples were used for the experimental validation of our proposed method.

4.2.1. Imaging *S. haematobium* eggs

S. haematobium produces oval-shaped eggs ($110\text{--}170 \times 40\text{--}70 \mu\text{m}$ [11]) with a characteristic terminal spine which is visible when examined under a microscope. According to the optical system analysis published in Agbana et al [12], it is evident that the size of the eggs, allows for a less stringent spatial resolution requirement. For this reason, we used a cellphone-based microscope with a reversed phone objective lens similar to the one reported in Switz et al. [13] for this proof of concept experiment. Since the focal length of the objective lens (F) and the tube lens (F_o) are approximately equal in this case, the maximum achievable magnification F_o/F is therefore close to $1\times$ allowing for a FOV that is equal to the size of the imaging sensor which has a typical size of $2 - 5 \times 3 - 6 \text{ mm}$.

For this study, we used the medium-range cellphone *Moto X-style* with sensor dimensions of $5.99 \text{ mm} \times 4.5 \text{ mm}$ with pixel size of $1.12 \mu\text{m}$. Based on the Nyquist criterion, the imaging system has a theoretical limit on its spatial resolution set at $2.24 \mu\text{m}$, sufficient for the purpose of resolving the morphological details of the eggs of *S. haematobium*.

The focal length of the phone lens is 4.61 mm , and the highest image resolution is 5344×4008 pixels. We added a reversed phone objective lens with the same focal length (4.61 mm) and aligned it to the phone optical interface. This configuration provides a FOV of almost the same dimension as the imaging sensor.

We obtained fresh *S. haematobium* eggs suspended in phosphate buffered saline which were isolated from hamsters infected with *S. haematobium* as part of the life cycle that is maintained at the Department of Parasitology of Leiden University Medical Center.

10 ml of urine sample provided by donors who gave their informed oral consent were collected from the sample collection cups spiked with isolated eggs. The choice of 10 ml was to adhere to the WHO standard for obtaining quantitative information (number of eggs per 10 ml of urine) [14]. We dispensed the contents of the syringe over a mapped circular area (3 mm in diameter), on a piece of stretched chiffon sieve material. Other low-cost filtration materials were also tested in our experimental set-up. Toilet papers and coffee filter papers provide easy filtration but the poor signal-to-noise ratio (SNR) makes them less ideal candidates for low-cost filtration methods. The chiffon sieve material however has a periodic structure. Its frequency is concentrated hence the sieve can be isolated from the target eggs by pre-processing a registered image in the spectral domain.

The chiffon material, with a pore size of $18\ \mu\text{m}$, is spread over a support structure. A cup placed beneath the support structure collects the filtered urine, and a white light emitting diode (LED) is placed beneath the filter material for illuminating the sample. Filtering the sample over a marked area enables the examination of the residue in a single FOV. The images show well-defined structures such as the edges, of the eggs that make it easy to detect and quantify manually. However, for automating this process, the presence of the periodic structure of chiffon material in the background complicates the detection of the eggs using simple image processing techniques like morphological processing. Hence, alternative procedures are needed to localize the structures that represent the eggs. These procedures need to be computationally inexpensive so that it can be executable in real-time, on a cellphone.

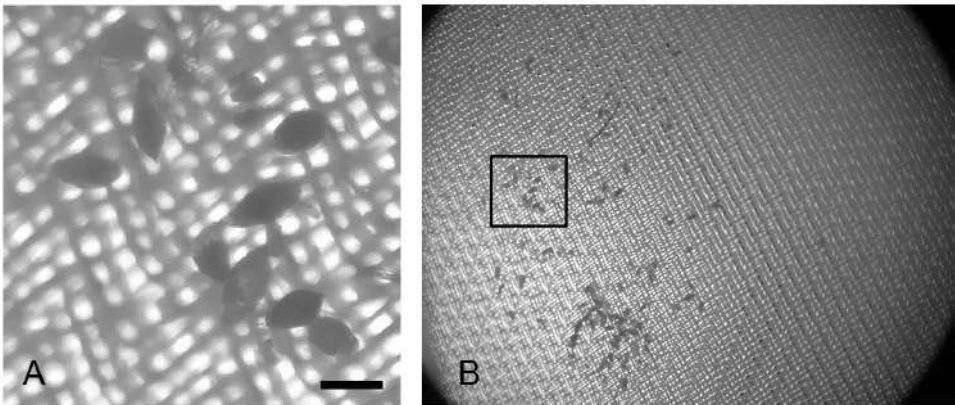


Figure 4.1: (A) is the zoomed-in version of the region in the image of the filtered 10 ml urine sample registered by a cell-phone based microscope as shown in (B). The black scale bar shown in (A) represents a width of $100\ \mu\text{m}$.

Egg detection, localization and estimation

Edge detection using simple mathematical morphological operations as reported in literature is a powerful tool for object detection in medical images [15–18]. However, these methods work well only in situations where the background of the image is plain and consistent.

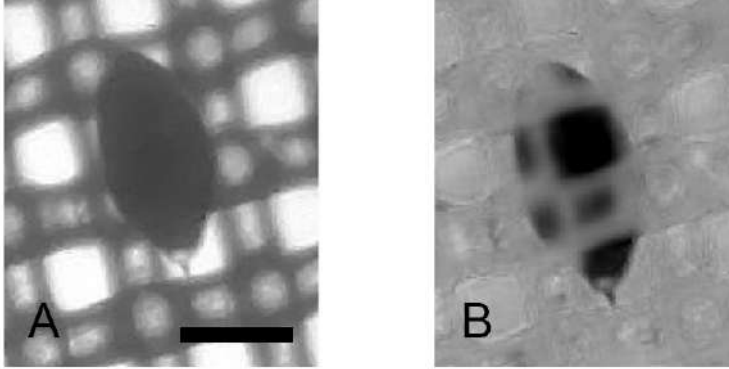


Figure 4.2: (A) shows a registered egg with the conflicting periodic sieve background, (B) is the processed image. Scale bar in (A) represents a width of $50 \mu m$.

Figure 4.2(A) is a cropped sub-image of an egg trapped by the chiffon sieve. The periodic pattern of the sieve is observed as spikes with high amplitude in frequency domain and was removed. The denoised sub-image is shown in Figure 4.2(B). Low contrast edges of the eggs as shown in Figure 4.2(B) makes accurate object segmentation and classification more difficult. We refer interested readers to the work of Sur et al as presented in [19] for a detailed discussion on the theory of the algorithm. Another valid alternative solution is to extract sub-image patches of size 64×64 pixels using the sliding window technique from the original gray-scale image. The extracted patches are fed to a trained classifier which predicts if the object of interest is contained in the patch. A patch without the egg is classified as a *not an egg* patch and discarded accordingly. However, the sliding window procedure will result in redundant detections and will require an additional overhead to resolve all the redundancies.

4.3. The proposed method

Given an acquired digital image $f(x, y)$, of size $M \times N$, its 2-D discrete Fourier transform (DFT), $F(u, v)$ - where u and v are the coordinates in the spectral domain - is computed using:

$$F(u, v) = \sum_{x=0}^{M-1} \sum_{y=0}^{N-1} f(x, y) e^{-j2\pi(ux/M+vy/N)} \quad (4.1)$$

The magnitude spectrum and phase images of the DFT computed on the original

image is shown in Figure 4.3.

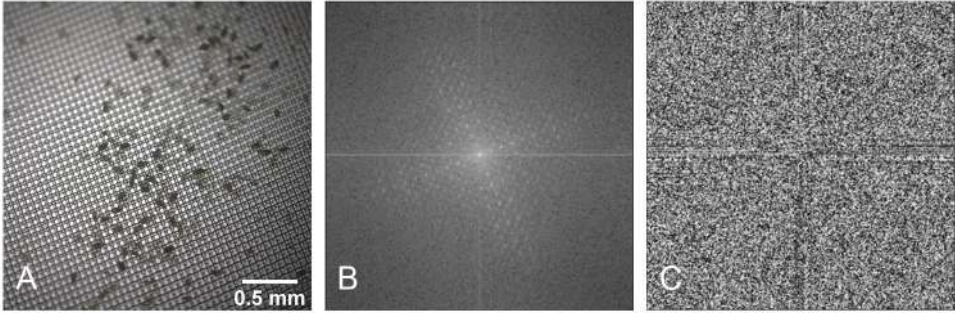


Figure 4.3: (A) is the original urine sample image, (B) and (C) are the magnitude spectrum and the phase information for the computed DFT on (A).

Applying an ideal low-pass filter (ILPF) to the computed spectral information and computing the inverse DFT using the new data, results in a blurred version of the original image with the chiffon sieve removed, as shown in Figure 4.4. The cut-off frequency used for the ideal low pass filter was set at 36Hz. At this frequency, background mesh periodic pattern was filtered out of the acquired image.

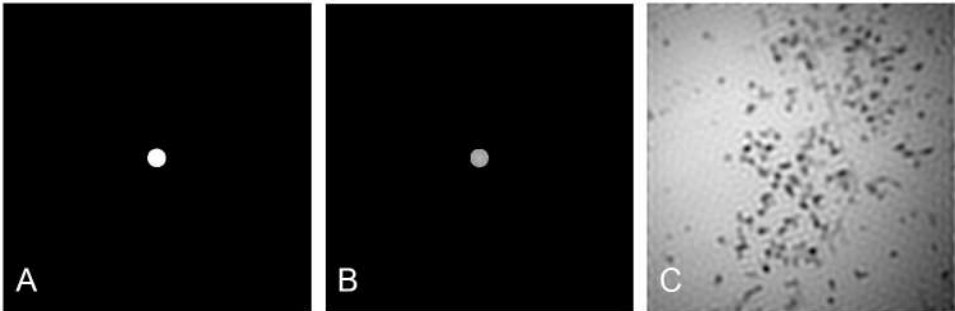


Figure 4.4: (A) is the low-pass filter mask, (B) is the filtered magnitude spectrum and (C) is the reconstructed image using the new spectral information.

The filtered image obtained in the previous section is free of the chiffon sieve. Hence, morphological operations can aid in localizing the positions of objects that are possibly eggs. We say *possibly eggs* because the image also contains other artifacts possibly due to manufacturing defects, folding of the sieve material or the presence of other unknown entities in the urine sample.

Applying an adaptive threshold procedure to the filtered image results in the image shown in Figure 4.5(C). Each white object in the resulting image is a potential candidate for an *S. haematobium* egg. The contour around each object is computable and using that data the approximate center of each object is estimable using the centers

of bounding boxes that envelop the contours. Mapping these centers to the original image provides the positions of potential eggs in the image.

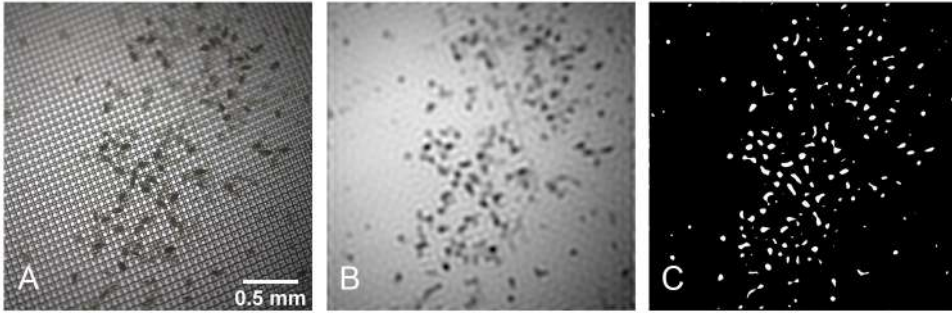


Figure 4.5: (A) is the original image of the filtered residue of a urine sample spiked with *S. haematobium* eggs. (B) represents the post low-pass filtered image and (C) is the threshold image.

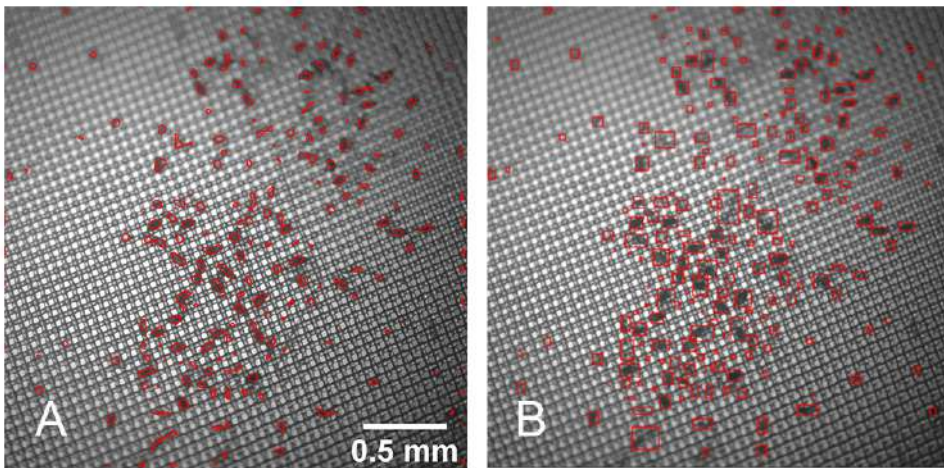


Figure 4.6: (A) shows the contours detected in the filtered image mapped to the original image and (B) shows the bounding boxes around the contours.

With the list of computed centers available, a binary classifier can classify the regions, with dimensions 64×64 , extracted about each center in the image.

4.4. Image classification using wavelet transform & statistical analysis

Egg detection can be done using a binary image classifier. In this work we compared the performance, robustness and accuracy of techniques based on wavelet decomposition and statistical analyses with a linear Support Vector Machine based classifier. Our choice of these algorithms is based on their demand for low computational power. Both algorithms are known to demonstrate fast training and prediction speed. Their memory usage demand is also minimized as compared to Neural Network, Nonlinear SVM, Logistic Regress etc. Although the Decision Trees algorithm has similar performance characteristic as our chosen algorithm, it is however prone to overfitting. Two-dimensional Discrete Wavelet Transform (2D-DWT) is applied to the input patches, formed around the expected egg centers. With this, the patch image labelled as *egg* or *not an egg* is decomposed into an approximation image and a sub-band of wavelet coefficients [16]. The wavelet representation, shown in Figure 4.7 & 4.8, is used to compute the singular value decomposition (SVD). The SVD reduces the large dataset into a lower dimensional space that exposes the underlying structure of the original data more clearly. Decision threshold level that distinguishes the *egg* class patches from the *not an egg* patches is estimated by using Linear Discriminant Analysis (LDA) on the SVD coefficient sets.

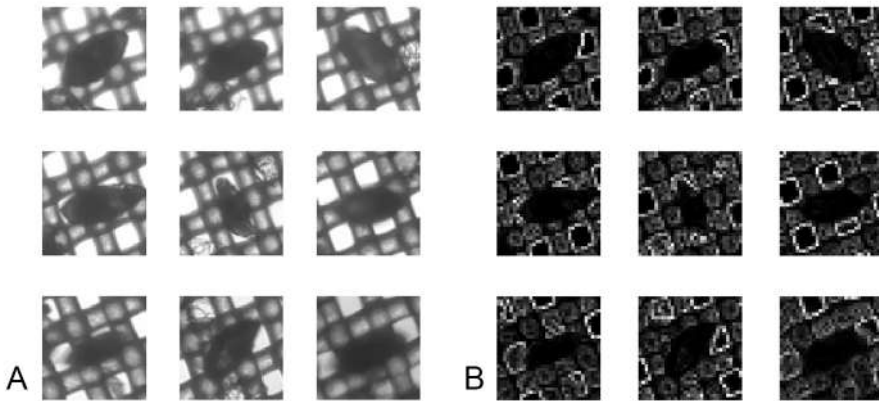


Figure 4.7: Extracted *egg* sub-image patches (A) and corresponding decomposed wavelet coefficient (B). The decomposed 2D-DWT represents the combined edge detection in the horizontal and vertical directions of the egg.

Using LDA, we find a suitable projection vector that maximized the distance between the inter-class data while at the same time minimized the intra-class data. The theory and mathematical formulation has been well described in [16].

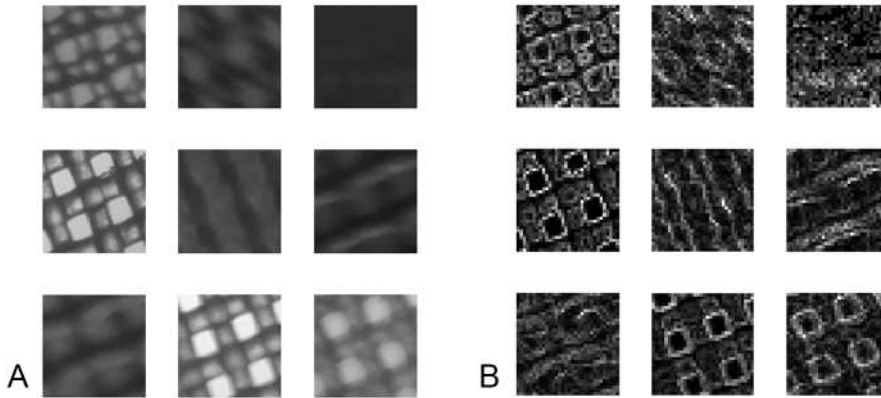


Figure 4.8: Extracted *not an egg* patches (A) decomposed into wavelet basis (B) representing the second class of data.

The training algorithm consists of four major steps:

- Image acquisition & pre-processing where the acquired image is converted from RGB into gray-scale image and resized to 2048×2048 pixels.
- Decomposition of pre-processed image into wavelet basis which provides an effective method for highlighting the edges and transitions in the sub-images.
- With the decomposed wavelet coefficients, we find the principal components/ proper orthogonal modes PCA/POD associated with the two object classes *egg* & *not an egg* using singular value decomposition.
- Based on the estimated principal components, we determine the statistical decision threshold that is sufficient to discriminate between the *egg* and the *not an egg* sub-images.

4.5. Image classification using a Support Vector Machine (SVM)

To develop this detection method, we used two classes of annotated images - *eggs* (Figure 4.7(A)) and *not eggs* (Figure 4.8(A)) - from the registered image, with 240 sub-images per class. Each cropped image is in a grayscale format, with an 8-bit depth, and has a resolution of 64×64 . We augmented the dataset to inflate it artificially, using label preserving transformations [20]. Specifically, we used rotations and flips of all the four orientations (by $90^\circ, 180^\circ$ and 270°). This step increased the dataset size by eight times, from 240 images to 1920 images in each class.

Next, we normalized all the pixel values from $[0, 255] \rightarrow [0, 1]$. We shuffled the images from each class, and split the dataset into two sets, the training set and the

test set, with 70% and 30% of the images respectively. The assigned class labels are 1 for *eggs* and 0 for *not eggs*.

The SVM formulation used is the *C*-Support Vector Classification (*C*-SVC) [21, 22] with a linear kernel. The normalised pixel values of the images are the features for training the classifier, and since the images have a resolution of 64×64 , the number of inputs to the classifier is 4096. The output of the classifier block is either a 0 (not an egg) or a 1 (an egg). On feeding the images extracted from the contour and centre detection step to the trained classifier, the procedure separates the eggs from the other objects.

We used the *Scikit-learn* [23] machine learning library for the SVM functionality. On a desktop machine with an Intel i7 7700HQ (@ 2.80 GHz) processor and 16GB memory, the average training time is 4.5 seconds. The trained model demonstrates an average accuracy of 96% on the test set.

The SVM classifier outperforms the 2D-DWT coupled with LDA procedure. The SVM classifier was used to demonstrate a simple classification model for the system. Convolutional neural networks (CNN) is an alternative model that can be used to replace the SVM. Also, the entire detection pipeline can be replaced with a deep-learning based object detectors but this will consequently increase the computational time as well.

4

4.6. Statistical analysis

For quantitative evaluation of our classification models, we calculated the sensitivity for *S.haematobium* egg detection at the object level as the percentage of true positive TP divided by true positives and false negatives (FN). The positive predictive value (precision) on an object level was estimated as the percentage of true positives (TP) divided by true positives and false positives (FP).

- Sensitivity provides the proportion of actual positives that were identified correctly,

$$\text{Sensitivity} = \frac{\text{TP}}{\text{TP} + \text{FN}} \quad (4.2)$$

- Specificity measures the proportion of non-eggs that are correctly identified by the algorithm as non-eggs in the reconstructed image,

$$\text{Specificity} = \frac{\text{TN}}{\text{TN} + \text{FP}} \quad (4.3)$$

- Positive predictive value estimates the proportion of positive predictions that was actually correct,

$$\text{PPV} = \frac{\text{TP}}{\text{TP} + \text{FP}} \quad (4.4)$$

The Null hypothesis applied in this case can be stated as: *oval shaped blob detected*

in an acquired image does not correspond to an *S.H* egg. Hence the type I and type II errors corresponding to the sensitivity and specificity of the model will be measured and determined as the performance metrics of the model. Also positive predictive value will also be evaluated.

4.7. Experimental results & discussion

An expert manually annotated a total of 320 *S. haematobium* eggs in 10 images, at a resolution of 64×64 pixels. For the *not an egg* sub-images, 320 patches are randomly cropped from the same 10 images annotated by the expert. With an imposed constraint that the center q of a *no-egg* patch can not be closer to an annotated centroid c by a distance of 32 pixels,

$$d(q_i, c_j) > 32 \quad \forall i, j \in \mathbb{N}$$

All *not an egg* training patches therefore contain either off-center eggs or no eggs at all. The patches are vectorized and represented by a vector consisting of 4096 elements and are stored as column vectors in a data matrix. A matrix of size 4096×80 generated for each class of data is therefore decomposed into wavelet coefficients using Haar wavelet. Decomposed wavelet coefficients were then used as input into an SVD algorithm. From the decomposed SVD basis, the statistical difference between the two classes was therefore estimated using the proposed LDA algorithm. A histogram of the *not an egg* and *egg* derived statistics estimated is shown in Figure 4.14. It is visually obvious that, some *not an egg* patches are mistaken for some *egg* and vice versa. This could be significantly reduced by tuning the feature to determine the optimal feature size. The red line indicates the decision threshold and patches which falls to the left of the line indicate an egg patch image and images to the right side of the line are *not an egg* patch.

The performance of the trained algorithm was tested on a test image set generated using the spectral pre-processing technique as described in the previous section. An independent expert labelled the *egg* sub-images to check the accuracy of the algorithm. Use of the pre-computed SVD matrix and LDA projection vector reduced the computational complexity of the algorithm. This makes it easily implementable on a low-cost Raspberry Pi 3B+ or cellphone.

Despite the limited number of samples available for training of the algorithm, it achieved a high sensitivity of 90.52%, a specificity of 90% and a positive predictive value of 87.5% when implemented on the cellphone. The sensitivity of the detection of the eggs correlates with the limited training data, and the use of a simple prediction model with low flexibility. Using state-of-the-art object detection models, which can today run on a modern cellphone, we can achieve a much higher sensitivity and specificity. As shown in Figure 4.10, including a bounding box around a detected target of interest (parasite candidates) allows a human expert to quickly confirm parasitic infection. This automated detection procedure could potentially result in faster sample analysis which enables the final diagnosis to be made by a human expert.

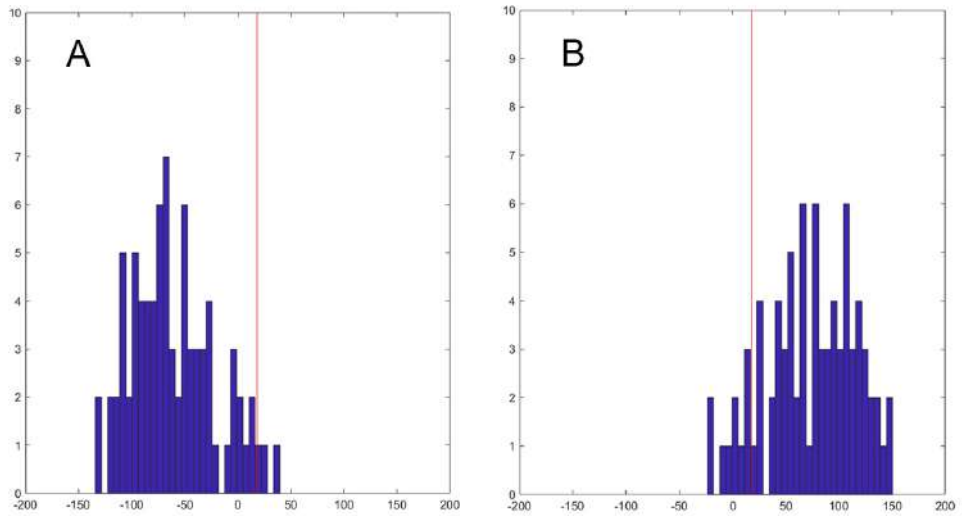


Figure 4.9: The histograms for the statistics associated with the *egg* and *not an egg* data projected onto the LDA basis. (A) is for the eggs and (B) is for *not an egg*. The red lines are the numerically computed decision thresholds. A new image will be projected onto the LDA basis and a decision will be made based on which side of the threshold line the result lies.

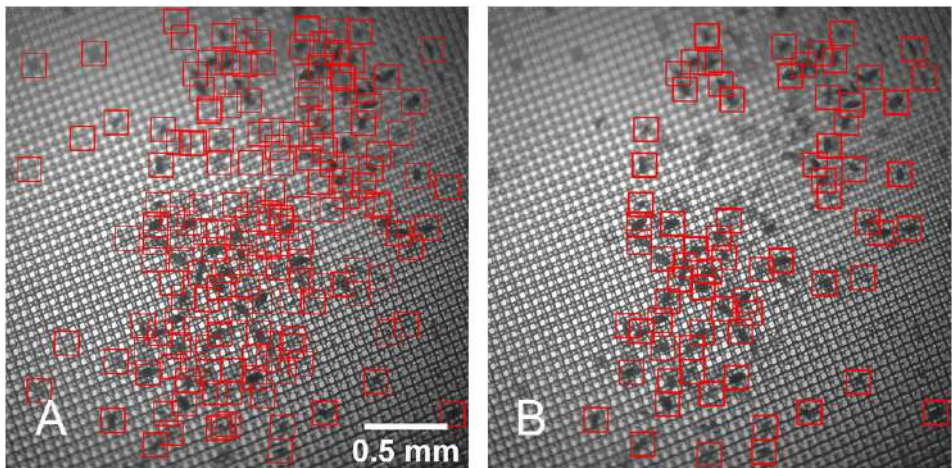


Figure 4.10: (A) shows all the 64×64 patches that are possibly eggs and (B) shows the output on filtering all the patches using the trained image classifier.

Our study adds to the findings of previous studies by showing that sample preparation process and rapid identification and detection of *S. haematobium* is feasible at the

point-of-care with a low-cost, cell-phone based microscope. Our proposed integrated smart algorithm for image analysis can be utilized to facilitate sample analysis and potentially reduce turnover time for sample evaluation. Compared to detection methods with high computational cost reported in [6, 8], our proposed method has minimal computational complexity and can be implemented on a cellphone making it deployable in resource-limited environments. Also, accurate infection load estimation by manual microscopy recommended as the gold standard diagnostic for *S. Haematobium* is prone to human error due to the manual counting of the visualized eggs. To reduce this error in practise, multiple microscopist are tasked with the responsibility of independent examination of the samples. The final documented result is based on the correlation or agreement of the individual outcome. This error of manual counting and the challenge of repeatability in measurement also constitutes a problem to the prescribed manual microscopy method. We believe that the error could be significantly reduced by our proposed method. A main limitation to this study is the limited number of samples analysed. Our goal is to test the possibility of realizing a device that provides simple and low-cost automated point of care detection of *S. haematobium* eggs in rural areas.

We have made no attempt to intensively evaluate the performance output of our device for parasite detection to conventional light microscopy method. We did not apply cross-validation in the training of the model because we observed that the cultured S.H eggs acquired with the imaging system and used in the training dataset did not fully represent what is obtainable on the field. Eggs were suspected to be calcified and appear as completely dark in our case. Although they are sufficient to verify and test our hypothesis, a larger study is being planned in Gabon. In the planned study, approximately 150-200 urine samples will be collected and analysed. From the acquired consistent dataset, various cross validation methods will be applied to increase the performance of our trained model. The success of our proposed model will eliminate the bottleneck of cloud-connected digital microscopy as samples can be locally processed, analysed and stored for future reference and analysis.

We believe that this will complement existing diagnostic method, potentially improve access to diagnosis in resource-constrained areas, decrease time for sample analysis and increase diagnostic accuracy, and larger field studies are being planned to validate these claims.

The software was written using a relevant programming language for each platform and the image processing tasks were handled using the open source computer vision library OpenCV [24]. The programming and implementation of this algorithm on a low-cost mobile-phone microscope was designed and reported as a master thesis project and the source code for the algorithm for ova detection can be obtained in [25].

The proof of concept system design was developed into a 3D printed device shown in Figure 4.11. Due to the slow development of the 3D printing technology as observed on our visit to Nigeria, we further optimised the embodiment design to reduce the amount of 3D printed parts. Using locally available aluminium sheet, the assembly parts of the third iteration of the device is shown in Figure 4.12. The optimised embodiment takes into consideration inputs obtained from stakeholders on the field.



4

Figure 4.11: Implementation of the algorithms on our device using a simple graphical user interface. The average execution time is 5 seconds on an android device. The algorithm is still being optimised for improved accuracy as some artifacts are categorized as eggs.

It features an aluminium frame and a 3D printed smart phone casing attached to it with screws and bolts. The smart phone has a small 3D printed phone objective lens holder which is aligned and attached to the phone's rear optical set-up using a double-sided tape. The focusing controller beneath consist of 3D printed parts assembled and mounted in an adjustable internal frame. Rotation of the controller provides sample translation along the z-axis to ensure the filtered sample is in focus. Adjustable internal aluminium frame is designed like a drawer to enable easy mounting and removal of the filtered samples. It also allows for easy cleaning of the device after use. Sample illumination in this case is done using a simple bike light shown in Figure 4.12. The sample mount is made of a material which is also used as a diffuser in the illumination path. The unit cost of our device is estimated at less than \$150.

A stored infected sample used for research and educational purpose at the ANDI Malaria research centre, Lagos, Nigeria was examined with our proposed diagnostic device. Figure 4.13(A) shows a typical image of an egg detected in an infected urine sample using the high-end microscope (40x objective used). Figure 4.13(B-E) shows eggs detected using our proposed, commonly available low-cost chiffon filter and our cell-phone based microscope. The detected eggs differ in colouration from the image obtained in our laboratory in the Netherlands due to the application of Lugol's iodine. We infer from the quality of the registered image, that our proposed algorithm will perform well if sufficiently large data set is acquired and used to train the model.

4.8. Discussion

Robust, simple and low-cost diagnostic tests are a necessity in low-resource settings. Wide availability of cellphones in such communities has great potentials in realizing diagnostic supports.



Figure 4.12: Assembly parts of the final iteration of the device. Parts are fabricated using 3D printed parts, locally sourced components and low-cost aluminium sheet.

In this proof of concept study, we have demonstrated a low-cost diagnosis of *S. haematobium* infection using widely available chiffon material and an inexpensive cell phone microscope integrated with smart oval eggs detection algorithms. With the chiffon material, quick filtration over a small area is realized using a 10 ml syringe potentially making diagnosis possible in just one measurement. This will translate to a reduction in diagnostic time, intensive manual labor and need for a specialized expert. Computer-assisted diagnosis is achieved using low computationally expensive feature extraction techniques. Image manipulation in both spatial and spectral domain and morphological processing have been combined with a simple binary image classifier for rapid egg detection in an acquired image. Results obtained from this analysis are promising. It

is our future research goal to optimise the robustness of the detection algorithm with datasets obtained from large number of samples from the field.

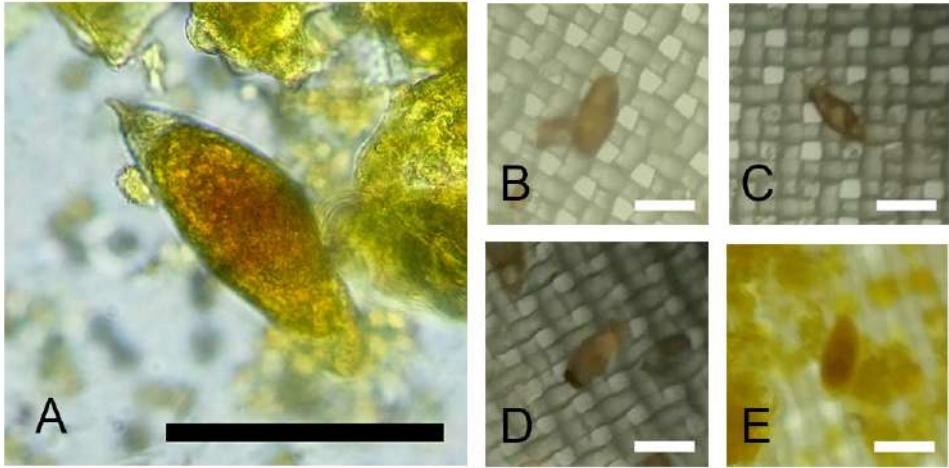


Figure 4.13: (A) is the image of an egg acquired with the Olympus microscope using the standard nylon filter. (B), (C), (D) and (E) are the images of eggs acquired with our cellphone microscope using the chiffon filter. All the scale bars shown in the five images represent a width of $100 \mu m$.

This proof of concept adds to previous research efforts in the development of low-cost point-of-care diagnostic platforms for Neglected Tropical Diseases in rural areas. Current efforts are underway to integrate the algorithm into a software application for field testing. Further validation of this technique is required before implementation in clinical settings.



Figure 4.14: The final iteration of the point-of-care diagnostics device. It can be carried in a simple, light-weight hand-held bag and can be locally produced at low-cost.

References

- [1] I. I. Bogoch, J. T. Coulibaly, J. R. Andrews, B. Speich, J. Keiser, J. R. Stothard, E. K. N'goran, and J. Utzinger, *Evaluation of portable microscopic devices for the diagnosis of schistosoma and soil-transmitted helminth infection*, *Parasitology* **141**, 1811 (2014).
- [2] D. J. Gray, A. G. Ross, Y.-S. Li, and D. P. McManus, *Diagnosis and management of schistosomiasis*, *Bmj* **342**, d2651 (2011).
- [3] S. Knopp, S. L. Becker, K. J. Ingram, J. Keiser, and J. Utzinger, *Diagnosis and treatment of schistosomiasis in children in the era of intensified control*, *Expert review of anti-infective therapy* **11**, 1237 (2013).
- [4] J. T. Coulibaly, M. Ouattara, M. V. D'Ambrosio, D. A. Fletcher, J. Keiser, J. Utzinger, E. K. N'Goran, J. R. Andrews, and I. I. Bogoch, *Accuracy of mobile phone and handheld light microscopy for the diagnosis of schistosomiasis and intestinal protozoa infections in côte d'ivoire*, *PLoS neglected tropical diseases* **10**, e0004768 (2016).
- [5] S. J. Sowerby, J. A. Crump, M. C. Johnstone, K. L. Krause, and P. C. Hill,

- Smartphone microscopy of parasite eggs accumulated into a single field of view*, The American journal of tropical medicine and hygiene **94**, 227 (2016).
- [6] O. Holmström, N. Linder, B. Ngasala, A. Mårtensson, E. Linder, M. Lundin, H. Moilanen, A. Suutala, V. Diwan, and J. Lundin, *Point-of-care mobile digital microscopy and deep learning for the detection of soil-transmitted helminths and schistosoma haematobium*, Global health action **10**, 1337325 (2017).
- [7] B. Gryseels, K. Polman, J. Clerinx, and L. Kestens, *Human schistosomiasis*, The Lancet **368**, 1106 (2006).
- [8] E. Linder, A. Grote, S. Varjo, N. Linder, M. Lebbad, M. Lundin, V. Diwan, J. Hannuksela, and J. Lundin, *On-chip imaging of schistosoma haematobium eggs in urine for diagnosis by computer vision*, PLoS neglected tropical diseases **7**, e2547 (2013).
- [9] J. Rajchgot, J. T. Coulibaly, J. Keiser, J. Utzinger, N. C. Lo, M. K. Mondry, J. R. Andrews, and I. I. Bogoch, *Mobile-phone and handheld microscopy for neglected tropical diseases*, PLoS neglected tropical diseases **11**, e0005550 (2017).
- [10] R. K. Ephraim, E. Duah, J. S. Cybulski, M. Prakash, M. V. D'Ambrosio, D. A. Fletcher, J. Keiser, J. R. Andrews, and I. I. Bogoch, *Diagnosis of schistosoma haematobium infection with a mobile phone-mounted foldscope and a reversed-lens cellscope in ghana*, The American journal of tropical medicine and hygiene **92**, 1253 (2015).
- [11] C. for Disease Control and PREVENTION, [Schistosomiasis infection](#), .
- [12] T. E. Agbana, J.-C. Diehl, F. van Pul, S. M. Khan, V. Patlan, M. Verhaegen, and G. Vdovin, *Imaging & identification of malaria parasites using cellphone microscope with a ball lens*, PloS one **13**, e0205020 (2018).
- [13] N. A. Switz, M. V. D'Ambrosio, and D. A. Fletcher, *Low-cost mobile phone microscopy with a reversed mobile phone camera lens*, PloS one **9**, e95330 (2014).
- [14] W. H. Organisation, [Manual of basic techniques for a health laboratory](#), .
- [15] T. R. Hiremath, S. M. Patil, and V. Malemath, *Detection and extraction of text in images using dwt*, Int. J. Adv. Res. Comput. Commun. Eng **4**, 533 (2015).
- [16] J. N. Kutz, *Data-driven modeling & scientific computation: methods for complex systems & big data* (Oxford University Press, 2013).
- [17] R. C. Gonzalez and R. E. Woods, *Digital image processing, prentice hall*, New Jersey (2002).
- [18] S. Livens, P. Scheunders, G. van de Wouwer, and D. Van Dyck, *Wavelets for texture analysis, an overview*, (1997).

- [19] F. Sur and M. Grediac, *Automated removal of quasiperiodic noise using frequency domain statistics*, *Journal of Electronic Imaging* **24**, 013003 (2015).
- [20] L. Taylor and G. Nitschke, *Improving deep learning using generic data augmentation*, arXiv preprint arXiv:1708.06020 (2017).
- [21] B. E. Boser, I. M. Guyon, and V. N. Vapnik, *A training algorithm for optimal margin classifiers*, in *Proceedings of the fifth annual workshop on Computational learning theory* (ACM, 1992) pp. 144–152.
- [22] C. Cortes and V. Vapnik, *Support-vector networks*, *Machine learning* **20**, 273 (1995).
- [23] F. Pedregosa, G. Varoquaux, A. Gramfort, V. Michel, B. Thirion, O. Grisel, M. Blondel, P. Prettenhofer, R. Weiss, V. Dubourg, *et al.*, *Scikit-learn: Machine learning in python*, *Journal of machine learning research* **12**, 2825 (2011).
- [24] G. Bradski and A. Kaehler, *Learning OpenCV: Computer vision with the OpenCV library* (" O'Reilly Media, Inc.", 2008).
- [25] S. Jujjavarapu, *Automating the diagnosis and quantification of urinary schistosomiasis*, (2020).

5

Optimizing The Resolution of Cell-Phone Based Microscope

And the light shineth in darkness; and the darkness comprehended it not.

John 1:5

We have optimized the design and imaging procedures, to clearly resolve the malaria parasite in Giemsa-stained thin blood smears, using simple low-cost cellphone-based microscopy with oil immersion. The microscope uses a glass ball as the objective and the phone camera as the tube lens. Our optimization includes the optimal choice of the ball lens diameter, the size and the position of the aperture diaphragm, and proper application of immersion, to achieve diagnostic capacity in a wide field of view. The resulting system is potentially applicable to low-cost in-the-field optical diagnostics of malaria as it clearly resolves micron-sized features and allows for analysis of parasite morphology in the field of $50 \times 50 \mu\text{m}$, and parasite detection in the field of at least $150 \times 150 \mu\text{m}$.

Parts of this chapter have been published in Imaging & identification of malaria parasites using cell-phone microscope with a ball lens, PLoS one 13,10 (2018) [1].

5.1. Introduction

Malaria is a life threatening disease prevalent in tropical and subtropical countries with high mortality and significant economic loss. Based on World Health Organization (WHO) report, 429,000 death cases were attributed to malaria in the year 2015. 212 million new cases of malaria worldwide was reported in the same year and about 3.2 billion people remain at risk of malaria globally [2].

Development of rapid diagnostic test (RDT) kits has enabled reliable detection of malaria infections particularly in remote areas with limited access to quality microscope services [3, 4]. However, RDTs performance have been reported in literature [5, 6] to degrade in tropical areas. Detection capabilities is low in sensitivity and specificity as compared to conventional diagnostic methods. Its current sensitivity threshold is reported to be greater than 100 parasite/ μl of blood and as such not sensitive enough to detect early-stage infections. Polymerase Chain Reaction (PCR) molecular detection methods are proven to be excellent diagnostics approaches with high efficacy. The cost of PCR equipment and the need for specialized trained personnel however restricts its usability to standard and sophisticated clinical laboratory settings. Microscopic examination of thick and thin blood smear still remains the recommended gold standard for clinical diagnosis of malaria [7, 8]. Widespread application and availability of conventional microscopy in remote low resource settings where malaria is prevalent is limited by (i) high cost, (ii) bulkiness of equipment, (iii) shortage of skilled personnel and (iv) lack of required equipment maintenance skills. Leveraging on the expansion in global cellphone network coverage, advances in cellphone imaging capabilities and computational power, simple high resolution diagnostic instrument useful in the global fight against malaria disease are fast becoming realizable. Optical techniques used in the design of cell-phone microscopy are based on (1) external optical attachment (2) on-lens design analysis and (3) on-chip optical design methodology.

Breslauer et al [9] implemented the external attachment technique by redesigning a standard microscope and attaching it to a cell-phone. The optical train attachment consist of a 60 \times achromat objective and standard eyepiece to achieve a spatial resolution of 1.2 μm . Although the authors demonstrated the application of the system in the imaging and analysis of malaria infected blood smear, the use of conventional microscope optics and the fabrication of a bulky attachments increases the cost, complexity and required maintenance skills of the instrument. To circumvent the disadvantages of the bulky optical attachment, on-lens optical design techniques offer a relatively simple and low-cost alternative. Using this technique, a refractive optical element is directly attached to the camera lens of a cell-phone. Smith et al [10] reports on using a single ball lens attachment to a cell-phone for successful diagnosis of iron deficiency and sickle cell anemia in a blood smear. The imaging capability of same technique in the detection of soil helminths in stool sample using a single 3 mm ball lens has been demonstrated in [11]. With this technique, achievable spatial resolution is limited by the aberration of the attached optics. As a result, imaging of malaria parasite within the red blood cell was difficult to realize. Using a reversed mobile phone camera lens attachment, a larger field of view with unity magnification and a spatial

resolution $< 5\mu\text{m}$ is reported in [12]. Detection of soil-transmitted helminth eggs in stool sample and imaging of red blood cells have been presented in their paper. Same technique with improved spatial resolution used for detection of *Shistosomiasis haematobium* infection on the field is reported in [13]. On-chip technique for holography based microscopy demonstrated by researchers in University of California (UCLA) requires major hardware modification [14, 15]. A fabricated holographic platform is used as a replacement for the original cell-phone objective lens. With this technique, a high field of view without loss in spatial resolution was reported. However, reconstructing a standard image from the recorded fringe patterns is computationally demanding. Furthermore, holographic microscopy requires a small sample to sensor distance [16–18]. This makes its application for imaging of blood smear and biological tissues a bit more cumbersome. Its application in the imaging of red and white blood cells as well as *Giardia lamblia* cyst has been experimentally validated.

Mobile-based optical polarization imaging device reported in [19] detects hemozoin crystals in infected blood smears. Integrated optics include low cost plastic lens assembly which increases system aberration and complexity. Since hemozoin crystals are formed at the later stage of the ring form of malaria parasite, imaging of the early ring trophozoite cannot be demonstrated.

Taking advantage of the low-cost cell-phone with high pixel resolution sensors, advances in low-power light-emitting diodes (LEDs) and 3-D printing technologies, a battery powered cell-phone based platform has been developed for field use. Optimized for use with immersion medium, our diagnostic instrument provides images with the morphology of the parasite at the early ring trophozoites and other mature stages of the parasite's developmental cycle. To the best of our knowledge, this is the first practical demonstration of imaging and morphological identification of malaria parasite using immersion based on-lens optical design techniques. This constitutes a major difference between our work and existing research works with similar optical design methodology. Giemsa staining is a simple protocol where blood smears are immersed in a staining solution containing Azure B and Eosin Y and then rinsed in with water. As the stains are chemically stable, low cost and do not require access to laboratory equipment, they can be rapidly deployed in low resource settings where access to efficient clinical laboratory infrastructure is unavailable.

5.2. Design and performance

The design of the mobile phone is optimized for photographic imaging, and imposes limitations to the optical scheme, when used in the microscope configuration. Fig 5.1 illustrates the two possible realizations of a mobile phone microscope, with the lens of the phone camera focused to infinity. In the first configuration, shown in the top

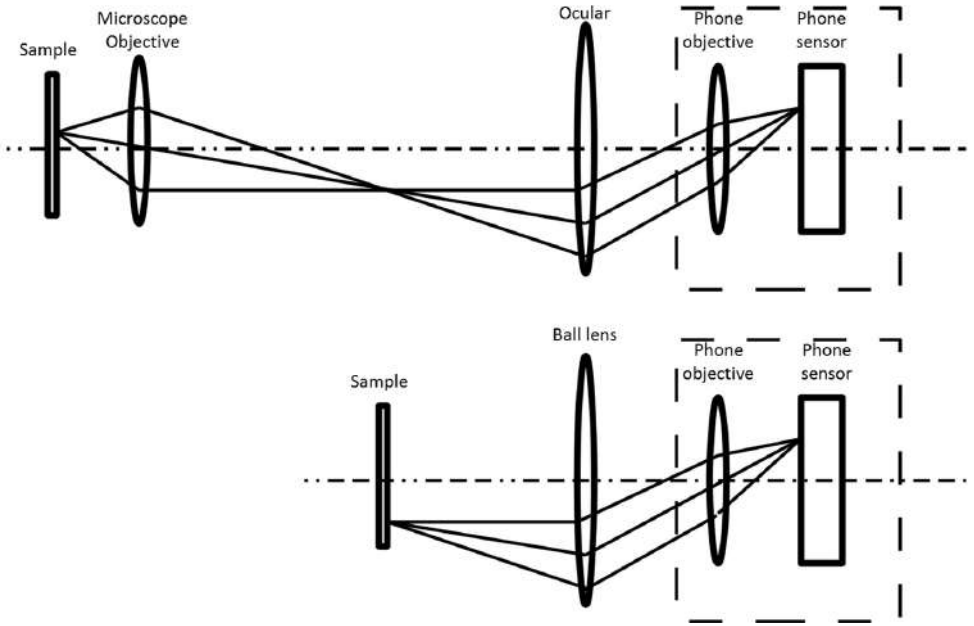


Figure 5.1: Cellphone camera coupled to classical microscope (top), and used as a tube lens coupled to external micro-objective (bottom).

of Fig 5.1, the phone camera replaces the human eye in the exit pupil of a classical microscope. Since the diameter of the phone lens (not to scale in the figure) is smaller than the average diameter of the pupil of the human eye, the phone lens tends to reduce the numerical aperture and the achievable resolution of the instrument. This scheme results in a rather bulky setup, as it requires a complete lab microscope to be present and properly coupled to the cellphone.

In the second configuration, shown in the bottom of Fig. 5.1, the mobile phone lens is used as the tube lens. It allows for a very compact implementation, with external lens mounted directly to the cellphone. However, to obtain an acceptable magnification $M \geq 1$ between the sample and the image, the external objective should have a very short focal length.

Human blood cells have disk-like shape with outer diameter in the range between 7 and 9 μm . For imaging of malaria parasite, nested inside the blood cell, the optical resolution r should be: $r \leq 1\mu\text{m}$. The corresponding minimum resolved spatial frequency is estimated as $F_{min} \geq 1/2r = 500 \text{ lp/mm}$.

The camera of a standard mobile phone has focal length in the range $F \sim 3 \dots 5$ mm, back numerical aperture of $NA \leq 0.25$, and the pixel pitch in the image sensor of $p \sim 1.25 \dots 2 \mu\text{m}$. According to the sampling theorem, one period of the maximum spatial frequency should cover at least two camera pixels:

$$p < \frac{\lambda M}{4NA}, \quad (5.1)$$

where NA is the numerical aperture. According to Rayleigh criterion, the resolution is given by:

$$r \approx \frac{0.61\lambda}{NA}. \quad (5.2)$$

So the minimum magnification M between the sample and the sensor of the phone should be at least:

$$M > 2\frac{p}{r}, \quad (5.3)$$

where p is the pixel pitch, and r is the required resolution. Assuming p in the range $1.25 \dots 2 \mu\text{m}$, and $r \approx 1 \mu\text{m}$, we obtain the condition:

$$M > 2.5 \dots 4. \quad (5.4)$$

Since the focal length of the phone objective ~ 4 mm is much smaller than the standard focal length of a tube lens, which is of the order of 200 mm, the maximum achievable magnification would be ~ 50 times smaller than with the standard tube lens. The focal length of the objective lens, according to 5.3 should be rather short:

$$F_o < F/M \approx 1.33 \text{ mm}. \quad (5.5)$$

Even $100\times$ standard microscope objective has a longer focal length, therefore glass ball lens, allowing for a very short focal lengths, is the natural choice.

References [9–11, 20, 21] mention cellphone as a promising diagnostic tool for malaria detection and exploit glass ball lenses as a cheap objective for the cell-phone based microscope. However up to date we are not aware of any practical imaging of malaria parasite with a ball-lens microscope, that allows for analysis of its morphology. It is of a great interest to perform the optimization of the optical design of the ball lens cell-phone microscope to its ultimate performance. The optimization should define the parameters, such as the material of the ball lens, the ball lens diameter, the distance from the ball lens to the phone objective, and the size and position of the aperture stop, that defines the numerical aperture and sets the diffraction limit to the achievable resolution. Optimized setup should provide the highest image quality in the widest field, with white light illumination.

For preliminary ray tracing we approximated the cellphone lens with a paraxial model. To obtain a better estimate, we used the raytracing model of a cellphone micro-objective, described by the US patent 20070024958, with focal length of $F \approx 4$ mm and the image space numerical aperture $A = 0.2$. The realistic model of

the objective allows to take into account the practically important vignetting factors. We found that for the rest, the standard phone objective has a very good correction and performs almost as good as the ideal paraxial lens. This is explained by the fact, that the numerical aperture in the image space is M times smaller than in the object space. Assuming maximum numerical aperture in the object space of $A = 0.2$ and magnification $M = 4$, we obtain $A/M = 0.05$, which corresponds to $F\# = 10$, where $F\#$ corresponds to the photographic focal number of the cellphone lens. Modern cellphone lenses are corrected for $F\# \leq 3$, therefore they are expected to have diffraction limited quality at $F\# \geq 10$.

The optical scheme of the cellphone microscope integrated with an optimized ball lens and the designed aperture, is shown in Fig. 5.2. Our multi-parametric optimization of the optical scheme, performed with Zemax Optics Studio, resulted in the following practical conclusions:

- The optimal object space numerical aperture of the glass ball microscope limited by the spherical aberration should not exceed ~ 0.2 , limiting the maximum achievable resolution. The optimal theoretical position of the system pupil is in the center of the ball lens. Since such a position is difficult (but not impossible) to implement, the next practically acceptable position for the aperture stop is directly behind the ball lens. The position and the size of the stop are rather critical for the image quality.
- The system is almost insensitive to the distance between the glass ball and the phone lens. In our simulation we have changed this distance in the range from 0.5 to 3 mm, without any significant change of the on-axis image quality. Longer distances result in significant vignetting in the off-axis areas, which are anyway strongly aberrated. Vignetting can be used to align the ball lens with the optical axis of the microscope objective, by centering the image circle on the cellphone screen.
- The field of view is limited by the off-axis aberrations of the ball lens, with major contribution from the field curvature.
- Due to high refraction difference between the cell tissue and air, the image of a blood cell in air has a very high contrast. This contrast is masking parasite inside the cell. Filling the space between the ball lens and the sample with immersion liquid mitigates the refractive index difference, allowing for clear imaging of the low-contrast parasite inside the cell. Immersion also reduces the amount of spherical aberration by eliminating the contribution of the front surface of the ball lens. The integral effect of immersion allows for a wider field of view. The type of immersion liquid is not of critical importance as long as its refraction index is close in the range between that of water $n \approx 1.33$ and glass $n \approx 1.51$.
- The chromatic aberrations did not contribute significantly to the resolution loss.

To mount the ball lens on the mobile phone, we used 50 μm aluminum foil. The ball lens was mounted between two pieces of foil with a double sided tape. The mounted

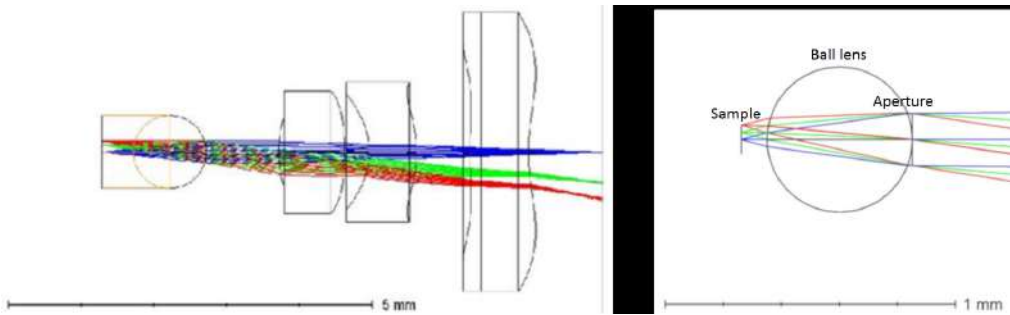


Figure 5.2: Ball lens coupled to the cellphone lens, to form a microscope and the zemax model of the aperture inserted behind the ball lens.

ball lens was aligned and attached to the cellphone with a 0.0625 mm scotch tape. The front piece, facing the sample, has aperture of about 200 to 300 μm , to provide for a sufficient field of view. The aperture stop was formed in the piece of foil facing the phone lens. The diameter of the aperture was chosen according to the results of optimization (see Table 5.1). The misalignment of the aperture stop within 10% of the aperture diameter does not constitute any serious degradation in the performance of the optical system. This is quite easily achievable in the practical implementation of the system. The glass ball was self-centered between two apertures and mounted directly on the phone. The lateral position of the ball lens assembly with respect to the phone lens was aligned by centering the defocused image circle produced by a remote extended light source.

The illumination was provided by an array of white LED, supplemented by a scatterer formed by a piece of white paper. We found that the position of the scatterer is not critical as long as the angular size of the scatterer exceeds $2NA$, where $NA \leq 0.2$ is the numerical aperture of the glass-ball microscope [22, 23].

Table 5.1 illustrates the visible polychromatic performance of the optimized glass ball microscope with 0.5 mm and 1 mm lenses in air and immersion (imm). The resolution is estimated on axis r_0 , and in the corner of the field of $50 \times 50 \mu\text{m}$ and $100 \times 100 \mu\text{m}$, r_{35} and r_{70} , where r is the *rms* radius of the geometrical point spread function. Obviously, the real resolution is limited by the diffraction limit r_{dl} for any $r < r_{dl}$. The theoretical cut-off spatial frequency at zero MTF contrast corresponding to the estimated numerical aperture (NA) at the wavelength $\lambda = 550 \text{ nm}$ is listed as F_m on table 1.

Table 5.1: Optical parameters of the ball lens microscope, optimized for the field of $100 \times 100 \mu\text{m}$, with different diameters of BK7 glass ball lens.

Ball size	Stop radius	M	NA	$r_0 \mu\text{m}$	$r_{35} \mu\text{m}$	$r_{70} \mu\text{m}$	$r_{dl} \mu\text{m}$	F_m lp/mm
0.5 air	0.09 mm	-8.5	0.24	0.95	1.28	3.6	0.95	872
0.5 imm.	0.11 mm	-11.5	0.23	1	1.5	3.1	0.85	836
1 air	0.16 mm	-6.1	0.21	1.3	1.5	2.7	1.3	763
1 imm.	0.2 mm	-4.6	0.19	1.6	2.1	2.3	1.6	690

5.3. Experimental validation

We have experimentally validated the performance of the cell-phone microscope with the optical parameters prescribed in table 5.1. The “Moto X-style” medium-range smart-phone used in our experiments has the following sensor specification: Sensor dimension is 5.99×4.5 mm with pixel size of $1.12 \mu\text{m}$. Focal length of the phone objectives is 4.61 mm and the image resolution is 5344×4008 pixels. We used 0.5 mm diameter, N-BK7 Ball Lens (Edmund Optics Stock #45 – 553) and 1 mm diameter N-BK7 (Edmund Optics #43 – 708). The aperture diaphragm prescribed in the model was created in the aluminum sheet using laser machine for maximum precision, and mounted directly on the back of the ball lens. To avoid uncertainty caused by the autofocus function, the camera phone was fixed to infinity. Self-timer was used to avoid any vibration due to touchscreen operation.

Fig 5.3 shows the image of the last group of the USAF1951 resolution target (PS7P from Pyser-SGI), obtained with a 0.5 mm ball lens. The optical system clearly resolves the maximum element in Group 9 with 645.1 lp/mm, with the width of resolved bar (r) = $0.77 \mu\text{m}$. A 1 mm ball lens, equipped with proper aperture, also clearly resolved this group, though with smaller magnification. The malaria parasites in the ring trophozoites stage have size of about $(1/5)^{th}$ of the diameter of red blood cell. Formally, the obtained spatial resolution is sufficient to detect the presence of parasite in a Giemsa stained thin blood smear. However, the parasite inside blood cell have a rather low optical contrast, therefore the practical detection of a parasite is the only ultimate criterion of the method applicability.

5.4. Practical detection of the malaria parasite

P. falciparum parasites from the NF54 strain were obtained from the Radboud University Medical Center (Nijmegen, The Netherlands). Parasites were in vitro cultured as described by Marin Mogollon et al [24]. In brief, parasites were cultured using the following conditions; RPMI-1640 culture medium supplemented with L-Glutamine and 25 mM HEPES (Gibco Life Technologies) to which was added 50 mg/L hypoxanthine (Sigma). Culture medium was supplemented with 10% human serum and 0.225% NaHCO_3 . Parasites were cultured at a 5% hematocrit under 4% O_2 , 3% CO_2 and 93% N_2 gas-conditions at 75 rpm at 37°C in a semi-automated culture system in

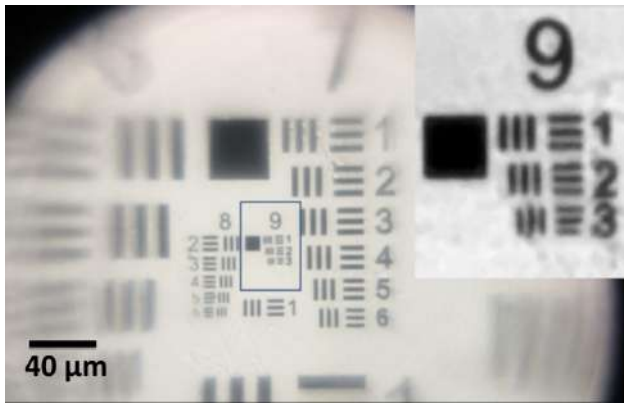


Figure 5.3: The third element of the last group of the 1951 USAF target, imaged without immersion, resolved with the optimized cellphone microscope, equipped with a properly stopped 0.5 mm ball lens. The width of the smallest resolved bar in the inset is $0.77 \mu\text{m}$, corresponding to $F_{max} = 645 \text{ lp/mm}$.

10ml flasks (Infers HT Multitron and Watson Marlow 520U). Fresh human serum and human red blood cells (RBC) were obtained from the Dutch National Blood Bank (Sanquin Amsterdam, the Netherlands; permission granted from donors for the use of blood products for malaria research and microbiology test for safety). RBC of different donors were pooled every two weeks, washed twice in serum free RPMI-1640 and resuspended in complete culture medium to 50% haematocrit. Human serum of different donors were pooled every 4 to 6 months and stored at -20°C until required. From the *in vitro* culture, thin blood smears were prepared of mixed infected Red Blood Cells (RBCs), early ring- to late schizont-stage parasites, slides were fixed in 100% methanol and stained with a 4% Giemsa staining to visualize the parasites of the blood-stage cycle as described in Janse et al [25].

Giemsa stained thin blood smears were examined using a cell-phone equipped with a 0.5 mm, NBK-7 ball lens with and without oil immersion as described in table 5.1. In the dry imaging, the light is mostly scattered on cell-to-air boundaries, resulting in cell imaging with high contrast, while the malaria parasites contained within the blood cells are hardly detectable as shown in the left of Fig. 5.4(a). Immersion in oil with refractive index ($n = 1.518$) reduces the refraction and visibility of the cell-to air interfaces and improves the relative visibility of the cell contents. Fig. 5.5 is an image of *in vitro* cultured *P. falciparum* parasites in Giemsa-stained thin blood smear taken with 1 mm ball lens cell-phone microscope using immersion oil. The *in vitro* blood sample contains infected red blood cells with parasites at different points of development. After staining, infected red blood cells are clearly visible including those containing very mature parasites (schizonts). System magnification is $4\times$ and an increased field of view of $\sim 150 \mu\text{m}$ is realized. This is an obvious gain as compared to the $100 \mu\text{m}$ field obtained with the optimized 0.5 mm ball microscope. Although

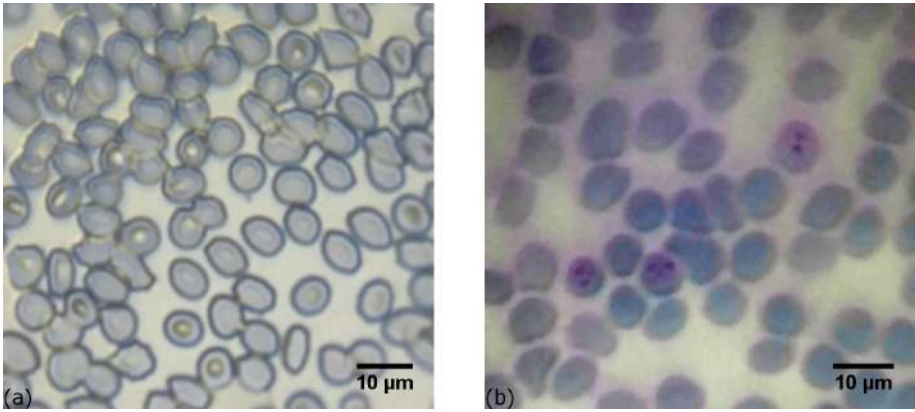


Figure 5.4: Images of *in vitro* cultured *P. falciparum* parasites in Giemsa-stained thin blood smears taken with 0.5 mm ball lens cell-phone microscope registered without immersion oil, with high contrast masking the cell contents (a) and with immersion revealing parasites inside blood cells (b).

5

this optimized design model is sufficient for the detection of *P. falciparum* infected red blood cells, the 4× magnification is, however, not sufficient for distinct discrimination of the morphology of the parasite.

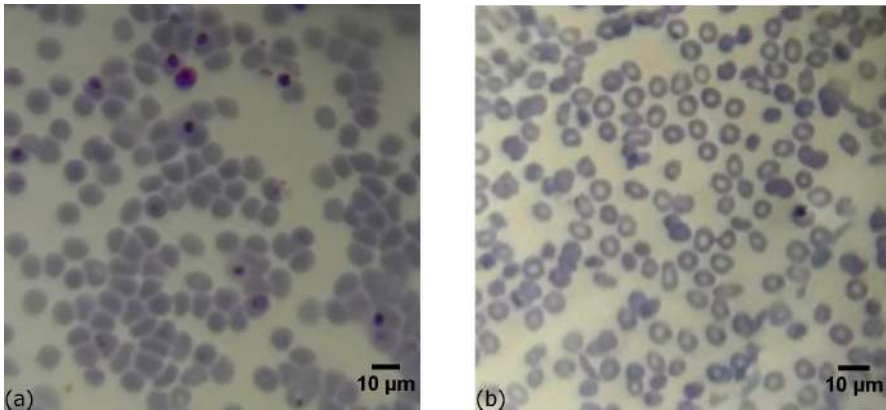


Figure 5.5: (a) depicts images of Giemsa-stained thin blood smears with *in vitro* cultured *P. falciparum* parasites taken with 1 mm ball lens cell-phone microscope and (b) is the non infected red blood cells.

To validate the presence of the parasites in the acquired images we conducted microscopic examination of healthy blood sample, subjected to the same fixation and staining process as the infected sample. An image obtained using this system configuration is shown in the right side of Fig. 5.5. The difference between the infected and the healthy samples is clearly visible.

The number of total fields required for a relevant diagnosis is determined by the field of view of the microscope. In the gold-standard case, it is approximately $180 \times 180 \mu\text{m}$ for 1.25 NA, $100\times$ oil immersion microscope objective. Current WHO standard requires 100 fields of view to provide the final determination of malaria infection. The standard limit of detection is 30 parasites/ μl of blood. The practically realized field of view of $100 \times 100 \mu\text{m}$ implies that a larger number of fields will be taken for proper diagnosis, as compared to the current standard. Considering the gains of mobility and simplicity, ball lens microscope still remains a usable tool for field diagnostics, where little or no diagnostic tool is available. The mobile phone can be used not only for imaging, but also for control and automation of the sample stage movement, providing automatic registration and pre-processing of a large number of images.

The contrast of the parasite images obtained with oil immersion is rather low as compared to results obtained from standard light microscopy, therefore post-processing algorithms that enhance the visual image contrast by extending the histogram to available dynamic range, are of great practical value. Fig. 5.6 shows the gain in contrast, obtained by registering the cellphone images in HDR mode. Since the HDR mode combines information from a number of images, the HDR mode improves both the visibility and the information contents of the image. In this particular case, it facilitates the detection of the early ring trophozoites.

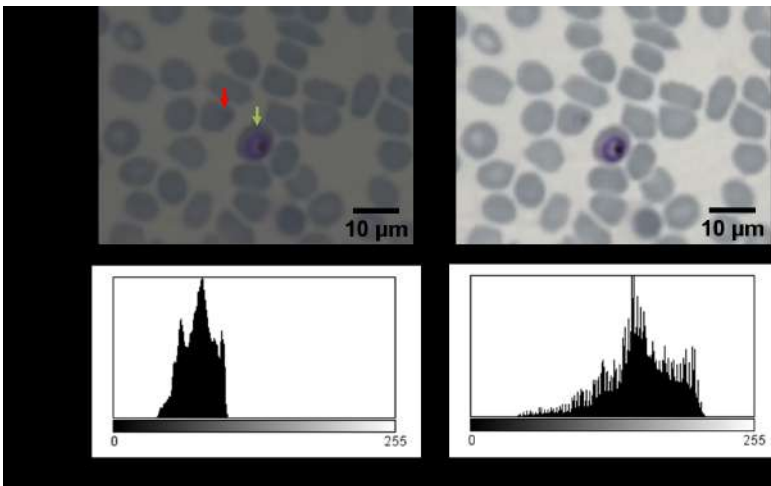


Figure 5.6: Images of *in vitro* cultured *P. falciparum* parasites in Giemsa-stained thin blood smears taken with 1mm ball lens cell-phone microscope using 4x digitally zoom. Visualizing an early ring stage trophozoite (red arrow) and a matured trophozoite (green arrow). Raw data from cell-phone microscope (a). HDR mode (b).

Fig. 5.7 compares the HDR and normal images. The (right) image is the reference, acquired using standard high resolution bright field microscope with 1.25 NA, $\times 60$ magnification and oil immersion, obtained using a high-end Zeiss Light microscope in Leiden University Malaria group laboratory. The High Dynamic Range (HDR) imaging

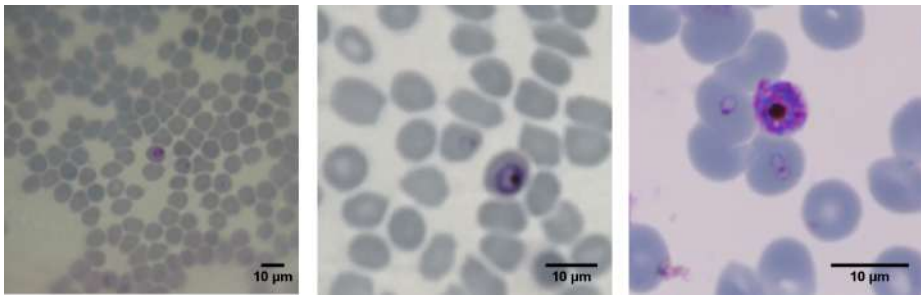


Figure 5.7: Images of *in vitro* cultured *P. falciparum* parasites in Giemsa-stained thin blood smears. Taken with 0.5 mm ball lens cell-phone microscope (left). Taken with 0.5mm ball lens cell-phone microscope, with applied 4× digital zoom and HDR mode (middle). Image of *in vivo* human *P. falciparum* infection taken by light microscope, ×60 objective obtained using a high-end Zeiss Light microscope in Leiden University Malaria group laboratory (right).

5

is especially useful for improved detectability with human operator. No other image manipulation was performed beyond reported.

The limited field of view requires a large number of images to be acquired for a reliable test outcome. To automate the procedure, we have built a simple device with an automated x-y translation stage (see Figs 5.8 & 5.9), that allows for motorized movement and easy manual image focusing of the blood smear sample. The stage is printed on a 3D printer and provides sufficient precision for acquiring a large number of sharp images over a significant field.

Our device is integrated with a single motor which provides a circular x-y movement of the blood sample. Although this rotational movement of the sample is uncommon in medical practices, we however confirmed with stakeholders that this is a viable solution since no field of view is repeated twice. This sample movement technique considerably reduces the size, price and power consumption of our device. A stepper motor 28BYJ-48 5V (with a unit cost of 1 euro) is integrated into the device using a low-cost micro-controller which cost approximately 10 €. An SP 10000 mAh Multi USB battery which cost 13 € provides a power back-up for situations of sudden power outages as common in remote settings. Total low volume cost which also includes the cost of 3d printed parts, illumination, ball lens holder, diffusers, screws and magnets used for the prototype is estimated at approximately 40 €. This price estimation excludes the cost of the integrated smart-phone. We expect that bulk production will imply a significant reduction in cost price. With image acquisition rate estimated to be in the range of 1-6 seconds per frame, diagnosis of patient sample could be completed in less than 30 minutes. The live demonstration of the system is available at: <https://www.youtube.com/watch?v=jnzKhMN1SiE&feature=youtu.be>.



Figure 5.8: Motorized prototype with automated x-y movement of blood sample, which enables fast acquisition of large number of images.



Figure 5.9: Overview of the system design (a) depicts the battery back up and micro-controller used for the digital control of the stepper motor (b) shows the circuitry while (c) depicts the attachment of the ball lens mounted in a piece of aluminum foil and attached to the smartphone with a scotch tape.

5.5. Discussion

Cellphone based microscope with a ball lens objective has been optimized for high resolution bright field imaging of malaria parasite in thin blood smears. Parasites in various stages of infection have been detected in sample infected smears. We found that the system based on the 0.5 mm glass ball lens using immersion enables morphological identification of the parasite, which is critical to accurate interpretation of the test results. It offers high spatial resolution, high system magnification ($8.5\times$) in a reduced field. The optimized system based on a 1 mm ball lens however offers a larger field of view of about $150\ \mu\text{m}$ and lower magnification ($\sim 4.5\times$), which is useful for preliminary detection. The performance has been critically analyzed with respect to optimal numerical aperture, field of view, camera pixel pitch, the system magnification, lens size, and immersion. Compared to the previously reported systems [9–11, 20, 21],

we have significantly improved the resolution of ball-lens cellphone-based microscope system. Use of immersion is instrumental for morphology identification as it allows for resolving the low-contrast contents of infected cells and reduces the field curvature, thus extending the field of view. Giemsa staining protocol is well simplified and can be implemented on the field by rural health field workers, patent medicine vendors etc. and the process of fixing with methanol is also realizable on the field. Our user design interaction interface survey with potential users and stakeholders on the field in Nigeria shows the potential of integrating our device with lab on the field diagnostic method.

References

- [1] T. E. Agbana, J.-C. Diehl, F. van Pul, S. M. Khan, V. Patlan, M. Verhaegen, and G. Vdovin, *Imaging & identification of malaria parasites using cellphone microscope with a ball lens*, PloS one **13**, e0205020 (2018).
- [2] WHO, *Malaria factsheet*, World Health Organization , cited 2018, March 4th (2016).
- [3] A. Butykai, A. Orbán, V. Kocsis, D. Szaller, S. Bordács, E. Tátrai-Szekeres, L. F. Kiss, A. Bóta, B. G. Vértessy, T. Zelles, *et al.*, *Malaria pigment crystals as magnetic micro-rotors: key for high-sensitivity diagnosis*, Scientific reports **3**, 1431 (2013).
- [4] J. G. Breman, M. S. Alilio, and A. Mills, *Conquering the intolerable burden of malaria: what's new, what's needed: a summary*, The American journal of tropical medicine and hygiene **71**, 1 (2004).
- [5] P. Yager, G. J. Domingo, and J. Gerdes, *Point-of-care diagnostics for global health*, Annual review of biomedical engineering **10** (2008).
- [6] A. Moody, *Rapid diagnostic tests for malaria parasites*, Clinical microbiology reviews **15**, 66 (2002).
- [7] W. H. Organization and C. for Disease Control, *Basic malaria microscopy* (World Health Organization, 2010).
- [8] F. Kawamoto, *Rapid diagnosis of malaria by fluorescence microscopy with light microscope and interference filter*, The Lancet **337**, 200 (1991).
- [9] D. N. Breslauer, R. N. Maamari, N. A. Switz, W. A. Lam, and D. A. Fletcher, *Mobile phone based clinical microscopy for global health applications*, PloS one **4**, e6320 (2009).
- [10] Z. J. Smith, K. Chu, A. R. Espenson, M. Rahimzadeh, A. Gryshuk, M. Molinaro, D. M. Dwyre, S. Lane, D. Matthews, and S. Wachsmann-Hogiu, *Cell-phone-based platform for biomedical device development and education applications*, PloS one **6**, e17150 (2011).
- [11] I. I. Bogoch, J. R. Andrews, B. Speich, J. Utzinger, S. M. Ame, S. M. Ali, and J. Keiser, *Mobile phone microscopy for the diagnosis of soil-transmitted helminth infections: a proof-of-concept study*, The American journal of tropical medicine and hygiene **88**, 626 (2013).
- [12] N. A. Switz, M. V. D'Ambrosio, and D. A. Fletcher, *Low-cost mobile phone microscopy with a reversed mobile phone camera lens*, PloS one **9**, e95330 (2014).

- [13] I. I. Bogoch, H. C. Koydemir, D. Tseng, R. K. Ephraim, E. Duah, J. Tee, J. R. Andrews, and A. Ozcan, *Evaluation of a mobile phone-based microscope for screening of schistosoma haematobium infection in rural ghana*, The American journal of tropical medicine and hygiene **96**, 1468 (2017).
- [14] S. Seo, T.-W. Su, D. K. Tseng, A. Erlinger, and A. Ozcan, *Lensfree holographic imaging for on-chip cytometry and diagnostics*, Lab on a Chip **9**, 777 (2009).
- [15] D. Tseng, O. Mudanyali, C. Oztoprak, S. O. Isikman, I. Sencan, O. Yaglidere, and A. Ozcan, *Lensfree microscopy on a cellphone*, Lab on a Chip **10**, 1787 (2010).
- [16] T. E. Agbana, H. Gong, A. S. Amoah, V. Bezzubik, M. Verhaegen, and G. Vdovin, *Aliasing, coherence, and resolution in a lensless holographic microscope*, Optics letters **42**, 2271 (2017).
- [17] H. C. Koydemir, Z. Gorocs, D. Tseng, B. Cortazar, S. Feng, R. Y. L. Chan, J. Burbano, E. McLeod, and A. Ozcan, *Rapid imaging, detection and quantification of giardia lamblia cysts using mobile-phone based fluorescent microscopy and machine learning*, Lab on a chip **15**, 1284 (2015).
- [18] O. Mudanyali, C. Oztoprak, D. Tseng, A. Erlinger, and A. Ozcan, *Detection of waterborne parasites using field-portable and cost-effective lensfree microscopy*, Lab on a Chip **10**, 2419 (2010).
- [19] C. W. Pirstill and G. L. Coté, *Malaria diagnosis using a mobile phone polarized microscope*, Scientific reports **5**, 13368 (2015).
- [20] R. Dendere, N. Myburg, and T. Douglas, *A review of cellphone microscopy for disease detection*, Journal of microscopy **260**, 248 (2015).
- [21] Y. Kobori, P. Pfanner, G. S. Prins, and C. Niederberger, *Novel device for male infertility screening with single-ball lens microscope and smartphone*, Fertility and sterility **106**, 574 (2016).
- [22] O. Goldberg, *Köhler illumination*, Vol. 27 (1980) pp. 15–21.
- [23] S. Bell and K. Morris, *An introduction to microscopy* (CRC Press, 2009).
- [24] C. Marin-Mogollon, M. van de Vegte-Bolmer, G.-J. van Gemert, F. J. van Pul, J. Ramesar, A. S. Othman, H. Kroeze, J. Miao, L. Cui, K. C. Williamson, et al., *The plasmodium falciparum male gametocyte protein p230p, a paralog of p230, is vital for ookinete formation and mosquito transmission*, Scientific reports **8**, 14902 (2018).
- [25] C. J. Janse, J. Ramesar, and A. P. Waters, *High-efficiency transfection and drug selection of genetically transformed blood stages of the rodent malaria parasite plasmodium berghei*, Nature protocols **1**, 346 (2006).

6

Smart Optical Detection of Malaria Parasites

*I am the light of the world whoever follows me
will never walk in darkness*

John 8:12

In this chapter we report on the novel implementation of computer-assisted dry fluorescent microscopy, optimized for efficient discovery of malaria parasite in the human blood. Computer analysis of an image containing a large number of blood cells establishes a robust statistics, resulting in the diagnostic recommendation, supplemented with the estimate of sensitivity and specificity, providing a foundation for making educated diagnostic recommendation. In our experimental implementation, the algorithm automatically identifies $\sim 10^6$ red blood cells on a thin blood smear in ~ 60 optical measurements, achieving reproducible and accurate detection of ~ 10 parasites per microliter of human blood. This performance is superior to the limit of ~ 50 parasites/ μl by WHO-recommended expert microscopy and 100-200 parasites/ μl by rapid diagnostic test. The technique, tested with *in vitro* and *in vivo* samples demonstrated its suitability for highly sensitive, robust and automated diagnosis of malaria. The method requires minimal human intervention, uses simple sample preparation, provides high degree of independence of expert judgement, and has a potential for massive community screening for malaria control and elimination programs.

The microscope has played a significant role in the diagnosis of malaria since its discovery by Laveran in 1881. Microscopy is specifically useful in cases where species identification of the parasites and assessment of the infection load is critical for appropriate treatment. It is however limited because of the requirement of a skilled microscopist and a well-maintained high power microscope facilities which are often lacking at the peripheral levels of the primary health care systems in endemic regions.

Rapid diagnostic test (RDT) represents an ubiquitous alternative to microscopy with good on-field diagnostic options [1]. Although important for epidemiological settings due to its low cost and field applicability, it achieves a detection limits in the range of 100 to 200 parasites per micro liter of blood as reported in literature [2]. Results reported in [3] confirm the high false negativity rate in PfHRP-2 detecting RDTs. The sensitivity and the robustness of the RDT diagnosis is further limited by the probability of using expired test sets, which, based on the practical experiences of the field experts consulted during this research, is quite high in rural areas.

Polymerase Chain Reaction (PCR) molecular detection has shown high efficacy and a detection level better than 1 parasite/ μ l of blood [4]. Most PCR techniques, however, remain impractical in field settings due to their cost, long processing time, and lack of appropriate laboratory facilities.

In this chapter we present a low-cost and highly sensitive method to detect malaria parasites using techniques based on fluorescent staining of the parasite. The use of fluorescent DNA stains for the detection of malaria parasite has been well studied in literature [5–7]. Its application in flow cytometry has shown increased speed, reproducibility, quantitative and quantitation estimates of malaria parasite [8, 9].

Cytometry-based fluorescent detection of malaria parasite is based on the fact that normal circulating red blood cells (RBC) lack DNA [5]. Although, the cytometry equipment has demonstrated high sensitivity (8 parasite/ μ l of blood), it is however comparatively expensive in clinical settings.

Quantitative Buffy Coat (QBC) analysis, combined with Acridine Orange fluorescent staining has demonstrated rapid, easy to interpret, and highly specific detection of malaria. The applicability, however, is limited by need for specialized equipment, cost & availability of QBC tubes [10].

In this chapter, we aimed at the following goals:

- The sample preparation procedure should be similar to the one used for the WHO-recommended gold standard test.
- The sensitivity and the specificity of the method should be significantly higher than the sensitivity of the WHO-recommended microscopy.
- The method should be based on computer processing of the data obtained from the test sample, to exclude the costly participation of trained microscopists. Such automation would extend the application of proposed test method in remote locations, where trained personnel is scarce.
- The method should deliver robust diagnostic recommendation, supplemented

with reliable statistical data derived from the composition of the blood sample, to help health workers make educated diagnostic decision.

The method described in this chapter addresses these issues. It is based on optical detection of stained fluorescent parasite in a smear containing large number of red blood cells using automated machine learning-based image processing algorithms integrated into a potentially low-cost multi-spectral imaging platform.

6.1. Statistics of the optical test

In the medical practice, the sensitivity, specificity and other statistical parameters of the test are determined by running statistical studies on population groups [11, 12]. Since optical analysis of blood samples operates with statistical probability of detecting the parasite in a large number of cells, it should be possible to derive statistical parameters such as sensitivity and specificity purely from the internal parameters of the test itself. Such an approach would result in individual estimates for robustness of the test for each patient, which is important, especially for automated diagnostic procedures, when the human expertise is not readily available.

Microscopic test for malaria relies on discovery and counting of the parasite in the image of blood smear. In practice, the total number of cells in the sample is limited to N . The parasitemia p is defined as the ratio of infected to the total number of blood cells in an infinitely large sample. The probability to discover even a single parasite is limited by the size of the sample. The smaller the sample, the higher the probability to miss the infected cell.

The sensitivity of the test S is defined as the probability to obtain positive diagnosis with diseased patient. The specificity Ω is defined as the probability to obtain a negative diagnosis with a healthy patient. Apparently, the ideal test correctly identifies all diseased and healthy cases: $S = \Omega = 1$. The probability of false identification γ is defined as the probability of a randomly chosen healthy cell to be falsely identified as infected. Accounting for the false positives, the expected number \bar{m} of positive counts in the test is given by $\bar{m} = N(p + \gamma)$.

With an ideal error-free method with $\gamma = 0$, the statistical probability P_m to detect m parasites in a sample with cell count N with parasitemia p is described by the Poisson statistics. For $p \ll 1$ (in medical practice $p = 10^{-7} \dots 10^{-2}$), the probability P_m can be approximated as:

$$P_m = \frac{(Np)^m e^{-(Np)}}{m!}. \quad (6.1)$$

Equation 6.1 describes the statistics of test outcomes, therefore it can be used to predict the test sensitivity and specificity without conducting statistical studies involving large groups of human patients. The probability to obtain a negative result with infected sample can be obtained by substituting $m = 0$ in 6.1:

$$P_0 = e^{-N(p+\gamma)}. \quad (6.2)$$

Then, the sensitivity S_0 of the method with cell count N and $\gamma = 0$ is limited by,

$$S_0 = 1 - P_0 = 1 - e^{-Np}. \quad (6.3)$$

Figure 6.1 illustrates the dependence of S_0 on the sample parasitemia p for different sample volumes N . To satisfy the condition $S_0 > T$, where T is the required threshold sensitivity, the test parameters p and N should satisfy the condition:

$$p > -\frac{\ln(1 - T)}{N}, \quad \text{or} \quad N > -\frac{\ln(1 - T)}{p}. \quad (6.4)$$

To achieve $S_0 > 0.9$ the test parameters should be: $p > 4.6 \cdot 10^{-5}$ for the WHO gold standard test with $N = 50 \cdot 10^3$, $p > 2.3 \cdot 10^{-6}$ for a test with $N = 10^6$, and $p > 2.3 \cdot 10^{-7}$ for a test with $N = 10^7$.

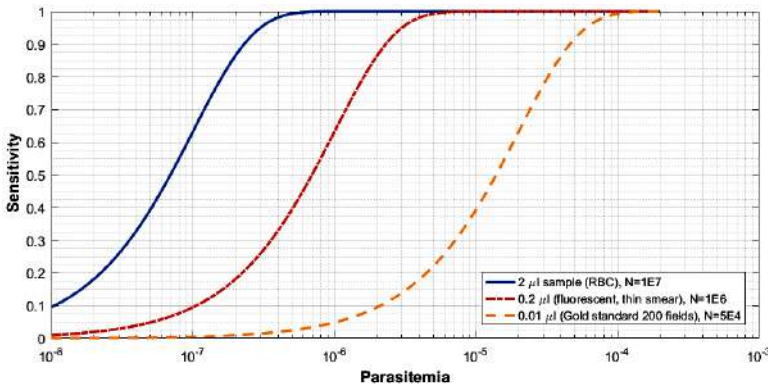


Figure 6.1: Theoretical sensitivity S_0 for different sample counts

If the probability γ of false positive identification is equal to zero, the test specificity Ω is equal to 1. However, if the false identification is possible, which is the case in optical diagnostics, then, similar to equation 6.3, the specificity Ω is given by

$$\Omega = e^{-N\gamma}. \quad (6.5)$$

Based on the preceding analysis, we have drawn the following conclusions:

- The maximum sensitivity is limited by the total cell count N in good agreement with Eq. 6.2, higher cell count N secures higher sensitivity.
- The test specificity is high at lower rate of false counts γ , however the number of false counts grows with N , so large values of N can be disadvantageous for high specificity.
- The statistics of healthy and infected blood cells in the blood smear can be used to make the estimate of the test robustness without addressing large groups of patients.

6.2. Experimental implementation

As follows from the analysis, the advanced method should provide the ability to analyze a large number of RBCs, provide high reliability of parasite identification and be very selective to false images of the parasite.

We developed a method that satisfies to these requirements. It is based on the use of very wide field medium resolution fluorescent microscopy in air, combined with computer image processing.

The test includes registration of images of fluorescent-stained dry blood smear:

- Fluorescent image: excitation of the DNA bound stains by illuminating the sample with a UV LED. Parasites, fluorescent in visible spectrum, are registered as bright spots on a black background.
- Acquisition of bright field images of the same region.

The microscope should be good enough to resolve the red blood cell, but it is not required that the parasite image is resolved in detail. In our experiments we used a 10×0.25 objective.

The parasites are counted as "true" and "false" by localizing their positions with respect to the positions of RBC. The image analysis is performed by a convolutional neural network. An image processing algorithm has been developed to perform the following tasks:

- Elimination of all spurious bright spots, including white blood cells and all spots that are much bigger than the parasite image.
- Detection of RBCs in the registered bright field image.
- Counting the bright fluorescent spots and classifying them as parasite by a neural network.

To validate the method, we built a multispectral microscope that included 10×0.25 achromatic microscope objective and CMOS camera UI-3070CP with $3.5 \mu\text{m}$ pixel size and sensor size of $\sim 5 \times 7$ mm. The combined light source included a 370nm UV LED for the parasite fluorescent imaging and white light LED for bright field RBC imaging. The design provides total field of view of about 0.9×1.25 mm in the sample plane.

6.3. Laboratory characterization

Plasmodium falciparum parasites from the NF54 strain were obtained from the Radboud University Medical Centre (Nijmegen, The Netherlands). Parasites were in vitro cultured as described in [13]. Infected thin blood smears were stained with Hoechst 33342 dye and fixed in methanol according to standard protocols. Registered bright and corresponding dark field fluorescent images are shown in Fig. 6.3.

To investigate the detection sensitivity of the proposed fluorescent diagnostic method, a dilution experiment was performed at the ANDI Center of Excellence for Malaria

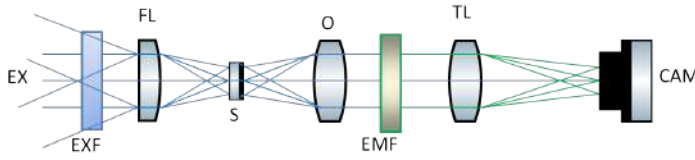


Figure 6.2: Diagram of trans-illumination fluorescence microscopy set-up. An ultraviolet LED excitation source ($EX = 370\mu m$) is placed beneath the sample. Excitation filter (EXF) enhances the spectral purity of the LED. The beam is focused to the sample (S) by a focusing condenser lens (FL). Emitted signals are collected by the objective lens (O) and filtered by the emission filter (cutoff = $490\mu m$). Filtered signal is focused to the CMOS sensor at the focal plane by the tube lens (TL).

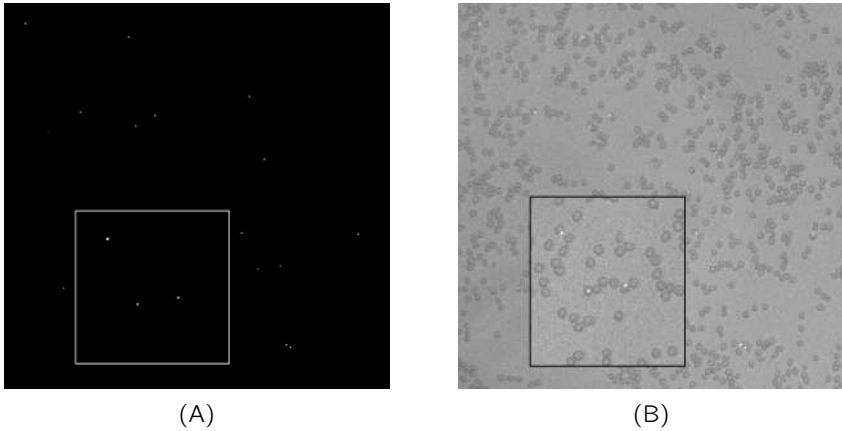


Figure 6.3: Dark field (A) and the sum of dark field and bright field images (B) of infected thin blood smear with fluorescent parasite clearly visible.

Diagnosis, Nigeria in January 2018. The samples were collected by the ANDI Malaria Diagnostic centre with an ethical approval by the Health Research Ethics committee of College of Medicine of the University of Lagos with the Number: CMUL/HREC/11/17/261. Written informed consent was sought from all participants.

Dilution analysis was done using the infected blood sample with the highest parasitemia ($70,307$ parasites/ μl of blood). The parasitemia was estimated by experts using WHO recommended standard Giemsa stained microscopy technique.

The blood sample was serially diluted with blood from an uninfected donor to realize parasitemia levels in the range $p = 1.4 \cdot 10^{-2} \dots 1.7 \cdot 10^{-6}$. To ensure the uniform parasite distribution, the diluted blood was mixed for one hour after each dilution. The result of the experiment is reported in Fig. 6.4. The experimentally measured parasitemia fits the curve

$$p = \exp(-C_1 D - C_2), \quad (6.6)$$

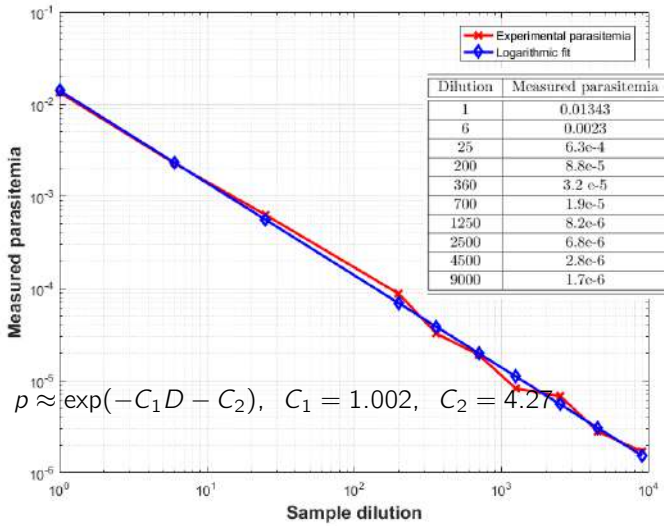


Figure 6.4: Detected parasitemia p as a function of dilution D .

where D is the dilution rate, corrected for the RBC concentration in the healthy donor blood, ($D = 1 \dots 22400$), $C_1 = 1.002$, and $C_2 = -4.27$. The good quality of logarithmic fit with $C_1 \approx 1$ preliminary confirms the validity of the method for samples containing as low as ~ 10 parasites per μl of blood. In this measurement, detection of the parasitemia at levels of ~ 10 parasites per μl of blood, required computer processing of more than 60 wide field images of thin blood smear, accounting for the total of $\sim 10^6$ RBCs.

6.4. Malaria detection in fresh patient samples

Forty fresh patient samples were collected from a secondary health facility in Lagos, Nigeria. The samples were labelled, and screened for malaria parasite using malaria microscopy, Rapid diagnostic tests, fluorescent diagnostic method and Polymerase chain reaction. The four different diagnostic techniques were implemented independent of each other to enable unbiased analysis as outlined below:

1. SD Bioline malaria Ag PF Rapid Diagnostic Test (RDT) kits were independently used to detect malaria infection in the patient samples.
2. Expert level malaria microscopy based on the WHO approved standard protocol. Each blood smear was made in duplicate and read independently at $\times 1000$ magnification by two experienced WHO certified microscopists. Malaria parasites were counted simultaneously with the white blood cells in every observed field of view.
3. Fluorescent diagnostic method (FDM) proposed in this work. The blood samples

were prepared and tested using computer-assisted analysis of fluorescent parasite signatures. The parasitemia was estimated according to the standard described by WHO in reference [14].

4. Real-time Polymerase Chain Reaction (PCR) analysis based on the method by [15] was performed at the Erasmus MC University Medical Center, Rotterdam The Netherlands. To realize the test in Rotterdam, forty $5 \mu\text{l}$ dried blood spots of patient samples prepared at the ANDI Malaria research centre were stored and transported to Rotterdam.

Due to its high sensitivity, specificity and accuracy, PCR analysis of the collected sample was used as our reference standard in this study. One of the 40 samples analyzed tested positive after sample analysis with standard microscopy. RDT detected three malaria positive samples, however one turned out to be a false positive when the results were compared with the outcome of PCR analyses. FDM detected 5 malaria infected samples. When compared to the standard reference PCR results, FDM realized a sensitivity of 100% and specificity of 97%. Malaria microscopy provides a sensitivity of 20% and a specificity of 100%. A sensitivity of 40% and specificity of 94% was reached by RDT respectively.

For high sensitivity S , a large number of fields has to be analyzed to reach the sufficient RBC count N . With multispectral fluorescent imaging and computer image processing of a thin smear, the procedure is much easier than the WHO gold standard method. However, to further efficiently reduce the diagnostic time keeping the computational complexity at minimum, a simplified method which uses a single thick smear with a large number of RBC in many layers was used. The image structure of a thick smear is more complicated, however the number of cells in one field can be very high, providing obvious practical advantages for quick screening. In the thick smear method only one dark field fluorescent image is registered. This image is filtered for white blood cells and all bright spots with deviating morphology. The remaining bright spots are designated as infection. Figure 6.5 illustrates the efficiency of filtering algorithm on the images of thick smears of infected and healthy blood.

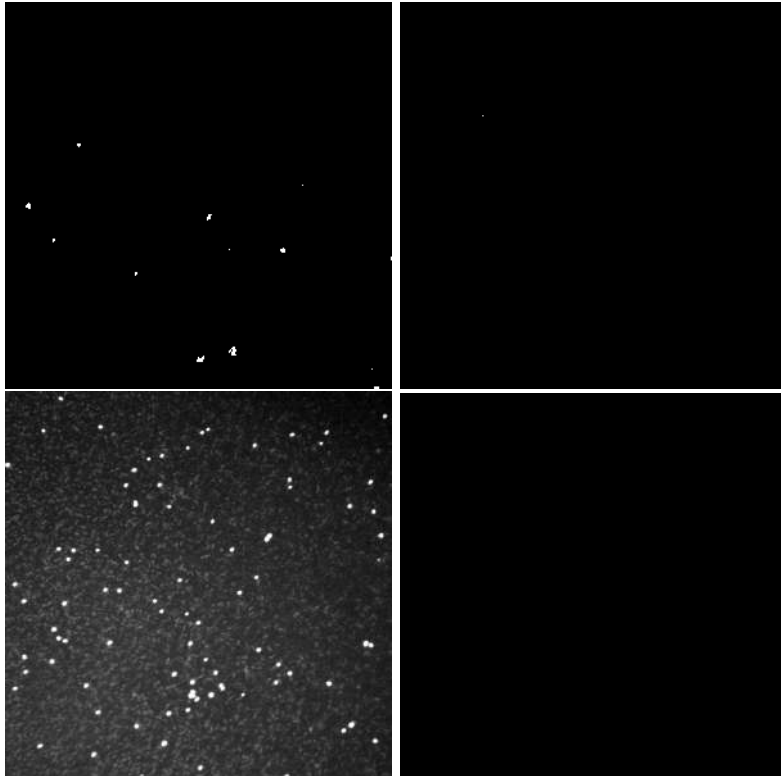
Quite obviously, the probability of false detection γ is expected to be higher for this method, compared to the method that takes into account the parasite localization in a thin smear. To obtain $S > 0.9$ & $\Omega > 0.9$ for $p > 5 \cdot 10^{-5}$, the number of RBC in the single field of view thick smear should satisfy to the condition $N > 5 \cdot 10^4$, which is easily achievable. Based on these preliminary estimates, the thick smear method offers a great promise for quick screening, however its practical applicability requires further investigation. Tab. 6.1 compares the outcome of the field diagnostic test performed in Lagos Nigeria. The performance output of the current standard diagnostic techniques is compared with our proposed diagnostic technique as shown in the table.

6.5. Discussion

We have developed a numerical model for a malaria test that takes into account total cell count N , the probability of false identification γ , and the count of infected

Table 6.1: Field diagnostic test performed in Lagos Nigeria. The malaria status (MS) of each patient is represented as positive (+) or negative (-) accordingly.

Patient	Fluorescence Diagnostic Method Detailed analysis				Polymerase Chain Reaction	WHO GS Microscopy	Rapid Diagnostic Test
	Counted RBC	TP	FP	MS	MS	MS	MS
1	100,342	0	0	-	-	-	-
2	486,810	0	2	-	-	-	-
3	280,900	0	0	-	-	-	-
4	650,495	0	2	-	-	-	-
5	721,531	0	1	-	-	-	-
6	528,395	0	0	-	-	-	-
7	770,376	0	0	-	-	-	-
8	9,576	110	0	+	+	+	+
9	676,000	0	0	-	-	-	-
10	720,088	0	4	-	-	-	-
11	595,600	0	0	-	-	-	-
12	78,345	18	1	+	+	-	+
13	461,250	0	2	-	-	-	-
14	288,600	0	2	-	-	-	-
15	602,500	0	0	-	-	-	-
16	782,300	0	0	-	-	-	-
17	67,228	27	0	+	+	-	-
18	576,110	0	0	-	-	-	-
19	834,250	0	5	-	-	-	-
20	753,670	0	6	-	-	-	-
21	663,850	0	5	-	-	-	-
22	788,800	0	4	-	-	-	-
23	860,000	0	0	-	-	-	-
24	230,000	0	0	-	-	-	-
25	241,550	0	4	-	-	-	-
26	348,000	0	0	-	-	-	-
27	623,500	0	0	-	-	-	+
28	434,870	0	3	-	-	-	-
29	230,000	0	0	-	-	-	-
30	282,350	0	2	-	-	-	-
31	635,000	0	3	-	-	-	-
32	399,220	0	2	-	-	-	-
33	183,500	0	0	-	-	-	-
34	278,500	16	0	+	+	-	-
35	873,000	0	0	-	-	-	-
36	783,000	0	0	-	-	-	-
37	768,000	0	0	-	-	-	-
38	650,000	0	0	-	-	-	-
39	100,000	18	0	+	-	-	-
40	345,000	0	0	-	-	-	-



6

Figure 6.5: Fluorescent image of infected thick smear sample before (top left) and after (top right) filtering. The image after filtering shows numerous parasites in the field of view. Fluorescent image of a thick smear of healthy sample before (bottom left) and after (bottom right) filtering. The image after filtering shows no parasite in the field of view. *Please note that the parasite represented by tiny bright spots may not be correctly reproduced in the screen or printed version of the manuscript.*

cells m . On the practical side we have realized a cost-effective optical microscope that efficiently uses the developed analysis to design the correct conditions for robust detection of malaria parasite in human blood smear.

The performance of the method was validated in preclinical field test with forty fresh human patient samples in Lagos, Nigeria. Proposed technique demonstrated 100% sensitivity and 97% specificity. Computer analysis of an image containing a large number of blood cells establishes a robust statistics, resulting in the diagnostic recommendation, supplemented with the estimate of sensitivity and specificity, providing a foundation for making educated diagnostic recommendation.

Aside the advantage of high sensitivity, this technique also offers rapid diagnosis and ease of result interpretation. The staining protocol for the fluorescent dye is easily performed and a field health worker can be trained to carry out this test accurately in less than one hour of instruction.

Given the performance shown in our preliminary field study, we believe that further optimization of the proposed method could potentially lead to high throughput malaria diagnosis with a performance superior to RDT with respect to sensitivity and specificity. Proposed method will compliment existing diagnostic techniques providing affordable quick screening of infected patients particularly in resource limited settings.

References

- [1] A. Moody, *Rapid diagnostic tests for malaria parasites*, Clinical microbiology reviews **15**, 66 (2002).
- [2] L. Wu, L. L. van den Hoogen, H. Slater, P. G. Walker, A. C. Ghani, C. J. Drakeley, and L. C. Okell, *Comparison of diagnostics for the detection of asymptomatic plasmodium falciparum infections to inform control and elimination strategies*, Nature **528**, S86 (2015).
- [3] A. Berhane, M. Russom, I. Bahta, F. Hagos, M. Ghirmai, and S. Uqubay, *Rapid diagnostic tests failing to detect plasmodium falciparum infections in eritrea: an investigation of reported false negative rdt results*, Malaria journal **16**, 105 (2017).
- [4] L. Golassa, N. Enweji, B. Erko, A. Aseffa, and G. Swedberg, *Detection of a substantial number of sub-microscopic plasmodium falciparum infections by polymerase chain reaction: a potential threat to malaria control and diagnosis in ethiopia*, Malaria journal **12**, 352 (2013).
- [5] B. T. Grimberg, *Methodology and application of flow cytometry for investigation of human malaria parasites*, J.Immunol Methods. **367**, 1 (2011).
- [6] J. B. Weiss, *Dna probes and pcr for diagnosis of parasitic infections*. Clinical Microbiology Reviews **8**, 113 (1995).
- [7] M. G. Ull4oranda, *The use of dna probes for malaria diagnosis: memorandum from a who meeting*, Bulletin of the World Health Organization **64**, 641 (1986).
- [8] P. H. van Vianen, A. van Engen, S. Thaithong, M. van der Keur, H. J. Tanke, H. J. van der Kaay, B. Mons, and C. J. Janse, *Flow cytometric screening of blood samples for malaria parasites*, Cytometry: The Journal of the International Society for Analytical Cytology **14**, 276 (1993).
- [9] C. J. Janse and P. H. Van Vianen, *Flow cytometry in malaria detection*, Methods in cell biology, **42**, 295 (1994).
- [10] M. Kochareka, S. Sarkar, D. Dasgupta, and U. Aigal, *A preliminary comparative report of quantitative buffy coat and modified quantitative buffy coat with peripheral blood smear in malaria diagnosis*, Pathogens and global health **106**, 335 (2012).
- [11] K. Raghavan, *Statistical considerations in the microscopical diagnosis of malaria, with special reference to the role of cross-checking*. Bulletin of the World Health Organization **34**, 788 (1966).
- [12] W. P. O'meara, F. E. McKenzie, A. J. Magill, J. R. Forney, B. Permpnich, C. Lucas, R. A. Gasser Jr, and C. Wongsrichanalai, *Sources of variability in determining malaria parasite density by microscopy*, The American journal of tropical medicine and hygiene **73**, 593 (2005).

- [13] C. M. Mogollon, F. J. van Pul, T. Imai, J. Ramesar, S. Chevalley-Maurel, G. M. de Roo, S. A. Veld, H. Kroeze, B. M. Franke-Fayard, C. J. Janse, *et al.*, *Rapid generation of marker-free p. falciparum fluorescent reporter lines using modified crispr/cas9 constructs and selection protocol*, PLoS One **11**, e0168362 (2016).
- [14] W. H. Organization *et al.*, *Microscopy for the detection, identification and quantification of malaria parasites on stained thick and thin blood films in research settings*, World Health Organization, Geneva, Switzerland. http://www.who.int/tdr/publications/microscopy_detec_ident_quantif/en (2015).
- [15] S. E. Shokoples, M. Ndao, K. Kowalewska-Grochowska, and S. K. Yanow, *Multiplexed real-time pcr assay for discrimination of plasmodium species with improved sensitivity for mixed infections*, Journal of clinical microbiology **47**, 975 (2009).

7

From The Lab To The Field

There will be no more night.

Revelation 2:5

In this chapter, we describe the design process of a low-cost smartphone-based microscope for rapid diagnosis of urinary Schistosomiasis. Field research conducted in Nigeria with the active involvement of key stakeholders in the research and development (R&D) process validated our assumptions and enabled the development of our proof-of-concept into a working prototype in three iterative design steps. Through this design process, we investigated the local development of technical optics for good quality imaging and explored the simplification of sample preparation techniques using commonly available materials. Starting from the first iteration, the output of each design step was used as the input to the subsequent iterations to optimize our system design. Insightful results and input from the field demonstrated that an adaptive design approach was needed to facilitate the rapid development and deployment of point-of-care diagnostic devices for use in low-resource settings. It is our goal that these devices will be locally manufactured and supported in Nigeria to expand access to quick and reliable diagnosis given her huge population and high disease burden.

Parts of this chapter have been published in Schistoscope: Towards a locally producible smart diagnostic device for Schistosomiasis in Nigeria, IEEE GHTC 42,(2019) [1].

7.1. Introduction

The neglected tropical diseases (NTD) are a group of disabling, chronic diseases that are prevalent in tropical and subtropical, resource-constrained areas with poor sanitation and weak health systems [2]. One of these NTDs is Schistosomiasis, a water-born parasitic infection which is transmitted through contact with the vector, snail-infested water bodies during routine domestic, swimming, household, agricultural activities and wading across streams/rivers. It is estimated that around 250 million people are currently infected by Schistosomiasis and 779 million people are at risk [3]. The infection results in impaired growth and development, diminished physical fitness and decreased neurocognitive abilities [2, 4]. Schistosomiasis specifically affects the poorest of the poor and it is prevalent among people living in rural, deprived urban or peri-urban settings. About 80% of the yearly infections are among the rural dwellers in tropical sub-Saharan countries where access to available diagnostic tests is limited [5–8]. These populations typically have low socioeconomic status, inadequate sanitation provision with limited access to clean water [3]. There are three major species of *Schistosoma*; *Shistosoma haematobium*, *Shistosoma mansoni* and *Shistosoma japonicum* [9]. We focus on *Shistosoma haematobium* in this research because it is the most prevalent among our target population.

7.2. Diagnostics gap

The WHO gold standard for diagnostics of *Shistosoma haematobium* relies on microscopy examination of urine samples prepared by filtration, sedimentation or centrifugation [2]. The availability of conventional microscopy in remote or rural communities is limited by high cost, bulkiness of equipment, shortage of required expertise and lack of required maintenance skills & parts [10]. Also manual microscopic examination of the filtered urine sample is time-consuming and prone to human-error [2]. Urine filtration method requires membrane filters which are expensive and are not commonly available at point of needs. In rural areas, the existence of tremendously erratic power supplies precludes the deployment of centrifuges. Furthermore, microscopy is cumbersome and requires highly trained personnel and therefore reduces the opportunities of deploying diagnosis for community surveillance as an aid of tracking the progress of control implementation and reporting. Safe and effective medication, praziquantel, is commonly available for treatment [9]. However, accurate diagnostic techniques for schistosomiasis is hugely underdeveloped and remains a critical challenge though reliable diagnosis is key for (early) treatment.

Severe reduction in the prevalence and intensity of infection is achieved by large scale administration of praziquantel to school-aged population and high-risk adults through the mass screen-and-treat program [11]. Besides the urgent need for treatment of infected patients, a rapid and easy-to-use test device with high performance is also critical for the successful implementation of control and elimination strategy. To ensure that national targets of the control and elimination program are met, there is a need for more accurate mapping of the disease. Consequently, a field adaptable

diagnostic test that fits the capacity of community trained personnel will not only provide access to diagnosis and reporting in the community but also enhances the understanding of the distribution of Schistosomiasis and help to guide program decisions for mass drug administration on a large-scale [3]. Based on all these limitations, there is, therefore, an urgent need for the development of new, reliable, sensitive, low-cost, and easy-to-use diagnostic instruments for the detection of *Shistosoma haematobium* infections in resource-limited communities.

7.3. Technological developments

Hand-held digital microscopes and cellphone-based microscopes are promising alternatives for diagnosis of Schistosomiasis. Rapid progress in optical and computational processing technologies has resulted in, sufficiently sensitive low-cost diagnostics for use in low-resource settings [12]. According to field reports, their portability makes them suitable for use outside of typical lab-setting [4, 7]. Recent studies have introduced novel diagnostic approaches with innovative image-capturing techniques for applications at the point-of-care. Integrating smart algorithms to automate the detection and quantification of *Shistosoma haematobium* eggs in samples will drastically reduce human intervention while increasing the sensitivity. The benefit of digital microscopy compared to light microscopy includes the option to share real-time digital healthcare and location data for mapping purposes for control programs.

The principle of digital microscopy is the starting point for the development of the Schistoscope as described in this paper.

7.3.1. Challenges and opportunities with digital handheld microscopes

Despite a wealth of technological innovation in this field which meets many technical and medical criteria, there remain key challenges in implementing mobile-microscopy devices in resource-constrained environments. We shortly discuss three of the current challenges as well as opportunities we foresee to overcome them.

Technical optics

Cellphones combined with glass ball lenses have been reported in [7]. This cellphone-based microscope provides relatively poor image quality due to the inherent aberration of the optics and the limitation posed by the numerical aperture. Furthermore, the limited field of view (FoV), results in the need for multiple measurements, which reduces the sensitivity and specificity of the diagnostic instrument [13]. A method which replaces the ball lens with a reversed phone lens has shown promising results. It provides a large field of view (the entire sensor plane), and an improved resolution.

An ideal diagnostic instrument should be integrated with an efficient Artificial Intelligence (AI) algorithm which enables automated detection and estimation of the eggs in a registered image. A desired feature of the AI algorithm is that it must be implementable on low-profile digital signal processors. To realize this, methods which drastically reduce the computational complexity must be investigated.

Complex sample preparation

There has been comparatively little work done on simple, low-cost, laboratory-free means for microscopy sample preparation. In contrast to centrifuge methods that concentrate urine for parasite detection, filtration is a much more simplified method. According to the WHO Microscopy standard recommendation, 10 ml of urine sample should be filtered using a disposable polycarbonate membrane of pore size $12\mu\text{m}$. Despite the simplicity of the filtration technique, the cost and availability of the filter and its holder limit its use in rural areas. From practical interactions with stakeholders on the field, filters and filter holders are imported and are delayed due to logistic reasons in most cases. Solving the filter availability challenge will enhance and facilitate the use of mobile microscopy in remote settings. To circumvent this limitation, a research group attempted urine filtration with towel papers. Egg detection was barely possible due to background noise [14].

In our attempt to propose a solution as well, we investigated the use of coffee filters. Results were not useable due to the poor signal to noise ratio. Finally, a locally sourced chiffon material with a pore size of $18\mu\text{m}$ was identified. The material filters the urine and the eggs were clearly visible when examined with a cellphone based microscope in our lab. The conflicting periodic background structure, however, reduces the capacity to automatically detect the eggs in a registered image. Therefore, we decided to explore computational methods to remove the structured background pattern of the material and enhance easy and quick detection of the *Schistosoma haemtobium* eggs in the residue. The success of the proposed filtration technique, will reduce the cost, eliminate the scarcity of filtration material and simplify the entire sample preparation procedure. ‘

Local production and maintenance

Most handheld microscopes, as well as the applied filters (for sample preparation), require sophisticated production facilities, which are not readily available where they are needed the most. Due to enormous logistics effort required, the diagnostic devices are expensive, scarce, and difficult to maintain (due to lack of spare parts and required technical skills) at the point of need. Most NTD diagnostics are currently produced from non-disease settings and this relies heavily on overseas importation that further increases cost at the point of use. The fragile economies of most of the poor countries whose source of revenue is on import duties and poor operational shipping processes would drive up the cost and make products inaccessible or expensive. Land-locked, Schistosomiasis endemic countries would also have to pay more for the devices due to the extremely high cost of shipping.

Mass production of components for the consumer electronics market in recent past has enabled the fabrication of low-cost, effective and portable digital imaging devices. Manufacturing these devices by using locally sourced materials could reduce costs as well as improve maintenance due to the general availability of spare parts in the target areas. Integrating this with innovative manufacturing pathways, we can overcome import dependency and unnecessary long value chains. Additive manufacturing tech-

nologies like 3D-printing offer new opportunities to set-up local production facilities which can supply devices and spare parts in the local context. We envisage that once these challenges are addressed, portable digital microscopy could provide high quality diagnostics at the point-of-need. It will also provide timely information on the distribution of disease, thereby enhancing treatment, control, surveillance, and elimination of NTDs at the point of need.

7.4. Research setup

To realize a decent digital microscopy system, we focused on three main challenges: (1) Optimization of the technical optics, (2) Simplification of the integrated sample preparation method and (3) Local production in Nigeria.

To develop a digital microscope which offers an integrated diagnostics solution (sample preparation and diagnosis) with the support of a smart algorithm for detection and quantification of the *Schistosoma haemtobium* eggs which can be produced and maintained in Africa). It is intended that the hardware and software design of Schistoscope will be shared through an open-source platform (to scale up).



Figure 7.1: Screenshot of Schistoscope kick-off movie indicating all possible target design requirement and goals.

Field research in Nigeria

Nigeria is a context in need of Schistosomiasis diagnostics for direct treatment as well as for control and elimination programs. The country is of particular interest because it has the largest number of people living in Africa with NTDs. It ranks first globally in the number of people infected with schistosomiasis with 29 million infected and 101 million at risk [15]. According to Hotez et-al, only 6% of the population receives access to praziquantel for the treatment of schistosomiasis [16]. Two specific Nigerian Universities were approached: The Faculty of Public Health of the University of Ibadan for its expertise in understanding the local healthcare system, and the Department of Biomedical Engineering of University of Lagos for its expertise in digital health technologies and distributed manufacturing. The ANDI Centre of Excellence

for Malaria Diagnosis Centre and Tropical Diseases Research Laboratory of the College of Medicine of the University of Lagos provided advice on the medical procedure and testing with real-time sample.

Design approach

Even though a wide range of digital diagnostic devices has been developed for low-resource settings, very few of them have been successfully adopted by local healthcare systems. Balsam et al for example mention that many modern and emerging diagnostic technologies are not affordable or compatible with the needs and conditions found in low- and middle-income countries. Likewise, Engel et al.[17] concluded that lack of end-user involvement in research and development, limited understanding of clinician, patient, and healthcare system behavior and insufficient test evaluation in target settings complicates the development, adoption, and scale-up of advanced diagnostics in low-resource settings. To develop a new diagnostic device which matches with the local healthcare context and successfully become adopted, it is crucial to engage with stakeholders in an early stage of the design. Conducting frequent experiments not only in the laboratory but also in real-world settings is critical for successful implementation. Based on these insights, we ensured two field visits to Nigeria.

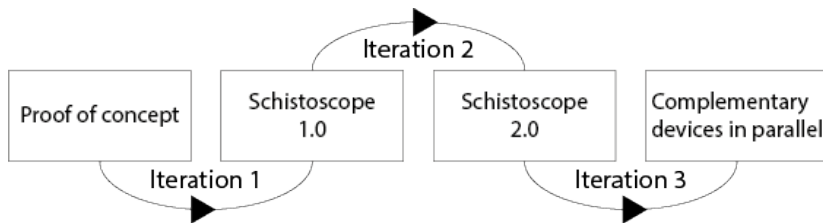


Figure 7.2: Iterative design process characterized by experimenting and frequent field research

For the design process, tools and methods as described in the Delft Design Guide [18] in combination with the framework for the holistic contextual design for low-resource settings [19] were applied. An iterative approach with multiple planned experiments was set out to develop the three consecutive Schistoscope concepts: Schistoscope 1.0 at the start of the project, Schistoscope 2.0 after the first field visit, and the further development in key directions emerged.

Methods

Our field research was executed (i) to gather data to elicit user- and context-requirements within the local healthcare system and, (ii) to validate and further improve the functionality of the system and technical specifications as well as the local manufacturability. To realize the goal of the first objective, we conducted expert interviews, organized focus group meetings, and staged system demonstrations with the potential users and stakeholders in Ibadan. For the second objective, we emphasized practical experiments using the prototypes in the local setting. We also organized iterative co-design sessions with Nigerian biomedical engineering students and engineering experts in Lagos.

During the first field visit, 12 expert interviews, 2 focus group sessions, and several co-creation sessions were held. The second field trip involved sample testing in the laboratory and peri-urban setting, and a range of discussion and co-creation sessions.

7.5. Field validation report

Feedback from potential stakeholders was promising as our proposed device was positively perceived. They shared the idea of the fact that the simplicity of the device will make it easily adopted by the primary healthcare workers. During each design iteration, the Schistoscope was adapted to become a better fit with the local healthcare system. It is perceived to be more specific to the end-user and matches with the locally available materials, components, and manufacturing methods. The intention behind the initial design choices was to ensure more frugality by simplifying the device and using low-cost, locally sourced materials.

The first iteration describes the trade-off between simplicity and standardization. Since our device will be used for medical diagnostics, diagnostic testing must be compliant with the WHO standard procedure and protocol.

In the second iteration, we described the development of the second prototype which demonstrates compliance and standardization with WHO protocols. In this phase of development, we discovered some basic challenges related to the technical specification of the optical instrument. Also, we realized that the local capacity of 3D-printing is still at a very early developmental stage making local manufacturing with 3D-printing more challenging than we envisaged. Finally, from field sample testing, we observed that urine filtration with local filtration materials did not produce a satisfactory result. We report our findings in the following section and used the obtained insights to optimize our system design. Further details will be described in third iteration.

7.5.1. First iteration

The first design iteration started with developing a technical demonstration of the concept as shown in Fig. 7.3(a).

The initial assumptions were quickly translated into a physical model 'Schistoscope 1.0' to represent the conceptual idea. The Schistoscope 1.0 is characterized by:

Optimization of technical optics

A smartphone Moto X-style with sensor dimensions of 5.99 mm x 4.5 mm and a pixel size of $1.12\mu\text{m}$ was used. We realized the appropriate magnification and resolution by aligning a reverse phone objective lens with similar focal length (4.61 mm) to the lens and camera module of the smartphone (See Fig. 7.3(b)). The main framework was made with wood, while the lens mount and sample holder were 3D-printed. By vertical translation of the smartphone, the optical focal plane is determined. The illumination comes from the bottom of the frame. After the acquisition of a focused image, the integrated algorithm is activated to detect and quantify the Schistosoma eggs in the sample.

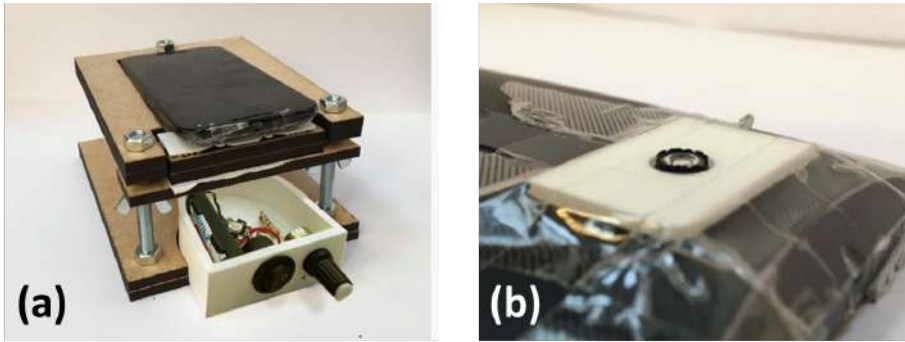


Figure 7.3: (a) Technical demonstration of concept Schistoscope 1.0, (b) Reverse phone objective lens added to the camera module.

Integrated sample preparation

To simplify the sample preparation process, the filtration-technique was our preferred choice due to local availability and low cost of material. We explored both nylon and chiffon filter materials with a pore size ranging between 18 and 36 microns. The filter material was cut into the size of dimension 10 by 10 mm, and fixed on a designed 3D-printed sample holder. The sample holder is directly positioned in the sample plane of the device for quick examination of filtered urine sample for target eggs.

Local production

For the first prototype, the main body was made with laser-cut MDF (Medium Density Fibre). The filter holder and the illumination case were 3D-printed. The adjustment of the focus is controlled by standard nuts and bolts (See Fig. 7.3).

7

7.6. Field research I

The aim of the first field research was to introduce the concept of digital microscopy to the local healthcare context and to test the envisioned diagnostic procedure. In general, the concept was positively evaluated for its potential functionalities and ease of use for the healthcare workers at the primary healthcare level with a minimal amount of training. A range of constraints such as unstable power supply, bumpy roads for transportation, and lack of resources to sterilize the device properly was identified by the local stakeholders. The insights gained from the three design challenges in this phase generated more context- and user-specific specifications for the second design iteration which will be described in detail in the following sections.

Optimization of technical optics

The outcome of the system design in phase 1 did not provide the required stability and precision needed for sample alignment due to the simplification of the system design and the wooden material used to fabricate the frame. The accurate vertical alignment

of the sample is essential for the acquisition of in-focus image of the sample. The choice of the smartphone for optimal optical performance was reconsidered. Familiarity of the smartphone interface, flexibility in its user flow and interface design which will lower the usage barriers to the healthcare workers was critical to design choices in this phase. However, an observed limitation of the smartphone was the short battery life. Therefore, an alternative solution for power supply was necessary. The possibility of using the smartphone for other irrelevant purposes was a major concern. To tackle that, customizing the smartphones and ensuring limited functionalities was our only option. Since the price of the smartphone was rather considered too high, inexpensive local phone brands were recommended.

Integrated sample preparation

The customized filter should comply with the medical standard. Proving the consistency in performance will be a challenge if we want to develop the customized urine filter with local sourced materials. Another major problem with the proposed locally sourced filter was the difficulty of tightly stretching the material over the 3D-printed sample holder (Fig.7.4). Hence it was difficult to realize an optimal image quality. From field interaction with stakeholders, we discovered that ordering WHO recommended filter was possible through online transactions from the warehouse in China. It was interesting to discover that the filters could arrive in the country within 48 hours. A common challenge with the standard filter compared to our proposed locally sourced filters however, was the fact that the standard filter has a larger surface area making it difficult to realize complete diagnosis in just one field of view.

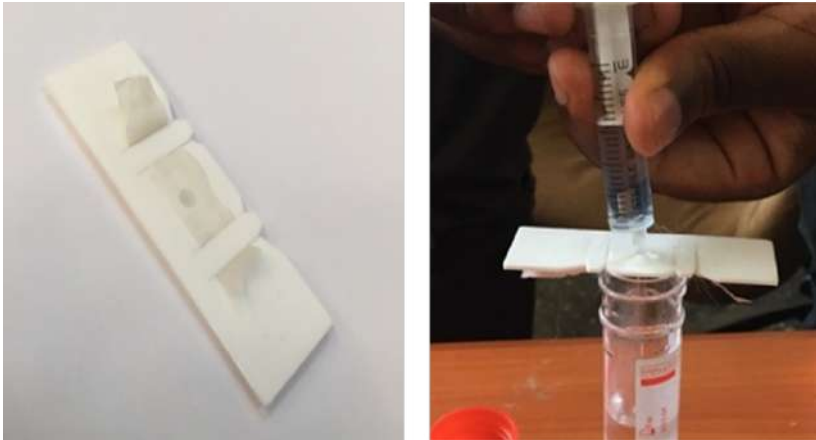


Figure 7.4: 1st iteration filter and its holder (left) and in use with a syringe (right)

A strong recommendation from the field was that standardized filters and diagnostic instruments widely used in the lab in Nigeria should be optimized, simplified and used as a design reference.

Local production

The possibility of local manufacturing was well validated as locals were not enthusiastic about importation of diagnostic products from Asia. Their usual experience when their imported medical product breaks down was saddening. Even though the sample holder and the illumination module were designed to be 3D-printed, the capacity of 3D-printing in the field is not advanced enough to produce our models with the desired quality. Based on this input, alternative types of materials and distributed manufacturing techniques should be considered to ensure smooth local production.

7.7. Second iteration

Our first prototype was optimized based on the insights from the first field research. A prototype of the improved output of the second design iteration Schistoscope 2.0 was developed as shown in Fig. 7.5.

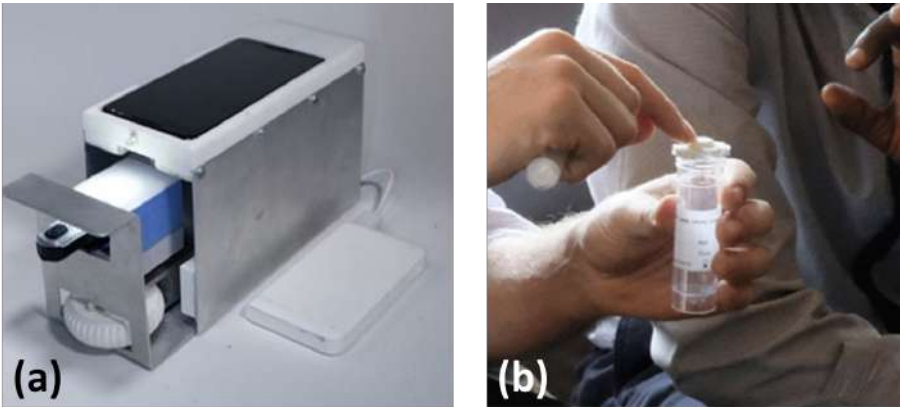


Figure 7.5: (a) 2nd Design iteration outcome with smartphone and (b) 2nd iterated design 3D-printed filter holder placed on urine collection cup

Optimization of technical optics

The new system design now has a more rigid metallic frame which is robust against vibration, and misalignment of the optical components. Translating the z-axis to ensure optimal sample alignment to focus point was attained by adjusting the focus knob which translates the sample plane with improved precision. A smartphone model manufactured in Nigeria was used in this design iteration. Unfortunately, the resolution of the phone camera and display were not sufficiently high enough for our desired goal.

Integrated sample preparation

The membrane filter commonly used in Nigeria was used to test the second prototype to ensure compliance with the WHO standard. The filter holder was separated from the main embodiment to prevent cross-contamination of urine. The new filter holder

(Fig.7.5(b)) is placed in the drawer attached to the frame without contacting other parts.

Local production

The material for the main frame was sheet metal which is stronger and more durable. The metal bending does not involve much complex production technique and it is repeatable at the local workshops in Nigeria. This will make the device easier to repair and maintain. The sample holder and the knob which controls the focus requires higher precision, hence, they were 3D-printed with ABS (Acrylonitrile Butadiene Styrene).

7.8. Field Research II

The key objective of the second field research was to demonstrate Schistoscope 2.0, confirm the improvements based on the input from the first iteration, and look for further opportunities for improvement. The Schistoscope 2.0 was tested with real samples at the University of Lagos. Furthermore, field visits were made to peri-urban settings for simulating the diagnostic test in practice. In parallel, discussions and co-creation sessions continued with relevant stakeholders (Fig.7.6).



Figure 7.6: Design students in discussion with health experts in Ibadan, Nigeria (Left) and demonstration at the peri-urban setting (Right)

All these planned activities, helped the design team to gain a deeper understanding of the potential problems of the context and the potential value of the Schistoscope. Some problems identified during the first field trip were found to be resolved. Still, there were recurring issues such as the material and structure of the metallic frame. The design of the filter and its holder still requires lots of attention also. Meanwhile, new challenges emerged:

Optimization of technical optics

Even though the overall stability was improved, the metallic frame was still not precise enough to support vertical alignment. Shape and size of the used smartphone reduced the degrees of freedom in the design of the desired embodiment. The relatively high

cost and reduced capacity of the backup battery were of major concerns also. Other issues relating to the maintenance and servicing of the device includes the fragility and difficulty to replace the phone screen and used lens. Therefore the need to engage with local phone repair shops is critical. The functionality of the developed AI algorithm (Fig.7.7) was well valued by local experts. The processing speed which allowed egg detection and estimation in barely 4 seconds, was considered highly sufficient. More feedback was required for users to prevent any human error. As the phone has a GPS sensor incorporated, the data collection and mapping seem realizable with much less effort.



Figure 7.7: Pictures of filtered *S. haematobium* eggs captured with Schistoscope 2.0

7

Integrated sample preparation

There were multiple drawbacks identified with the sample holder (Fig.7.8). First, the syringe was not well secured in the holder which causes spillage of the urine samples. Due to the small pore sizes and amount of volume injected through them, the pressure on the mesh is high and since the sample holder does not have a handle, easy spillage of content is observed. An interesting outcome from the frame design is that the drawer for the sample holder worked smoothly in terms of usability on the field.

Local production

The main material, sheet metal, was found as too expensive for local production. It should not be neglected that the sheet metal corrodes easily in such humid weather. To allow more precise and durable manufacturing and maintenance, 3D-printing was considered to be a more promising option. However, the limitations that were found in the previous iteration should be overcome to realize this.



Figure 7.8: The difficulty of using the customized holder (Left) and the standard filter and filter holder (right)

7.9. Discussion

During the iterative design process, we were able to validate our assumption on the field and adapt our design to match with the local healthcare context and need of the end-users. For the remaining challenges, we determined the key problems to focus on to further improve the Schistoscope. The key insights and the current directions we are exploring are summarized in Fig.7.11. The third iteration in progress is aimed at optimizing the main challenges indicated below. Afterward, we will continue with the validation and iteration of the results in a lab setting and in the field with the stakeholders.

Optimization of technical optics with Raspberry Pi

Although a smartphone has the advantage that it is locally repairable, it also severely limits the possibilities of the technical design. We concluded that there is a need for a customized imaging system for optimal effectivity of the algorithm. Therefore, the use of a Raspberry Pi or similar development board was suggested. Working with the development boards directly is more efficient in terms of coding rather than running on an android system. Adopting Raspberry Pi will enable the modular design and make it more efficient in terms of physical embodiment, battery capacity, and illumination. Adapting to a new component or expanding the functionality would be relatively easier. Nevertheless, working with a smartphone still has many benefits such as its ease of use, availability and familiar interface. The current prototype is being developed as in Fig.7.9.

Integrated sample preparation: exploring both centrifuge and filtration methods

For the urine filtration method, the holder has to be re-designed to prevent the spillage and solve usability issues in the next iteration (Fig 7.10(a)). The locally produced customized filter will have a high potential value in terms of sustainable supply and efficiency of field of view. Moreover, the filter size relates to the required number of



Figure 7.9: 3rd design iteration with Raspberri pi and development of dedicated 3D Printer.

field of view (FoV) which influences the design of the technical optics. The cost and benefits of the two options will be considered more thoroughly in the next iteration.

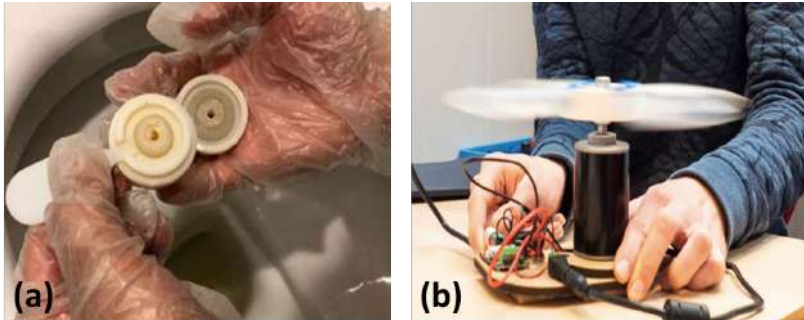


Figure 7.10: (a) Outcome of the third iteration: filter holder design, (b) Low-cost, locally manufacturable and maintainable centrifuge.

Staining: As mentioned, the staining will increase the contrast of the target eggs against the background. This will increase the sensitivity of the algorithm. However, the supply of the staining chemicals and the accompanying training should be considered in this case especially in the remote settings. Based on input from the field, we decided to develop a Frugal Centrifuge (Fig.7.10 (b)), which optimizes the design of a lowcost centrifuge specifically for the detection of eggs in urine. It is our goal to ensure that the product is low-cost, locally manufacturable, and easy-to-use.

Sample contamination: Sample contamination plays a major role in the overall quality of the diagnostic output. Some urine samples obtained from the field were observed to be highly contaminated with either blood, or other strange sediments. These sediments forms very thick residue on the filtered membrane when observed with a microscope. Our proposed hypothesis is that residue from a contaminated urine sample will not

yield a sufficiently high resolution image on which the AI algorithm will perform well. This hypothesis will however be tested with real infected human samples from the field in our planned field study.

Local production with optimized 3D-printer

Many local experts suggested the use of plastic for the embodiment design considering the context. To enable more detailed and easy-to-clean embodiment, 3D-printing seems to be the most promising option for manufacturing for the first batch of Schistoscopes. As the local capacity of 3D-printing is not ready, we aim at setting up a local manufacturing unit with several optimized 3D-printers (see Fig.7.9) with independent power supply systems. We hope that our current 3D-printer modification will overcome the current limitations on the field.

7.10. Conclusion

We conceptualized the novel ideas for digital microscopy by iterative design process of Schistoscope in three different design iterations. To fill the diagnostic gap of Schistosomiasis in Nigeria, we believe that our method to explore with the potential stakeholders outside the lab-setting provided useful insights for the optimization of our technical system design during the design process. Engaging local stakeholders from the early stage of the R&D process has improved our design methods to meet local healthcare needs. In the next stage of this research, we will further develop the three focus areas, and validate again with the potential stakeholders. We plan to repeat this cycle until a practical product that can be validated with a large sample size is realized. After the validation in the lab, we will start testing with communities based on standard ethical approval. We believe that this design thinking and process will benefit researchers focused on using science and technology for societal benefit.

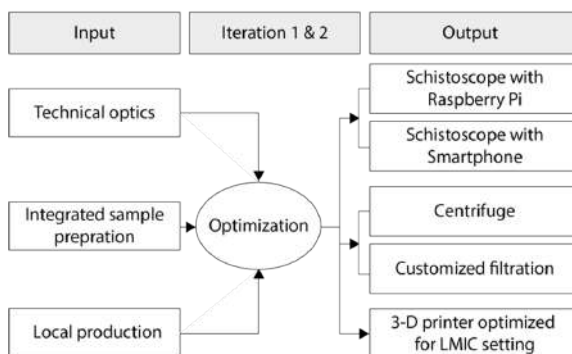


Figure 7.11: An iterative process that has led to the current work-in-progress

References

- [1] T. Agbana, G. Van, O. Oladimeji, G. Vdovin, W. Oyibo, and J.-C. Diehl, *Schistosomiasis in africa: Improving strategies for long-term and sustainable morbidity control*, IEEE GHTC (2019).
- [2] O. Holmström, N. Linder, B. Ngasala, A. Mårtensson, E. Linder, M. Lundin, H. Moilanen, A. Suutala, V. Diwan, and J. Lundin, *Point-of-care mobile digital microscopy and deep learning for the detection of soil-transmitted helminths and schistosoma haematobium*, *Global health action* **10**, 1337325 (2017).
- [3] L.-A. T. Tchuenté, D. Rollinson, J. R. Stothard, and D. Molyneux, *Moving from control to elimination of schistosomiasis in sub-saharan africa: time to change and adapt strategies*, *Infectious Diseases of Poverty* **6**, 42 (2017).
- [4] H. C. Koydemir, J. T. Coulibaly, D. Tseng, I. I. Bogoch, and A. Ozcan, *Design and validation of a wide-field mobile phone microscope for the diagnosis of schistosomiasis*. *Travel medicine and infectious disease* (2018).
- [5] B. Gryseels, K. Polman, J. Clerinx, and L. Kestens, *Human schistosomiasis*, *The Lancet* **368**, 1106 (2006).
- [6] D. J. Gray, A. G. Ross, Y.-S. Li, and D. P. McManus, *Diagnosis and management of schistosomiasis*, *Bmj* **342**, d2651 (2011).
- [7] J. Rajchgot, J. T. Coulibaly, J. Keiser, J. Utzinger, N. C. Lo, M. K. Mondry, J. R. Andrews, and I. I. Bogoch, *Mobile-phone and handheld microscopy for neglected tropical diseases*, *PLoS neglected tropical diseases* **11**, e0005550 (2017).
- [8] I. I. Bogoch, J. T. Coulibaly, J. R. Andrews, B. Speich, J. Keiser, J. R. Stothard, E. K. N'goran, and J. Utzinger, *Evaluation of portable microscopic devices for the diagnosis of schistosoma and soil-transmitted helminth infection*, *Parasitology* **141**, 1811 (2014).
- [9] Y. Vonghachack, S. Sayasone, V. Khieu, R. Bergquist, G. J. van Dam, P. T. Hoekstra, P. L. Corstjens, B. Nickel, H. Marti, J. Utzinger, *et al.*, *Comparison of novel and standard diagnostic tools for the detection of schistosoma mekongi infection in lao people's democratic republic and cambodia*, *Infectious diseases of poverty* **6**, 127 (2017).
- [10] T. E. Agbana, J.-C. Diehl, F. van Pul, S. M. Khan, V. Patlan, M. Verhaegen, and G. Vdovin, *Imaging & identification of malaria parasites using cellphone microscope with a ball lens*, *PLoS one* **13**, e0205020 (2018).
- [11] M. D. French, D. Evans, F. M. Fleming, W. E. Secor, N.-K. Biritwum, S. J. Brooker, A. Bustinduy, A. Gouvras, N. Kabatereine, C. H. King, *et al.*, *Schistosomiasis in africa: Improving strategies for long-term and sustainable morbidity control*, *PLoS neglected tropical diseases* **12**, e0006484 (2018).

- [12] J. Balsam, M. Ossandon, H. A. Bruck, I. Lubensky, and A. Rasooly, *Low-cost technologies for medical diagnostics in low-resource settings*, Expert opinion on medical diagnostics **7**, 243 (2013).
- [13] N. A. Switz, M. V. D'Ambrosio, and D. A. Fletcher, *Low-cost mobile phone microscopy with a reversed mobile phone camera lens*, PLoS one **9**, e95330 (2014).
- [14] R. K. Ephraim, E. Duah, J. R. Andrews, and I. I. Bogoch, *Ultra-low-cost urine filtration for schistosoma haematobium diagnosis: A proof-of-concept study*, The American journal of tropical medicine and hygiene **91**, 544 (2014).
- [15] S. Dawaki, H. M. Al-Mekhlafi, I. Ithoi, J. Ibrahim, A. M. Abdulsalam, A. Ahmed, H. Sady, W. M. Atroosh, M. A. Al-Areeqi, F. N. Elyana, *et al.*, *Prevalence and risk factors of schistosomiasis among hausa communities in kano state, nigeria*, Revista do Instituto de Medicina Tropical de São Paulo **58** (2016).
- [16] P. J. Hotez, *Blue marble health: an innovative plan to fight diseases of the poor amid wealth* (JHU Press, 2016).
- [17] N. Engel, K. Wachter, M. Pai, J. Gallarda, C. Boehme, I. Celentano, and R. Weintraub, *Addressing the challenges of diagnostics demand and supply: insights from an online global health discussion platform*, BMJ Global Health **1**, e000132 (2016).
- [18] A. Van Boeijen, J. Daalhuizen, R. van der Schoor, and J. Zijlstra, *Delft design guide: Design strategies and methods* (2014).
- [19] C. B. Aranda-Jan, S. Jagtap, and J. Moultrie, *Towards a framework for holistic contextual design for low-resource settings*, International Journal of Design **10**, 43 (2016).

8

Conclusion

*The leaves of the tree shall be for the
healing of the nations.*

Rev.22 vs.2

According to the World Health Organisation, microscopy still remains the reference diagnostic method for most parasitic diseases. As outlined in the introduction of this thesis, microscopy allows for parasite detection, quantification, species identification and morphological analysis. Realizing effective malarial microscopy in low-resource settings is however difficult due to the need for highly skilled human operators, intensive manual labour, high cost of equipment and training of staff. Furthermore, considering the large amount of red blood cells to be screened in the case of malarial microscopy, the constraint of spatial resolution and achievable field of view increases the amount of manual measurement required for conclusive diagnosis.

This poses a major limitation in realizing point-of-care devices that will alleviate the complexity of standard optical diagnostic procedure. To address these problems, this thesis explored distinct methods which combines data driven algorithms with optical imaging techniques to realise reliable and robust detection of parasites in infected samples.

In this work we have examined, analysed and optimised both coherent and incoherent optical imaging techniques to develop potential solutions towards point-of-care diagnosis of parasitic diseases.

The following steps have been taken towards the realisation of our research goals: The first step covered in Chapter 3 was to define the resolution limit of a lensless microscope and its practical application to the detection of *S.haemtobium* eggs in urine sample; the second step was the combination of cellphone based microscope & data driven algorithm to realize automated smart detection of *S. hametobium* as reported in Chapter 4. The resolution limit of cellphone-based microscope for the imaging of malaria parasite was defined and reported in Chapters 5 & Chapter 6, reports on our

novel smart multimodal imaging of malaria parasite circumventing the resolution limit of a standard microscope. Chapter 7 discusses practical design iterations and field validation steps followed to realize functional prototypes for field testing in Nigeria. Hereafter is a summary of accomplishments and the potential for future work.

Defining the resolution limit of lensless microscope

The purpose of this work focused on the derivation of optimal configuration that delivers maximum resolution in a digital inline holographic microscope. This imaging modality is particularly of interest because it has the capability to provide high spatial resolution concurrently with large field of view. From the analysis of the coherence property of the illumination and the pixel size of the imaging sensor, maximum achievable resolution limits without aliasing is defined.

Based on the results obtained, we propose a novel diagnostic method for rapid point-of-care diagnosis of urinary schistosomiasis. This method combines flow cytometry, lensless imaging and artificial intelligence for the detection of *S. haemtobium* in urine sample. The robust diagnostic method avoids the cost and complexity of the standard sample preparation method.

The performance of a prototype device (SODOS - Smart optical diagnosis of Schistosomiasis) developed based on our proposed method has been pre-validated with experts on the field in Ivory Coast. Results shows that proposed diagnostic methodology is robust, smart, easy-to-use and can be used to map the disease. Disease mapping is critical for effective disease control and elimination programs. Suggestions for future work would therefore be to optimise image acquisition and processing time so as to significantly reduce diagnostic delay.

Fig 8.1 shows a working point-of-care diagnostic device for the optical detection of schistosomiasis. Prototype was developed as a master project at the faculty of Industrial Design, TU Delft based on this project. The performance of the device is compared to a conventional microscope used in the lab.

8

Smart optical diagnosis of urogenital schistosomiasis

Standard WHO recommended diagnostic method for *S. haemtobium* involves urine filtration using standard membrane filters with an approximate pore size of $12\mu m$. These filters are not widely available in low-resource communities where they are needed the most. Using widely available chiffon materials for filtration and combining developed data driven algorithms with a cellphone-based microscope, we realized automated detection of *S. haemtobium* eggs in filtered urine samples. With a sensitivity of 90.52% and a specificity of approximately 90% we present the first offline automated detection of *S. haemtobium* using cellphone-based microscope to the best of our knowledge. Developed methodology has been implemented with other low-cost consumer grade electronics such as raspberry pi etc. We believe that this point-of-care devices will empower low skilled community health care workers to provide quick detection of *Schistosoma haemtobium* in rural areas. Fig. 8.2 & Fig. 8.3 shows developed working prototypes based on cellphone-based methodology developed in this thesis.



Figure 8.1: A Smart Optical Diagnosis of Schistosomiasis (SODOS) point-of-care device developed as a master project at the faculty of industrial Design based on the concept proposed in (chapter 3 of this thesis).

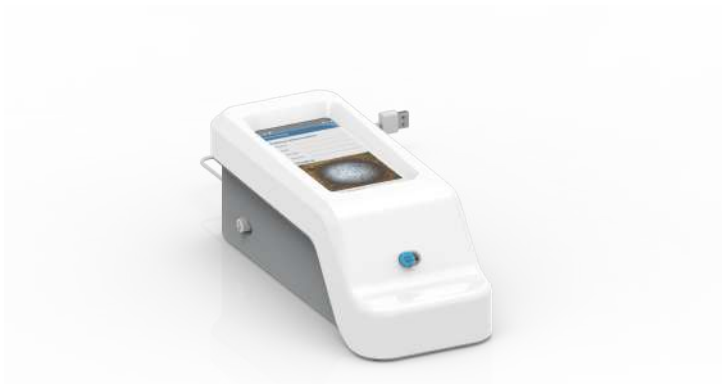


Figure 8.2: Developed cellphone based microscope towards point-of-care diagnosis of *Schistosoma haemtobium*. This design is aimed at realizing conclusive diagnosis in one measurement. The working prototype was developed as a master project at the faculty of industrial Design based on the concept proposed in (chapter 4 of this thesis).

Fig. 8.4, shows the testing of a working prototype in Lagos, Nigeria. The performance is compared with standard microscope as shown in the picture. Fig. 8.5, shows a robust, low-cost Schistofuge. A centrifuge specially designed for centrifugation of urine samples on the field. This device is envisaged to minimize the complexity of sample preparation, reduce power requirement and enhance diagnostic throughput.



Figure 8.3: Developed automated microscope using low-cost consumer grades electronics and optics based on the methods described in Chapter 3. It is a simplification of the WHO approved diagnostic method and requires minimal technical skill, we envisage that this methodology will be of practical interest to the primary health care community. (a) shows the first working design of the prototype and (b) is the designed implementation. Functional Prototype was developed as a master project at the faculty of industrial Design based on the concept proposed in (chapter 4 of this thesis).



Figure 8.4: Working prototypes used to image *Schistosoma haemtobium* at the ANDI Malaria research centre in Lagos, Nigeria. An expert is seen looking through a standard microscope while the developed cellphone based microscope also provides automated detection of the eggs (2018).

Future development of this work will be to optimise the system for multiple fields of

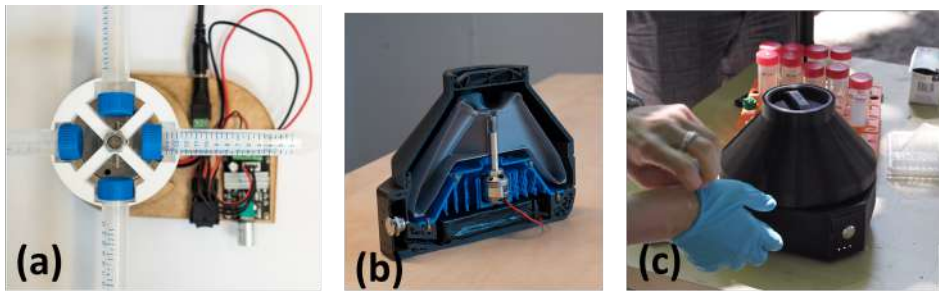


Figure 8.5: Developed low-cost schistofuge, designed specifically for the diagnosis of schistosomiasis. The centrifuge has been optimised for use in remote and rural areas where access to consistent power is really limited. It can operate continuously for three days without any dependencies on external power supply. The prototype was developed as a master project at the faculty of industrial Design within the scope of this thesis.

view by developing and integrating precision sample control softwares.

Optimizing the resolution limit of cellphone-based microscope

Cellphone-based microscopes are being adopted for use in emerging point-of-care diagnostic due to the integrated optics, imaging sensor and electronics. In this thesis, we optimised the technical optics of a cellphone to resolve the malaria parasite which is $1\mu m$ in size. Using a single ball lens and a specially designed apertures prescribed in our design model, malaria parasites in cultured samples were imaged with sufficient resolution. Although the achievable field of view is limited, the diagnostic procedure can be automated using integrated control softwares to move the samples. The proof-of-principle was further developed into a working prototype as shown in Fig.8.6. Further work will include integrating autofocus control software. Developing and integrating automated parasite detection algorithms will be a follow-up future direction to go.

Smart optical detection of malaria parasites

Using multimodal imaging techniques combined with smart algorithms, we propose wide field detection of malaria parasite in an infected sample. The proposed method is easy to use, potentially low-cost and requires little or no technical expertise. Although it does not provide additional information on parasite morphology or specie identification, it is capable of detecting very low infection load. Proposed method has been tested with limited amount of samples at the ANDI Malaria research centre in Lagos, Nigeria in January 2018 and results obtained are promising. Developed prototype is shown in Fig. 8.9. Further work will be to explore the possibility of optimising this device for specie identification and morphology analysis using data-driven computational methods.



Figure 8.6: Cellphone-based microscope (Excelscope 2.0) developed towards the point-of-care detection of malaria parasite. The diagnostic device was developed as a master project at the faculty of industrial design based on the concept proposed in (chapter 5 of this thesis)

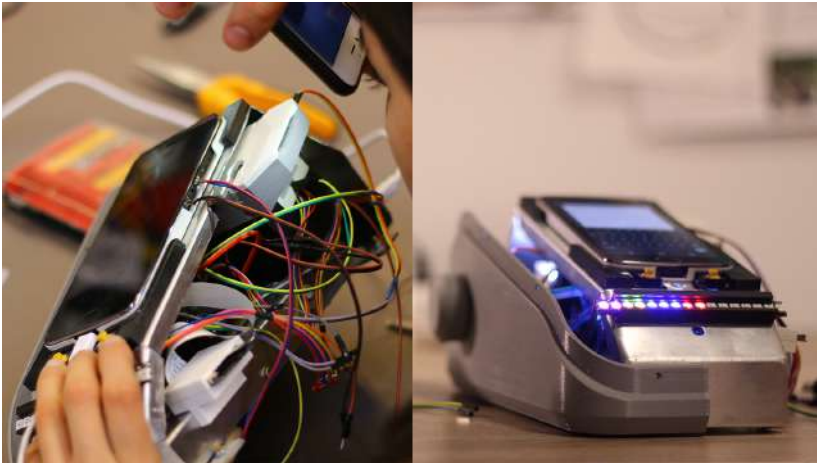


Figure 8.7: System design and development of Excelscope 2.0.

From the lab to the field

Translating developed proofs-of-principle to practical working prototypes required series of field validation processes. To ascertain the desired practical system specifications such as robustness, power dependencies, system resistance to temperature, pressure, dust, etc, a design process was carefully planned and implemented. During this research, different design-based field researches on diverse parasitic diseases were conducted. Endemic countries visited include Nigeria, Ghana, Ivory-coast, Gabon and Uganda. Results obtained from these different field trips provided practical insights into realizing reliable working prototypes. The design iteration and steps to realize working models of Schistoscope from conception to implementation were discussed in



Figure 8.8: A second design of Excelscope 2.0 for imaging of parasitic diseases. System has the capacity to resolve $1 \mu\text{m}$ sized parasites. Device was developed as a master project at the faculty of industrial Design based on the concept proposed in (chapter 4 of this thesis)

the corresponding chapter. Conclusively, it is my humble submission that most of the parasitic diseases currently ravaging endemic low income countries can be eliminated. I am deeply convinced that access to quick and reliable diagnosis of malaria and other neglected tropical disease should not be a privilege but a fundamental right of every human being. Thankfully, this is attainable!



8

Figure 8.9: AiDx assist, a working prototype of a multimodal imaging device for malaria detection. The development of the functional prototype was co-ordinated by a non-profit Medical Optics fund, based on the concepts proposed in this thesis. The developed prototype was being tested for the quick diagnosis of *Loa loa* and malaria parasite in prepared blood samples at the CERMEL (Center of Medical Research Lambaréné) laboratory facility in Lambarene, Gabon. Picture was taken in January 2020.

*The limitation of science is that it lacks the capability to discern
the heart which is the source of fundamental human problems.
Thankfully, the word of God has the capacity to do so.*

Hebrews 4 vs.12.

Acknowledgements

It all started when I received a mail from Prof. Michel Verhaegen asking if I am interested in participating in the Delft Global Initiative (DGI) challenge. I was excited by this opportunity and immediately wrote a proposal with strategic inputs from Prof. Gleb Vdovine and Michel Verhaegen on Optical Smart Malaria Diagnost. The proposal, submitted in collaboration with Prof. Oladimeji Oladepo (a public health expert in University of Ibadan Nigeria) was granted by the Delft Global Initiative. This initiated my interesting journey into the world of Smart optical diagnosis of parasites.

On this journey, I have worked with amazing people whose contribution to this work has brought me thus far. I will like to start with my Promotors: Gleb Vdovine and Michel Verhaegen. Thank you for your support, your guidance, your encouragement and your deep insight that guided me through this work. To my "unofficial" supervisor from Delft Global Initiative – Dr. Jan Carel Diehl, thank you for your support, useful collaboration and for organising our ideas and concepts into beautiful functional prototypes which has regularly won many James Dyson Design Awards in the last years. I deeply appreciate Prof. Oladimeji Oladepo for his support and commitment to this project. You gladly received a call from a stranger 4 years ago and since then, it's been an interesting journey. Thank you!

Next, I would also like to thank my family, especially my wife, Irene Agbana, for her unflinching support, encouragement, prayers, sacrifice and awesome advises that kept me going. To Anthony, Kelvin, Jeremy, Jaella and Jacinth I am super grateful for allowing me do this work peacefully. You all stand out and I am grateful to God for making me an integral part of your lives.

To my parents, Dr. Steve & Yemi Agbana, you nurtured me, prayed for me and implanted virtues and values with strong capacity to produce results anywhere in the World. Thank you for always being there for us, thank you for your ground breaking prayers, thank you for your sufferings, thank you for your love, thank you for everything! You mean so much to us. Mama Fester Imoh you are simply amazing, you care about everything and desire the best for our family. God bless you abundantly for being there throughout this journey and being a mother indeed. You are special.

Dr. Peter & Hazzel Uwaibi, thank you for your prayers and for sharing in our joy. Dr. Anthony Yao Dzegede, your life has been an encouragement from the beginning, You are a shining light and I look forward to the day I can be a great blessing to you sir. To Abraham Sam & Grace Aiyedogbon, amazing and wonderful times we have shared together in time past, may the great works you have done continue to speak for you. Pastor Stanley & Celeste Dissels, thank you for your revival blessings and for great times of refreshing that we have shared and that are ahead, thanks for being a blessing. To Pastor Dele & Bucky Olowu, thank you for your constant encouragement

and support. Chief & Dr. Abudu Mahe & Patience Adamu, I am grateful I met you in this life time. Your energy, passion, love and diligence has always been an inspiration. So suprised that age has not made you otherwise.

Many thanks to Delft Global Initiative team: Sophie, Esther, Annelies and Claire. You are such an amazing team! To Jennifer Kockx, thank you for being there at the beginning and for standing with me all the way. I specially want to thank Roel Kamerling for his amazing advises and deep insights whenever we prepare for corporate meetings. Working with you Roel has been a great blessing! your selflessness baffles me. To my Delft Global fellows, thanks for supporting me.

Michel, thanks for always being there to support and encourage, I sometimes feel we should have combined our work for even greater impact, I wish you well on the development of your technology. Roos, I wish you all the best in the days ahead. Mitasha, its always amazing talking with you. Keep up the good work and the cheerful face. Dominik, Juan Carlo! Saqr, Pieter, Anteneh, Rachel, you guys are simply amazing. Thanks Yask for being so supportive and ensuring I get the original version of your wife's drawing of my Tedx talk. Your work is inspiring and I look forward to its global impact. Camille, Petra, Merel, Christine, Mona, Hendrik—keep up the great work. And the new fellows: Monica, David, Daniel, Prosper and Adeola welcome to the group and I wish you greater days ahead. To all of you, keep making impact in your space.

I will like to thank my colleagues for the great times we shared together. I specifically thank Oleg for introducing me to the principles of adaptive optics, Hans for his invaluable contribution to my understanding of optimisation algorithms. Many thanks to Paolo for sharing his practical experience on how to build and align optical systems with me. To Dean, Elisabeth, Reinier, Pieter, Peter, Hai, Tijmen, Laurens, Baptiste, Thao, Shrinivas, and the rest I may have forgotten at this moment, thank you for being amazing colleagues to work with. To my office mates and colleagues - Lukasz & Leonoor, thanks for your encouraging and motivating words while I was writting my thesis, I wish you both the very best. I acknowledge the Master's students whose labour has profited our work: Riemer, Alex, Satyajith, Patrick, Mirte, Julia, Max, Derk, Casper, Noor and all the Industrial Engineering Design Masters students (on different project groups) too numerous to mention. You all make this story complete!

There are so many others without which this would not have been possible: Will and Kees for their technical supports, the amazing DCSC secretariat of Marieke, Heleen, Kiran, and formerly Kitt; Mascha the Graduate School coordinator and Erica our departmental manager. Many thanks to the amazing department of Parasitology at the Leiden Medical Centrum under the leadership of Prof Maria Yazdanbakhsh. Thank you for providing all the samples we needed for this project. Thank you Maria for supporting this project, thank you for believing in me, and thank you for guiding me. Abena, Lissette, Angela, Maryam, I enjoyed collaboration with you all. Thanks for the Schisto samples too. Fiona, Shahid, Jar and Chris from the Malaria group, thanks for your support, insight and provision of all malaria samples needed to test and verify our proposed techniques.

Special thanks to Prof. Wellington Oyibo and all staff of ANDI malaria research center. Thank you for opening your laboratory to us and hosting our students. Thank you also for your insightful comments and advises. To the Dean, staff and students of the Industrial Design Engineering (TUDelft), thanks for the beautiful collaboration we have enjoyed these last years. To Gyoung, Mirte, Max, and many others too numerous to mention. Thanks for always being there to share design ideas and think together. Thanks Mirte for helping with the dutch translation of the project summary and propositions. To my colleagues, Deborah and Fatima I am happy to have met you guys during our graduate school course. To Britta, thanks for a beautiful cover design and above all, a cheerful spirit with which you did the job.

To the AIDX Team : Seva, Mirte, Max, and many others that will come onboard, I believe the best is yet to come. Special appreciation to Anouk, Alexandra, Toine, Martijn, Annelies and the entire Tedx team. Thanks for helping in spreading my ideas I have graciously benefited from this kind gesture. To YES Delft & EIT Health, thanks for helping to finance us to get out of the building and talk to expert from which we got very useful inputs that enabled the robust development of our devices. Noor, Ruben and Tjarda are simply amazing people. To all the CEO's of the startups that participated during the validation lab – Gaia, Addoptics, Munevo, Envision, Gyrafit, Tympany, Viewpoint, Recognize, Eyemic, I truly believe in you guys. Keep advancing and hope to meet you all at the top.

Charloite koster it was really great practising our Tedx delft talk together, you have made DNA editing less scary for me. Keep up the good work because I Know you “really love your job – that’s what you do for a living”! Jos Wassink thank you for following up our story. Reading your writtings is always refreshing. You are very good at what you do! To Dr. Rob, how I dreaded coming for the oral exam of that very difficult course you taught me during my MSc many years ago. Oh, I passed it with an 8 by the way! but I never cease to wonder at your very inspiring and absolutely funny side whenever we catch bus 40 from Rotterdam to Delft. Meeting you on the bus is super relaxing and entertaining- its like therapy. I seem to enjoy you speak in the bus than in the classroom!

To my amazing friends, Barka & Jessica the precious times of prayer and intercession in those small cubicles in the University when we were less than 17 years of age still resonates with me. It is still a mystery how I found you again right in my office in Delft (The Netherlands) after 15 years of loss in contact. Dayo Adewole my dear friend, we grew up together doing great things, and so glad to still see you doing greater works thank you for your prayers.

Odigwe & Beth (now the Okonjis’) I cannot stop remembering our days together in Abia State Nigeria 15 years ago. Isaiah 53 vs.2 is an accurate description of our state as National Youth Service Corp members. All we had was God, each other, a clear vision and very strong passion for all we did back then. Years have gone bye and I am grateful to God for His evident unreserved grace towards us. Keep advancing my people! - Proverbs 4 vs.18. To Alfred & Favour Eyimife, such a wonderful brother and sister you have been to us. I deeply appreciate your friendship, brotherhood and

prophetic insight. May the Lord advance you in all areas of your lives. We love you guys so much!

Wolfi & Alison thanks for being so encouraging and committed to our friendship. David & Geeta the hours of interactions we share either in your home or in our home sharing and edifying one another is amazing. You guys are simply amazing and wonderful. We love you and your whole family. Regilio & Ingrid- fantastic people, loving people, great people we really love you guys. John & Eugenia my dear "American-Dutch friend" I appreciate all the times we shared together. Emmanuel & Ediseh cannot forget the great and precious times we have shared, you have inspired me so much. God bless you my dear friend. To Pastor Guno Hannah Veux, you guys are simply amazing. We love your passion for Christ, your love for people and your ministry! God bless you our dear great friend.

To Owanle Mathias & Mama Hilda, such a blessing you have been to us and not to us only but to this generation. We love you so much, you are an example. May the Lord keep you and uphold you in all ramification. Farai & Busi my big brother from another mother – "God will see us through" is our prayer that God has not failed to answer. You and Pastor Busi are simply amazing we love you both forever. To my dear brother Taslim & Nike Alade, thank you for the great times we shared in the library, in our home and in yours, you are really wonderful people. May the Lord perfect all that you do. Together we laboured on our thesis and I will sure attend your defence next tomorrow - 8th May 2020. We love you guys! To Priscillia Imoh, Peter & Christabel, thanks for being a family indeed, I always feel at home with you guys either in Ireland or in Newcastle. You all inspire me.

Emmanuel & Grace you are more than words can describe, you are my friends, my scientific collaborator, family, and prayer partner. I thank you copiously for editing the medical part of this work. Kayode & Seyi, thanks so very much for the fun times, the brain storming, the challenges and the great times we have been through. Better days are ahead brother! Major my General, thank you for the great times we have shared and we will continue to share. I will see you live out your dreams by Gods power. Rejay, Edor & Uyor, what would I have done without you guys. I love you all loads! Elder John Timi your rugged faith inspires me, your determination and doggedness is contagious, I learn so much from you. To our beloved friend and family, Apostle Claire Revealed, may the Lord bless you more and more. Thank you for your friendship and "sisterhood". Keep moving on.

Pastors - Ola & Rudsella Asubiaro, Ardy & Rose Fer, Moses & Angel Eboh, Moses Adekanye, David Olugosi the precious times we shared in prayer remains ever green. Thank you for staying true to your calling despite the challenges. Dele Balogun, Chamberlain Brown, Kayode Adelowo, Henry Praise, Ben Musa, Osayemi, Anointing Bitrus, Ayodeji, Toyin, Godwin Nath Ayo, Ayo & Tutu thanks for your prayerful support and great words of encouragement. Andy Kluivert, thank you for organising the social media promotions, your passion and commitment is a key that can open many doors for you. Abdoulrahim & Innocent, thank you for your constant encouragement. Chagall so bright is your future, keep holding on to God, thank you for offering to re-type the

manuscript of a book for youths which I wrote more than sixteen years ago. It will surely be published soon!

To the Compassion Church Family worldwide thank you for your prayers and support. To Compassion Rotterdam, thanks for your love and prayers. Your love for God is encouraging and together we shall do greater works for God. Many thanks to Jim Lafoon for praying and speaking the mind of God concerning this project right from the beginning. I believed every word, and I testify to God's grace revealed through those words.

To my Best family for real – Kay, Rejay, Lanre, Wemi, Edor, Major, Uyor, John, "Uluba", Feyi, Pelumi – You guys have been there from the beginning and together we will make it to the end. To my beloved big brothers, Kingsley Uwagbale, Femi Olukotun, Biodun Osasona, Dele Agbana, Samuel Osasona, thank you so much for your many encouragement and admonitions. Again to Kingsley Uwagbale, you saw the future and you challenged me to go for it, you inspire me deeply.

Engr Smith & Yomi, thank you very much for your prayers and your love from the beginning, you are amazing and I can never forget the great times we spent together doing life in the heat of Borno back in the days. Days in Smith Compuserve were amazing, I look back with great pleasure. Rotimi Olukotun, can never forget you, may the Lord lift you up. Mummy Abigail Ojo, I am so grateful for your love and care for us. May the Lord bless you.

Uncle Jide & Lola thank you for being there for me. Can never forget how you rushed down to the accident scene in Gbgogan many years ago, brought me to the hospital in Lagos and nursed me to recovery. Thank you so very much. To Owanle Toba, Bobolante, Anslem & Emeka, I enjoyed every moment we spent together in Italy and Lagos. To Auntie Cordellia thank you for affording me your address to fill my ESTA immigration form whenever I visit the US for my conferences. To my dear and amazing friends, Dr.Keshinro, Dr.Gidado and Dr.Akin thank you very much for your deep insight and great support. Talking with you is always refreshing. Ireti you are such an inspiration, God bless you for what you do! Pastor Goke & Toni, so awesome to reconnect with your family after 30 years. Pastor Segun & Sade Oyediran and our lovely Appointed who came at the appointed time, thank you for your support, prayers and prophecies.

Joshua Selman Nimmak, I cannot but add you to this acknowledgement, each time I see you something leaps for joy in me. It feels like I have known you for years. You greatly inspire me, its a spiritual connection and I am grateful to God that this is happening in my days. Keep advancing dear brother. To you reading this page! Thank You very much. To my very wonderful and special friend Dr. Charles Usie, you really inspire me and I mean every word of it. Thank you for your friendship and for standing out above all, thank you for what you do for our people (the very poor of the poor). You, your wife and kids are simply amazing. Much love bro!

eck

Curriculum Vitæ

Summary

I am currently a researcher and my research focuses on the development and deployment of affordable, field-compatible and easy-to-use biomedical diagnostic instrument. I work on developing methods that combines both optical system design and data-driven algorithms specifically for the diagnosis of parasitic diseases common in low-income countries. Conception of new ideas and methodology, design of smart optical systems with sufficiently high resolution to realize diagnostic instruments with high sensitivity and specificity is my main research interest. I am experienced in building, managing and motivating teams to realize set goals and targets. I have practical experience in proposal writing, public presentations, project coordination and supervision.

Work Experience

2013–2016

Delft University of Technology

Researcher- Delft Centre for Systems and Controls

Develop data-driven algorithms for Adaptive Optical Systems,
Design and development of imaging systems.

2011–2013

Delft University of Technology

Research Assistant- Delft Centre for Systems and Controls

Participated in STW Project - Develop data-driven algorithms-
and new measurement methodology for temperature-drift-immune -
wavelength meter based on an integrated micro-ring resonator.

2006–2010

Mobile Telecommunication Network Nigeria (MTNN)

Team Lead - RF & BTS Operations

Leading a team of 8 Engineering staff and over 100 contract staff

Function: Coordinate the mobile network availability & optimising system network.

Education

- 2016–2020 **Doctor of Philosophy**
in Systems & Control Engineering
Delft University of Technology, Netherlands
Thesis: Smart Optics against Smart Parasite
Promotor : Prof. Gleb Vdovine
- 2010–2013 **Master of Science**
Microwave sensing, signal & systems
Delft University of Technology, Netherlands.
Model-based Wavelength Estimation with Tunable Color
Filter and Single Photodiode
- 1997–2002 **Bachelor of Engineering**
Electrical & Electronics Engineering
University of Maiduguri, Nigeria
Design & simulation of magnetic levitation
system

Grants & Awards

- 2017 Edmund Optics Award Silver recipient
- 2018 National winner - James Dyson Award
- 2018 International runner up - James Dyson Award.
- 2018 Open mind grant awarded by NWO- Netherlands
- 2018 INSPIRED Project awarded by NWO - Netherlands

Teaching Skills & Experience

- 2017–2018 **MSc Thesis Supervision**
 Student Riemer Sorgedragter
 Thesis Automated malaria diagnosis using convolutional neural networks in an on-field setting: The analysis of low quality smartphone based microscope images.
- 2017–2018 **MSc Thesis co-supervision**
 Student Vendel, Mirte
 Thesis The EC: a device to diagnose urinary schistosomiasis in Ghana
 Designed for local facilities as well as large-scale community screening sessions.
- 2018–2019 **MSc Thesis Supervision *cum laude***
 Student Heemels, Alex
 Thesis Development towards a robust low-cost Fourier Ptychographic microscope: For the detection of malaria parasites.
- 2018–2019 **MSc Thesis Supervision**
 Student Satyajith, Jujjavarapu
 Thesis Automated Optical Diagnostic Of Schistosomiasis
- 2018–2019 **MSc Thesis Supervision**
 Student Patrick Nijman
 Thesis Smart Optical Diagnostic Of Schistosomiasis (SODOS)
- 2016–2019 **Co-supervision of Student Project - Integrated Product Design**
 Student Supervision of 7 project groups consisting of approx. 6 students each.
 Project Translating proof of concept described in this thesis into functional prototype.
- 2014–2019 **Teaching Assistant**
 Course *Control for High Resolution Imaging & Adaptive Optics Design*
 Function Developing & and teaching laboratory and practical sessions.
- 2019–ongoing **MSc Thesis Supervision**
 Student Derk van Grootheest
 Thesis Lensless Imaging of Urinary Schistosomiasis
- 2019–ongoing **MSc Thesis Supervision**
 Student Casper van Engelenburg
 Thesis Towards label free imaging of plasmodium falciparum in blood samples
- 2019–ongoing **MSc Thesis Supervision**
 Student Noor van Driel
 Thesis Automated detection of plasmodium falciparum in Giemsa stained blood samples

Leadership & Presentation skills

- European Institute of Innovation & Technology Validation Lab - 2018
- Advanced Leadership Workshop - Politecnico de milano - 2019
- Dutch Optical Centre Discovery Day - Winner best start up pitch.
- TEDx Delft Opening speaker - 2019

Research skills & Interest

- Technical Optics design and development.
- MATLAB, Machine Learning, Data-driven algorithm development .
- Development of point-of-care diagnostics for parasitic diseases.
- Adaptive Optics, Sample preparation.

List of Publications

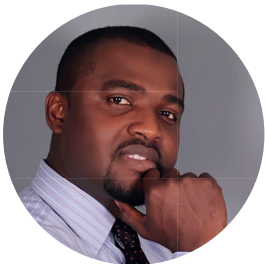
Journal publications

1. *Aliasing, coherence, and resolution in a lensless holographic microscope*, **TE. Agbana**, H. Gong, AS. Amoah, V. Bezzubik, M. Verhaegen, and G. Vdovin. [Optics Letters 42, 2271-2274 \(2017\)](#)
2. *Optical path difference microscopy with a Shack–Hartmann wavefront sensor*, Hai Gong, **TE. Agbana**, P. Pozzi, O. Soloviev, M. Verhaegen, and G. Vdovin. [Optics Letters 42, 2122-2125 \(2017\)](#)
3. *Imaging & identification of malaria parasites using cellphone microscope with a ball lens*, **TE. Agbana**, JC Diehl , FV Pul , SM. Khan, V. Patlan M. Verhaegen, and G. Vdovin. [PloS one, 10,\(2018\)](#)
4. *Discrete wavelet transform detection of Schistosoma haematobium using a cellphone microscope*, **TE. Agbana**, S. Jujjavarapu, JC. Diehl, AS.Amoah, M. Yazdanbakhsh, W. Oyibo, O. Oladimeji, M. Verhaegen, G. Vdovin. [Submitted\(2019\)](#)
5. *Highly sensitive automatic optical detection of malaria*, **TE. Agbana**, F. vanPul , SM. Khan, JC. Diehl, J. vanHellemond, W. Oyibo, O. Oladimeji, V. Bezzubik, M. Verhaegen, G. Vdovin. Yet to be published (2019)

Conference publications

1. *Wavefront coding with adaptive optics*, **TE. Agbana**, O. Soloviev, V. Bezzubik, V. Patlan, G. Vdovin, M. Verhaegen. [Proc. of SPIE BiOS Vol 93350Q,\(2015\)](#)
2. *Sensorless adaptive optics system based on image second moment measurements*, **TE. Agbana**, H. Yang, O. Soloviev, G. Vdovin, M. Verhaegen. [Proc. of SPIE Vol 9896, 989609 \(2016\)](#)
3. *Single Si₃N₄ Micro Ring Resonator as Integrated Wavelength Meter with Long-Term Reproducibility*, C. Taballione, **TE. Agbana**, G. Vdovine, M. Hoekman, L. Wevers, J. Kalkman, M. Verhaegen, P. J. M. van der Slot, and K. Boller. [Optical Society of America, \(2017\)](#)
4. *Temperature-drift-immune wavelength meter based on an integrated micro-ring resonator*, C. Taballione, **TE. Agbana**, G. Vdovine, M. Hoekman, L. Wevers, J. Kalkman, M. Verhaegen, P. J. M. van der Slot, and K. Boller. [Proc. of SPIE Vol 10242, 1024206 \(2017\)](#)
5. *Temperature-immune wavelength meter based on an integrated micro-ring resonator*, C. Taballione, **TE. Agbana**, G. Vdovine, M. Hoekman, L. Wevers, J. Kalkman, M. Verhaegen, P. J. M. van der Slot, and K. Boller. [19th European Conference on Integrated Optics, ECIO \(2017\)](#)

6. *Schistoscope: Towards a locally producible smart diagnostic device for Schistosomiasis in Nigeria*, **TE. Agbana**, GY. Van, O. Oladimeji, G. Vdovin, W.Oyibo, Jan-Carel Diehl. [Proc. of IEEE GHTC \(2019\)](#)
7. *Towards a robust, low cost Fourier Ptychographic device*, A. Heemels **TE. Agbana**, S. Pereira, JC.Diehl, M. Verhaegen, G. Vdovin. [Proc. SPIE. 11251, Label-free Biomedical Imaging and Sensing \(LBIS\) 2020](#)
8. *Towards label-free point-of-care diagnosis of urinaryschistosomiasis*, **TE. Agbana**, N. Patrick, M. Hoeboer, A. Diepen, L. VL, M. Yazdanbaksh, JC Diehl, M. Verhaegen, and G. Vdovine. [Proc. SPIE. 11247, Optical Diagnostics and Sensing XX: Toward Point-of-Care Diagnostics](#)



ABOUT THE AUTHOR

Temitope Ebenezer Agbana, obtained a bachelor of Engineering in Electrical Electronics Engineering from the University of Maiduguri, Nigeria in 2004. He managed a team of RF/BTS Engineers and contractor in a multinational telecommunication engineering company which delivered the best phone network availability and quality in the country at the time.

With a passion to make a difference in his generation, he resigned and pursued a postgraduate education at the Delft University of Technology where he obtained an MSc in Electrical Electronics Engineering (Telecommunication Track). He joined the Delft Centre for Systems and Controls as a researcher in 2011 and worked with the adaptive optics group of Michel Verhaegen until 2016.

Together with Prof. Gleb Vdovine and Prof. Michel Verhaegen, he obtained the Delft Global initiative funding for the Optical Smart Malaria Diagnostics (OSMD) proposal, a project on which this thesis is based. He has since obtained several awards, grants and recognition for his work from the NWO, Netherlands Organization for Scientific Research – Open Mind Program, Edmund Optics Educational Award, James Dyson Award etc. in collaboration with other colleagues and team members.

Temitope continues to do science for the benefit of people and serves as the Chief Executive Officer of AiDx Medical BV. A company that aims at developing the proof-of-concept into working, affordable, easy-to-use, field compatible product which will be deployed for field use.